A Universal Centralized Protection Scheme for Feeders of AC Microgrids using IEC-61869-9 Digital Instrument Transformers

by

Jigyesh Sharma

A thesis submitted to the
School of Graduate and Postdoctoral Studies in partial
fulfillment of the requirements for the degree of
Masters of Applied Science
in
Power Systems and Power Electronics

Department of Electrical and Computer Engineering
University of Ontario Institute of Technology (Ontario Tech University)
Oshawa, Ontario, Canada
October,2023

THESIS EXAMINATION INFORMATION

Submitted by : **Jigyesh Sharma**

Master of Applied Science in **Power Systems and Power Electronics**

An oral defense of this thesis took place on October 12,2023 in front of the following examining committee:

Chair of Examining Committee: Dr. Khalid Elgazzar
Professor, Dept. of Electrical and Computer Engineering,
Ontario Tech University

Research Supervisor: Dr. Tarlochan S Sidhu
Professor, Dept. of Electrical and Computer Engineering,
Ontario Tech University

Examining Committee Member: Dr. Vijay Sood
Professor, Dept. of Electrical and Computer Engineering,
Ontario Tech University

Examining Committee Member: Dr. Sheldon Williamson
Professor, Dept. of Electrical and Computer Engineering,
Ontario Tech University

Thesis Examiner:	Dr. Martin Agelin-Chaab Professor, Dept. of Mechanical and Manufacturing Engineering, Ontario Tech University

The above committee determined that the thesis is acceptable in form and content and that a satisfactory knowledge of the field covered by the thesis was demonstrated by the candidate during an oral examination. A signed copy of the Certificate of Approval is available from the School of Graduate and Postdoctoral Studies.

ABSTRACT

This thesis underscores the escalating importance of microgrids powered by renewable energy sources and inverters in modern power systems. Despite offering significant environmental and economic advantages, their decentralized and dynamic nature poses unique protection challenges. Traditional protection methods struggle to adapt to the diverse conditions within microgrids. Past protection techniques relying on current or voltage detection have limitations affecting system reliability and security. To address this, the thesis proposes a pioneering protection approach based on 'discrepant impedance.' This concept calculates impedance disparities using both feeder ends' positive sequence voltage and current measurements. This value approximates zero during normal operation but deviates during a fault, enabling effective fault detection.

The proposed protection philosophy was rigorously tested through simulations, real-time experiments using RTDS®, and validation on the IEEE-9 bus system with inverter-based resources, a benchmark system by the National Renewable Energy Laboratory National Renewable Energy Laboratory (NREL). Comparative assessments with traditional methods underscore the effectiveness and adaptability of the discrepant impedance-based protection scheme. The thesis concludes by discussing practical implementation options, showcasing the approach's versatility across varied microgrid configurations and control strategies, and ultimately demonstrating the feasibility and effectiveness of discrepant impedance-based feeder protection for modern microgrid systems.

AUTHOR'S DECLARATION

I hereby declare that this thesis consists of original work of which I have authored. This is a true copy of the thesis, including any required final revisions, as accepted by my examiners.

I authorize the University of Ontario Institute of Technology (Ontario Tech University) to lend this thesis to other institutions or individuals for the purpose of scholarly research. I further authorize University of Ontario Institute of Technology (Ontario Tech University) to reproduce this thesis by photocopying or by other means, in total or in part, at the request of other institutions or individuals for the purpose of scholarly research. I understand that my thesis will be made electronically available to the public.

Jigyesh Sharma

STATEMENT OF CONTRIBUTION

In my thesis titled "A Universal Centralized Protection Scheme for Feeders of Microgrid," a part of the work described in chapter-2 has been published as:

J. Sharma, K. T. Lulbadda, A. Golder, T. Sidhu and S. S. Williamson, "Fault Analysis of Microgrids with Inverter Interfaced Resources in Grid-Connected and Islanded Modes," 2022 *IEEE 1st Industrial Electronics Society Annual On-Line Conference (ONCON)*, kharagpur, India, 2022, pp. 1-6, doi: 10.1109/ONCON56984.2022.10127023.

Part of the work described in chapter-3 and 4 has been published as:
Jigyesh Sharma, Tarlochan S Sidhu, A new protection scheme for feeders of microgrids with inverter-based resources, *Journal of Electric Power Systems Research, Elsevier* Volume 224, 2023, 109632, ISSN 0378-7796, https://doi.org/10.1016/j.epsr.2023.109632. (https://www.sciencedirect.com/science/article/pii/S0378779623005217)

Part of the work described in chapter-5 has been submitted for publication
A Low Voltage Microgrid Protection Scheme Using Digital Instrument Transformers, *IET Renewable Power Generation*

ACKNOWLEDGEMENT

I want to express my sincere gratitude to all those who have supported me throughout the journey of completing this thesis.

First and foremost, I would like to extend my heartfelt thanks to my supervisor, Prof.(Dr) Tarlochan Singh Sidhu, for their unwavering guidance, patience, and invaluable insights. Your mentorship and dedication to my academic and personal growth have been instrumental in shaping the direction of this research.

I extend my appreciation to the faculty and staff of Ontario Tech University for providing a stimulating academic environment and access to valuable resources that supported my research endeavours.

My deepest gratitude goes to my family for their unwavering support, love, and encouragement throughout my academic journey. Your belief in me has been my constant motivation, and I am forever thankful for your sacrifices and understanding during this time.

I also want to acknowledge my friends and peers who encouraged me, shared ideas, and offered assistance when needed. Your camaraderie made this academic journey more enjoyable and fulfilling.

Lastly, I would like to thank all the participants and individuals who contributed their time and insights to this research. This thesis would not have been possible without your cooperation and willingness to participate in this study.

Financial support provided by Ontario Tech University is thankfully acknowledged.

Table of Contents

List of Figures

List of Tables

List of Abbreviations

BESS Battery Energy Storage System. xii, 9, 10, 12, 14, 60, 71

CERTS Consortium for Electric Reliability Technology Solutions. 59, 60, 82

CPU Central Processing Unit. 31, 46

CT Current Transformer. 34

DFT Discrete Fourier Transform. 32, 38, 39

GFL Grid-Following Inverter. 6–8

GFM Grid-Forming Inverter. 6, 7

GPC Gigabit-Processor Card. ix, 41–43, 46

GTNET Gigabit-Transreceiver Network. ix, 41–43

GTNETx2 Gigabit-Transreceiver Network version 2. ix, 41

GTWIF Gigabit Work Station Interface. ix, 41–44

HMI Human Machine interface. 62

HSR High-availability Seamless Redundancy. 31

IBR Inverter-Base Resources. 80

IED Intelligent Electronic Devices. 2, 3, 31

LAN Local Area Network. 41

LPIT Low Power Instrument Transformer. 35–37

NREL National Renewable Energy Laboratory. iv

PCC Point of Common Coupling. 26

PLL Phase Lock Loop. 7, 38

PRP Parallel-Redundancy Protocol. 31

PV Photo Voltaic. xii, xiii, 1, 9–13, 21, 22, 71

PWM Pulse Width Modulation. 7

RTDS real-time digital simulator. 4, 41–44, 82

SNTP simple Network Time Protocol. 31

SV Sampled Value. 36, 37, 41

WTG Wind Turbine Generator. xii, 9–13

Chapter 1

Introduction

1.1 Context

All over the world, climate change and concerns about global warming have sparked massive efforts to transition toward clean energy generation and utilization. The International Renewable Energy Agency (IRENA) has reported that renewable energy's stake will increase from 25% in 2017 to 85% by 2050 [1]. In 2021, the Canadian Renewable Energy Association (CanREA) estimated deploying 3,800 MW of wind energy and 1,600 MW of solar generation annually for 29 years to achieve net-zero GHG emissions by 2050 [2]

Renewable energy resources such as solar Photo Voltaic (PV), wind turbines and battery energy storage systems interface with the electrical network through power-electronic devices known as inverters. This energy conversion method is very different from traditional generating plants such as coal-fired, hydropower, and gas-fired, equipped with turbines coupled with synchronous generators. As a result, the penetration of inverter-based resources presents technical challenges in operating and managing the grid, which differs from the synchronous-based generators. Among the many challenges, this thesis focuses on the protection challenges brought by inverter-based resources in microgrids.

Microgrid is a group of interconnected loads and distributed energy resources with clearly defined electrical boundaries that act as a single controllable entity for the grid. It can connect and disconnect from the grid to enable it to operate in grid-connected

or off-grid modes [3].

1.2 Causes of Faults in Power System and Types of Faults

The faults in the power systems are due to natural phenomena such as lightning, storms or earthquakes. The major technical reasons for faults are insulation degradation, equipment malfunctioning, and equipment overloading. Sometimes the faults occur due to poor operation and maintenance.
Broadly, the faults are classified as symmetrical and asymmetrical faults. In symmetrical faults, all three phases are involved. Commonly known as three-phase faults. Asymmetrical faults comprise faults involving one-phase to-ground (AG, BG or CG), two-phase to-the-ground (ABG, BCG, and CAG), phase-to-phase (AB, BC, CA), and open circuit faults.

1.3 Microgrid Protection

In electrical power systems, feeders, transformers, generators, and bus bars, are protected by relays. The function of relays is to identify and distinguish between faults and healthy conditions. For the past two decades, microprocessor-based relaying technology has been widely used in electrical power systems, and most of them are commonly known as Intelligent Electronic Devices (IED) or numerical relays. These numerical relays provide many advantages over electro-mechanical relays, such as multiple setting groups, a wide range of settings and protection functions, and the ability to communicate and store disturbance records [4]. Whenever a fault occurs, the corresponding relay identifies a fault and gives the command to the associated breaker.

The protective principles employed in microprocessor-based relays are primarily the same as those used in electro-mechanical relays. Microprocessor-based relay pro-

vides multiple protection functions such as over current, earth fault, directional over current and earth fault, under voltage, over-voltage, under frequency and over frequency in a single unit. Some critical equipment, such as transformers, generators, and motors, are protected by differential relaying [5], [6] [7], and other IEDs provide backup protection.

Currently, the power system is protected using a conventional approach based on changes in quantities such as voltage and current. These traditional protection measures are still used to protect microgrids, even with or without inverter-based resources. Consequently, there are many challenges faced by conventional protection techniques due to the proliferation of inverter-based resources [8–11].

The primary emphasis of research on the protection of microgrids is on designing a strategy for grid-connected and off-grid modes of operation. Initial designs for microgrid protection were similar to rule-based overcurrent coordination [12–15]. They used relays for each feeder under protection and coordinated the relays for each mode of microgrid operation. A signal is always required for the relays to switch their settings from one group to another when the microgrid changes its mode of operation. Such strategies work in a microgrid with a defined topology since a microgrid comprises a PV solar generator, wind and battery energy storage system, which are intermittent and may only sometimes be available. This increases the possibilities of different settings with different microgrid topologies. Recently some strategies have been reported in the literature that does not rely on the coordination principle for microgrid protection; one of them is the use of wavelet transform [16–18]. These techniques use wavelet energy of the currents and voltages to identify a fault in a microgrid. But such a technique needs fixing due to downsampling.

Conventional microgrid protection techniques have limitations, which a new approach must address. This thesis reports on developing and testing a universal microgrid protection technique in real time.

1.4 Objective of the Research

Unwanted faults in electrical power networks are unavoidable. However, steps are being taken to keep the grid operational and minimise the effect of faults in the system through protective devices. Grid protection devices continually monitor the power system for faults and provide the desired protection. However, these protective devices were designed considering the synchronous generator's characteristics in the event of a fault. Inverter's response to the fault depends on its controls [19]. Therefore, the conventional protection scheme faces challenges in the present and future, with increased penetration of inverter-based resources in the power system and should be replaced with an advanced protection system [20].

The primary objectives of the work reported in the thesis were to

1. To develop a new protection technique for microgrid independent of topology, type of resources and control strategy.
2. Design, implement and test the protection scheme on an offline simulation software.
3. Design, implement and test the protection scheme in a real-time environment on a real-time digital simulator (RTDS).

1.5 Reseach Outline

The thesis is organized into six chapters and two appendices. The first chapter introduces the subject of the thesis and describes its organization. Chapter 2 reviews the fault analysis in a microgrid and the response of each inverter for various types of faults. This illustrates the significance of positive sequence quantities for the protection of microgrids. Chapter 2 also reviews the previously proposed protection methods. Limitations of these protection methods are identified.

A technique for the protection of feeders of microgrids with inverter-based resources is proposed in Chapter 3. This technique is then used to develop the sampled

value-based central protection technique on a real-time operating system, RTDS®. The protection technique is simple and requires voltages and current inputs from feeder ends. The performance of the protection technique was verified using software simulations ®PSCAD/EMTDC.

Chapter 4 discusses the performance of the protection technique on a high voltage IEEE-9 bus system, and Chapter 5 evaluates the performance on a low-voltage CERTS microgrid using a real-time digital simulator RTDS®. Some results obtained from the simulations are included.

Chapter 6 includes a summary and conclusion drawn from the work reported in this thesis. A list of references is included in the reference section.

Chapter 2

Microgrids Fault Behaviour and their Protection Issues: Setting the Scene

This chapter is based on the following publication: **J. Sharma**, K. T. Lulbadda, A. Golder, T. Sidhu and S. S. Williamson, "Fault Analysis of Microgrids with Inverter Interfaced Resources in Grid-Connected and Islanded Modes," *2022 IEEE 1st Industrial Electronics Society Annual On-Line Conference (ONCON)* doi: 10.1109/ONCON56984.2022.10127023.

2.1 Introduction

Before delving into the microgrid protection challenges, some fundamental principles are explained in this chapter. First, the commonly used inverter for interfaced inverter-based generation, such as Grid forming and following inverters, are outlined. Second, the response of different types of inverters at different locations in microgrids. Finally, the protection issues in a microgrid with inverter-based or non-inverter-based resources are discussed. This chapter is organized as follows. Section 2.2 introduces the Grid-Forming Inverter (GFM) and Grid-Following Inverter (GFL) control architectures used in the simulations. In Section 2.3, the fault behavior of inverters in microgrids is introduced. Protection issues and current practices are presented in

section 2.4. Section 2.5 concludes this chapter.

2.2 Inverter Control: Grid Following vs Grid Forming

Renewable energy resources are interfaced with the microgrid through an inverter. An inverter is an electric device that converts DC power to AC power. The inverter has a primary source with a DC link. The power electronic switches, based on the pulse provided to them, convert DC to desired AC voltage. The control system generates a reference signal to Pulse Width Modulation (PWM) based on the measurement of voltages and currents [21]. Based on the control system, the inverters are classified as GFL and GFM. A grid-following inverter follows the phase angle of the grid voltage and controls the AC side current. While grid forming inverter controls the AC voltage and forms a voltage source. [22].

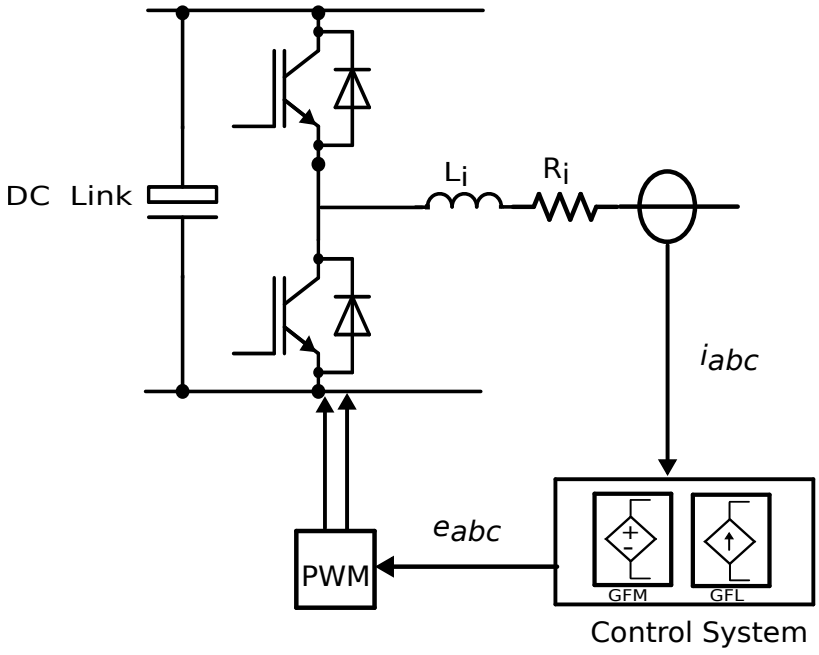

Figure 2.1: Basic schematic of grid interface inverter

The grid-forming inverter regulates the power output by measuring the grid voltage angle using a Phase Lock Loop (PLL) and injecting the current into the grid.

Grid-following inverter does not control voltage and frequency and maintains power output according to the desired set point [23, 24]. GFL inverters are represented as the current source as illustrated in Fig. 2.2.

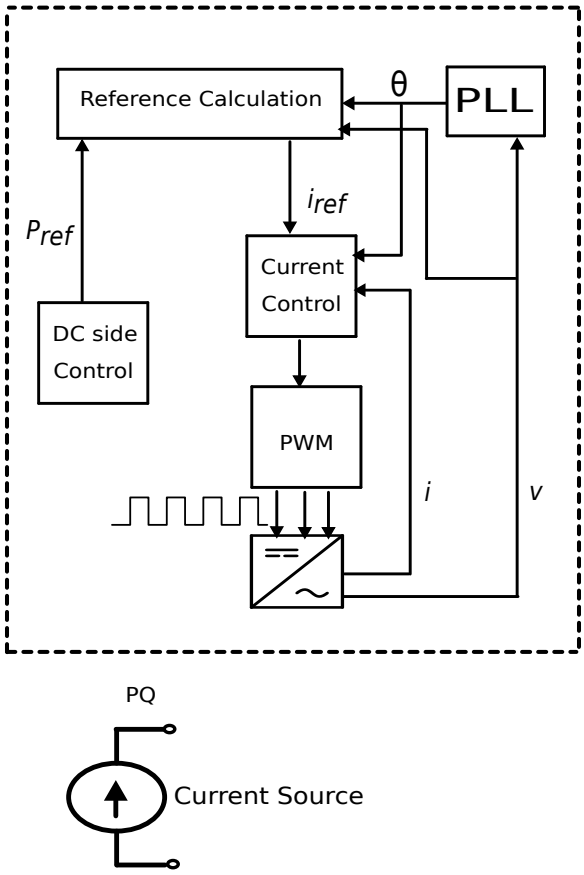

Figure 2.2: Functional block diagram of the grid following inverter

In contrast, the grid-forming inverter regulates the voltage and frequency and can work with or without a grid [25]. The grid-forming inverter does not require PLL. The commonly used control for grid-forming inverters is droop control, a virtual synchronous machine, and a virtual oscillator. The voltages and currents measured at the output of the inverter generate reference voltage and angular frequency [22].

2.3 Fault in Microgrid and Their Response

A fault in a microgrid or any electrical network is inevitable. There are many causes of faults which are explained in chapter-1. In general, faults are classified into short-

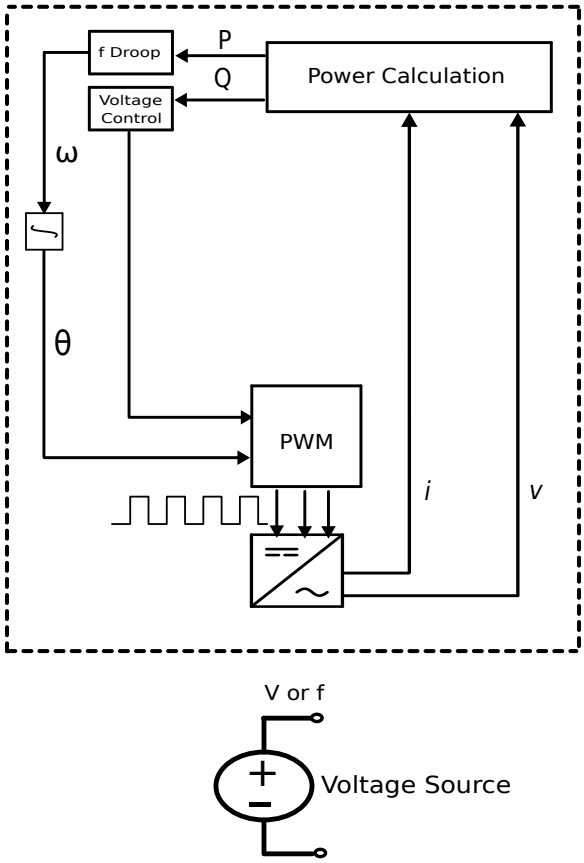

Figure 2.3: Functional block diagram of the grid forming inverter

circuit and open-circuit faults. In a three-phase network, four types of short circuit faults can occur: three-phase fault(LLL or LLL-G), line-to-line(LL), line-to-line-ground(LL-G), and line-to-ground(L-G). Each of these faults provokes different results. To illustrate the fault response of various energy resources, consider a microgrid in Fig. 2.4. The microgrid shown in Fig. 2.4 is a medium voltage 3.3 kV microgrid connected to a utility at 230 kV. This microgrid consists of three inverter-based resources solar PV(2.5 MW), Battery Energy Storage System (BESS) (250 kW), and Wind Turbine Generator (WTG) (2.5 MW). Three loads are connected in microgrid load-1, load-2, and load-3 of 1 MVA, 0.4 MVA, and 1.5 MVA, respectively. Solar PV and WTG inverters are modelled as a PQ source and BESS as a V/f-P source.

A single-line-to-ground fault F-1 is applied on the load-1 feeder to analyze the behavior of the inverter-based resources while the microgrid operates in grid-connected mode. This fault was created at 1.0 s for a duration of 50 ms. The current response

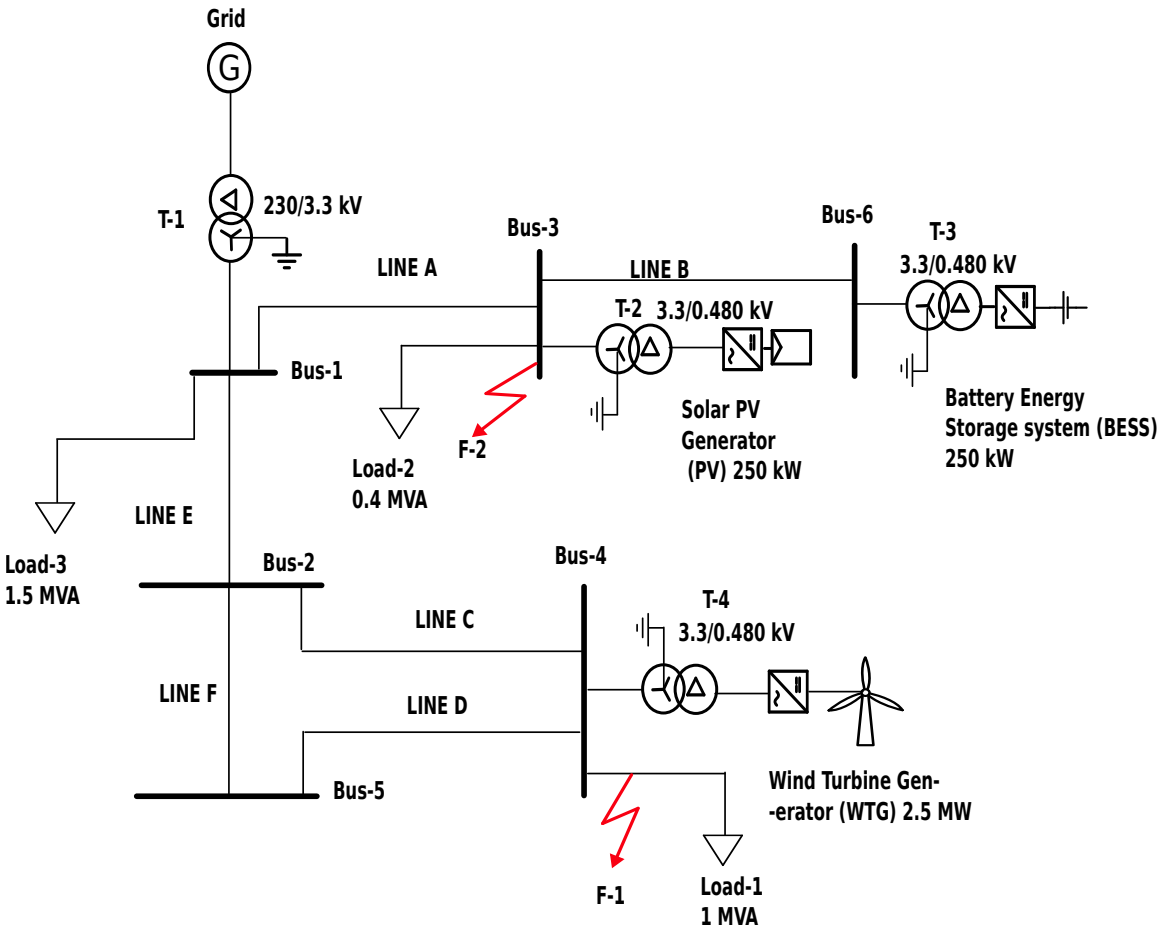

Figure 2.4: Single line diagram of a microgrid

of the BESS, PV and WTG is shown in Fig. 2.5, 2.6 and 2.6, respectively.

It can be observed from Fig. 2.5 that the current in A-phase reaches 2.5 p.u, while the current in B and C-phase remains unchanged. In the case of the PV inverter, the currents in all phases rise from 0.1 p.u. to 0.2 p.u, and the current in all the phases is balanced. At the same time, the current supplied by the BESS inverter is almost balanced with a spike in A-phase current after 20 ms from fault inception. When the utility is disconnected, the microgrid operates in off-grid mode. In this mode, the microgrid sources BESS, WTG, and Solar PV generator supply power to connect load-1, load-2, and load-3. A single-line-to-ground fault F-1 on the load feeder is applied. The currents from the resources WTG, PV and BESS are recorded in Fig. 2.8, 2.9 and 2.10, respectively.

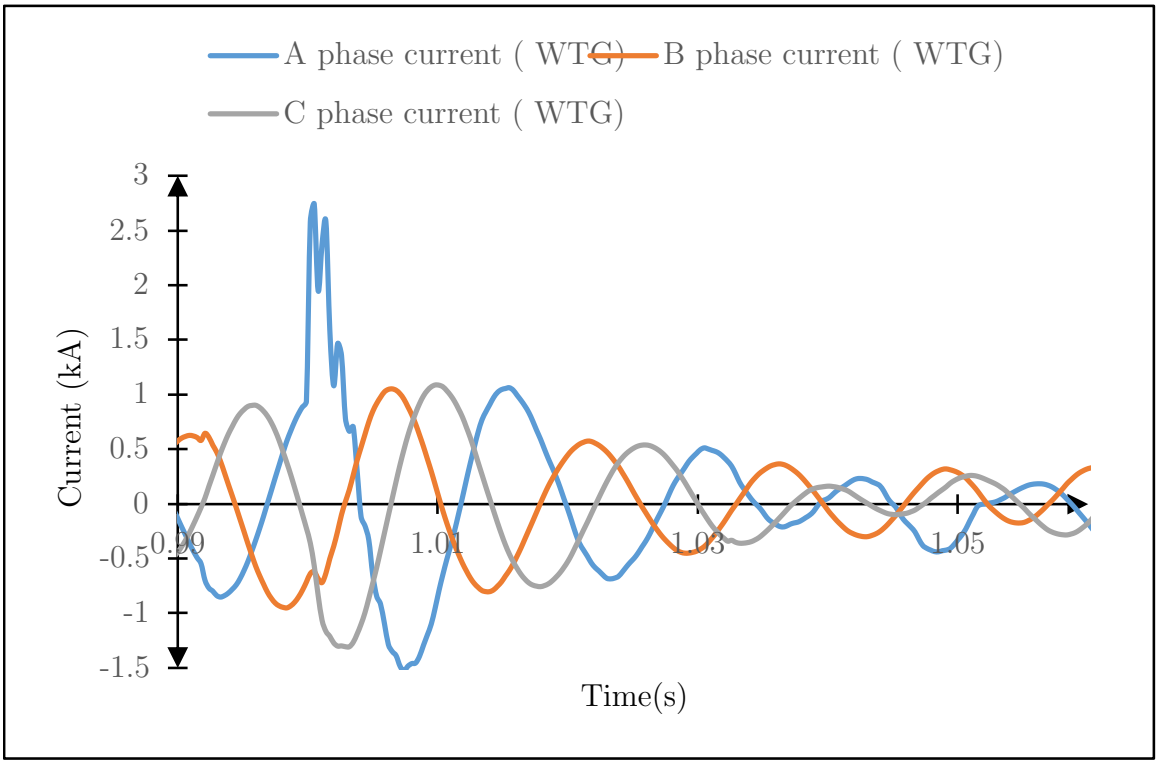

Figure 2.5: Currents waveform of WTG for F-1 fault in grid-connected mode

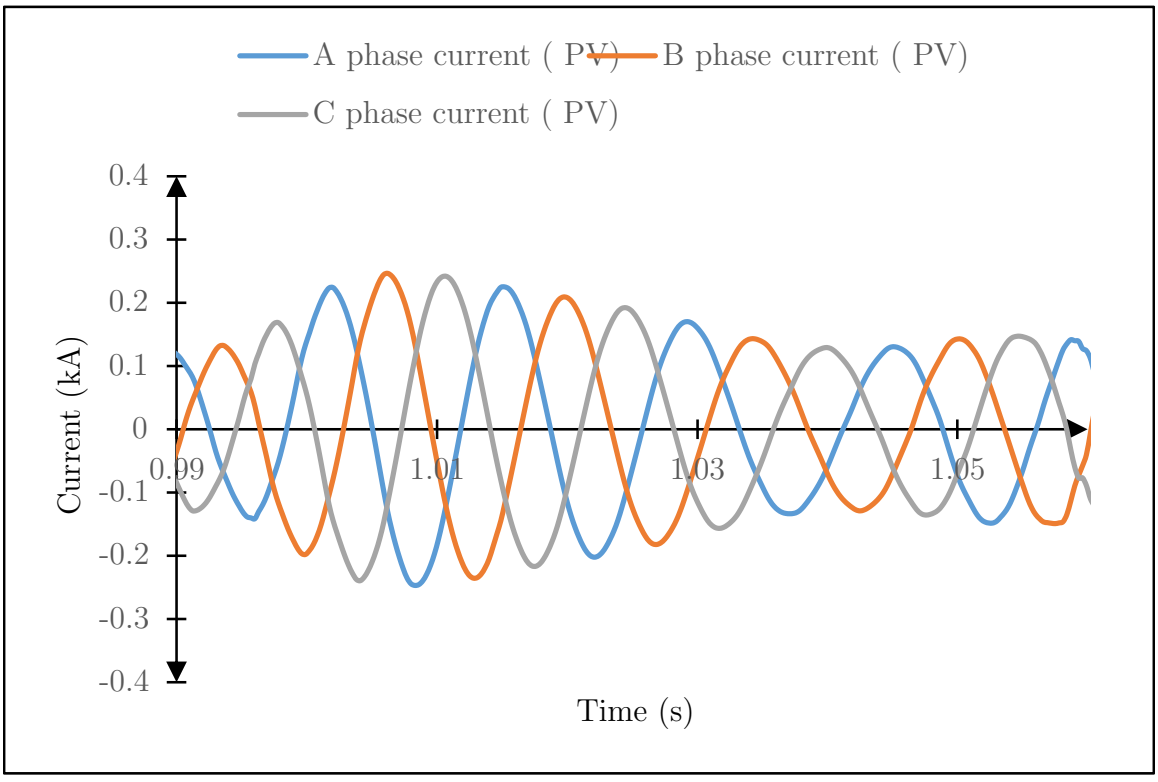

Figure 2.6: Currents waveform of PV inverter for F-1 fault in grid-connected mode

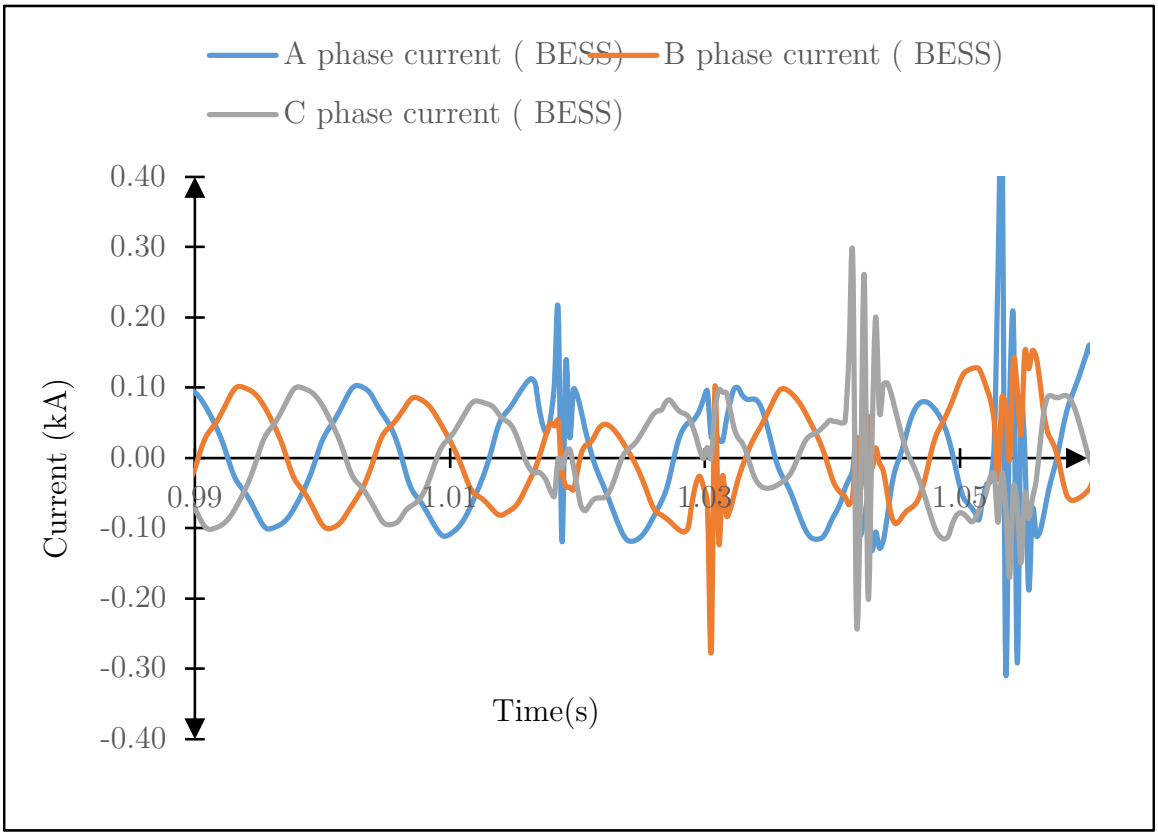

Figure 2.7: Currents waveform of BESS inverter for F-1 fault in grid-connected mode

It can be depicted in Fig. 2.8 that in islanded mode, the magnitude of the A-phase current rises to 1.5 kA while the currents of other phases increase to 0.6 kA for WTG. At the same time, the current contribution from solar PV inverters is almost unchanged and balanced; it is shown in Fig. 2.9. The current supplied by the BESS changes from pre-fault values after a few cycles from the fault occurrence. Also, the currents in all the phases are unbalanced, which is shown in Fig. 2.10.

Compared with grid-connected and off-grid modes, it can be concluded that the magnitude of the fault current supplied by the inverter-based resources significantly reduces in off-grid mode. Also, the current from inverter-based resources is non-linear. The reduction in the magnitude of the fault current supplied by the inverter is because it is governed by its controller and thermal withstand capacity of power electronic devices [26]. The response of voltages at different buses in the grid-connected mode is shown in Fig. 2.11, Fig. 2.12, Fig. 2.13, Fig. 2.14, Fig. 2.15 and Fig. 2.16. The voltage

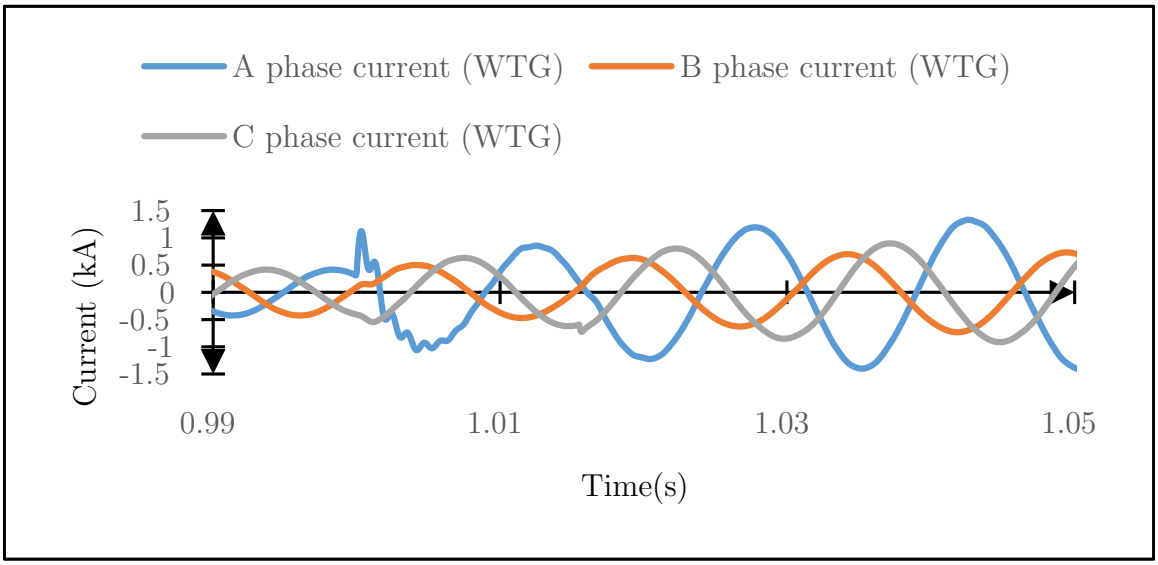

Figure 2.8: Currents waveform of WTG for F-1 fault in off-grid mode

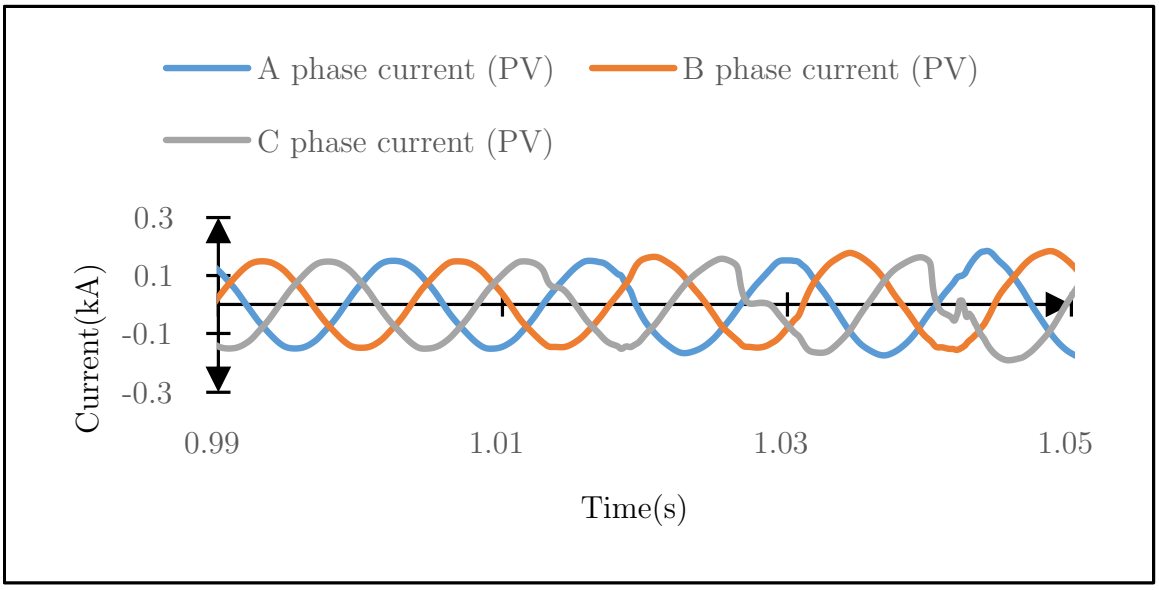

Figure 2.9: Currents waveform of PV inverter for F-1 fault in off-grid mode

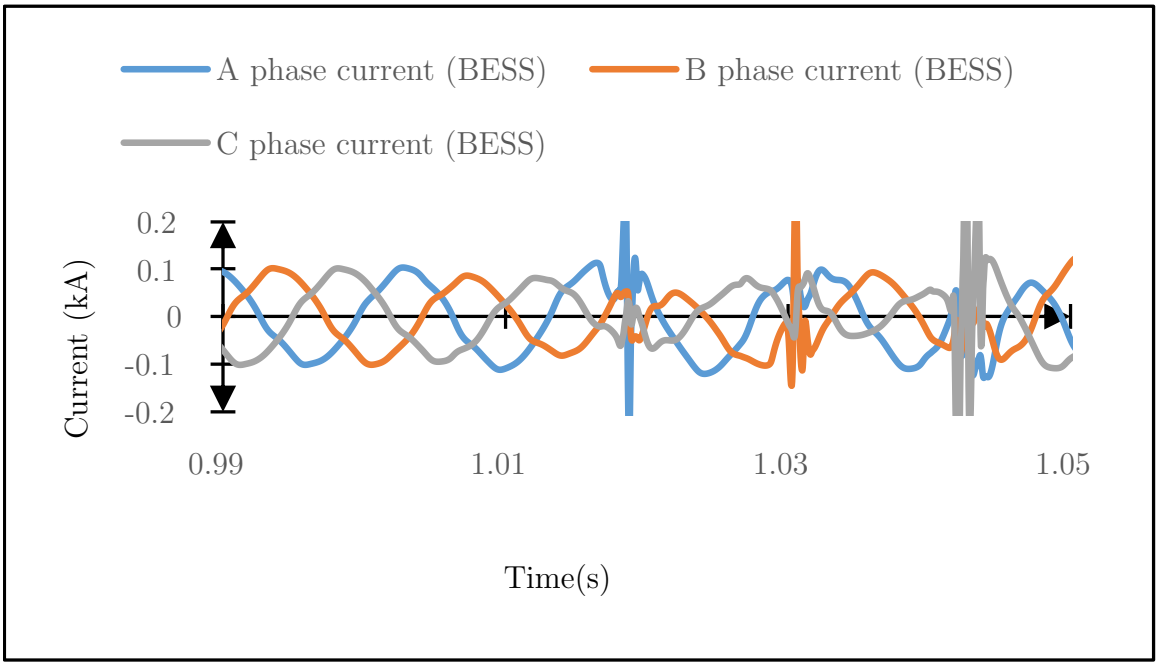

Figure 2.10: Currents waveform of BESS inverter for F-1 fault in off-grid mode

at bus-1, as shown in Fig. 2.11, is perfectly balanced since it is supported by the grid, which is a strong source. The voltages at other bus-2 and bus-5 observe some dip due to their proximity to the fault. However, the phase A voltage at bus-4 is zero since it is a single-to-ground fault, and the other two healthy phases are increased to 4 kV.

The voltages of bus-3 and bus-6 are balanced since they are far away from the fault. The scenario is different when the microgrid is operating in off-grid mode. The voltage waveform for fault F-1 in the off-grid mode for bus-1,bus-2, bus-3, bus-4, bus-5 and bus-6 is shown in Figs. 2.17 to 2.22 respectively.

In off-grid mode, a fault in any section of the microgrid causes a disturbance in voltages on each bus. From Fig. 2.17, Fig. 2.17, Fig. 2.21 it can be depicted that there is a huge disturbance in voltage in comparison to the voltages of the buses in grid-connected mode. In the off-grid mode of operation, the microgrid strength is defined by the short circuit capacity of the resources, and the short circuity of a microgrid is less in the off-grid mode of operation than in the grid-connected mode.

Consider a single-line-to-ground fault F-2 on Bus-3 at 1 s for 50 ms. It can be

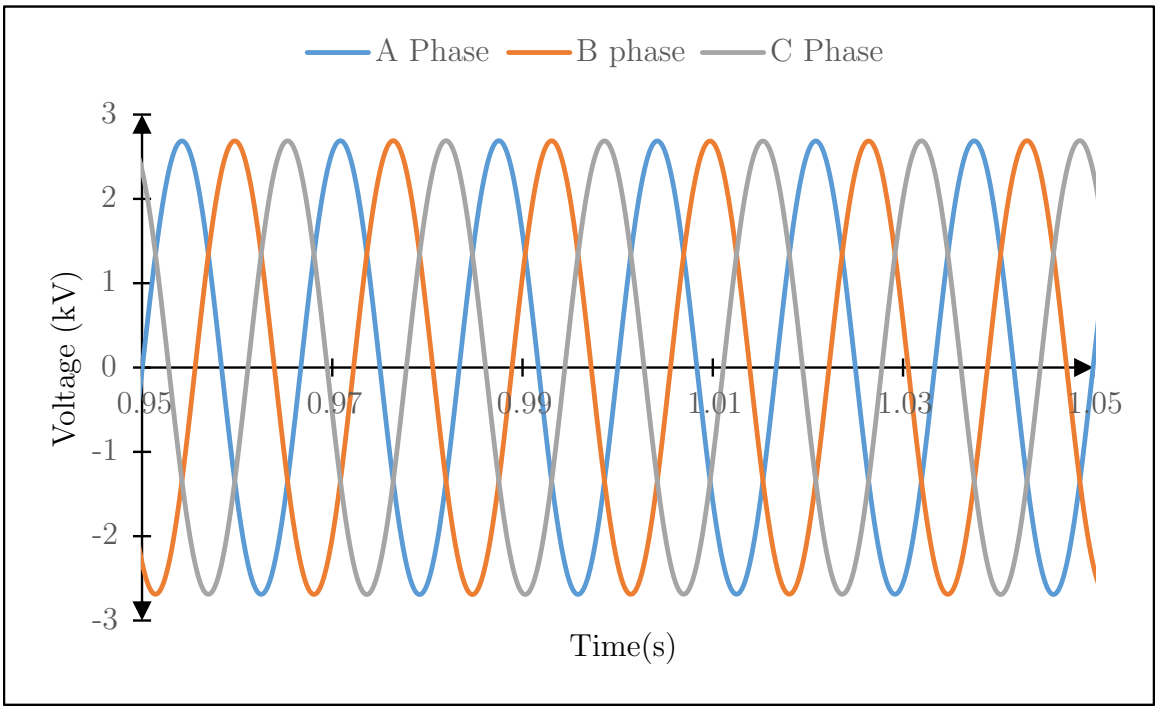

Figure 2.11: Voltage waveform of Bus-1 in grid-connected mode for fault at F-1

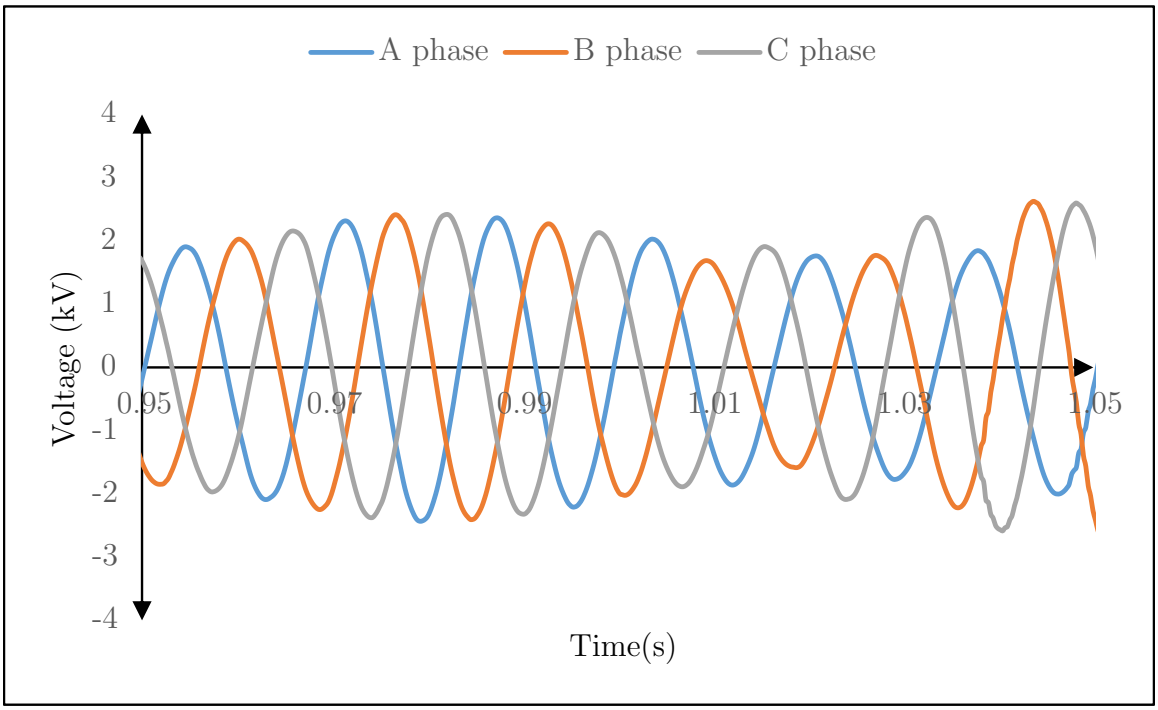

Figure 2.12: Voltage waveform of Bus-2 in grid-connected mode for fault at F-1

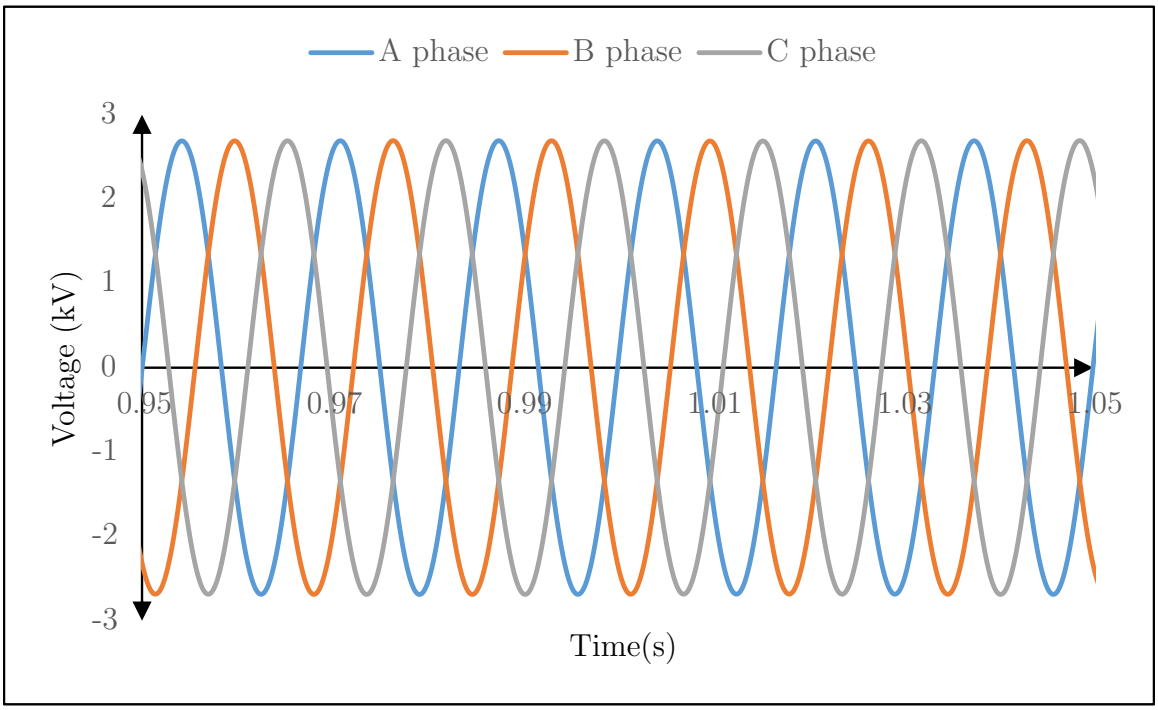

Figure 2.13: Voltage waveform of Bus-3 in grid-connected mode for fault at F-1

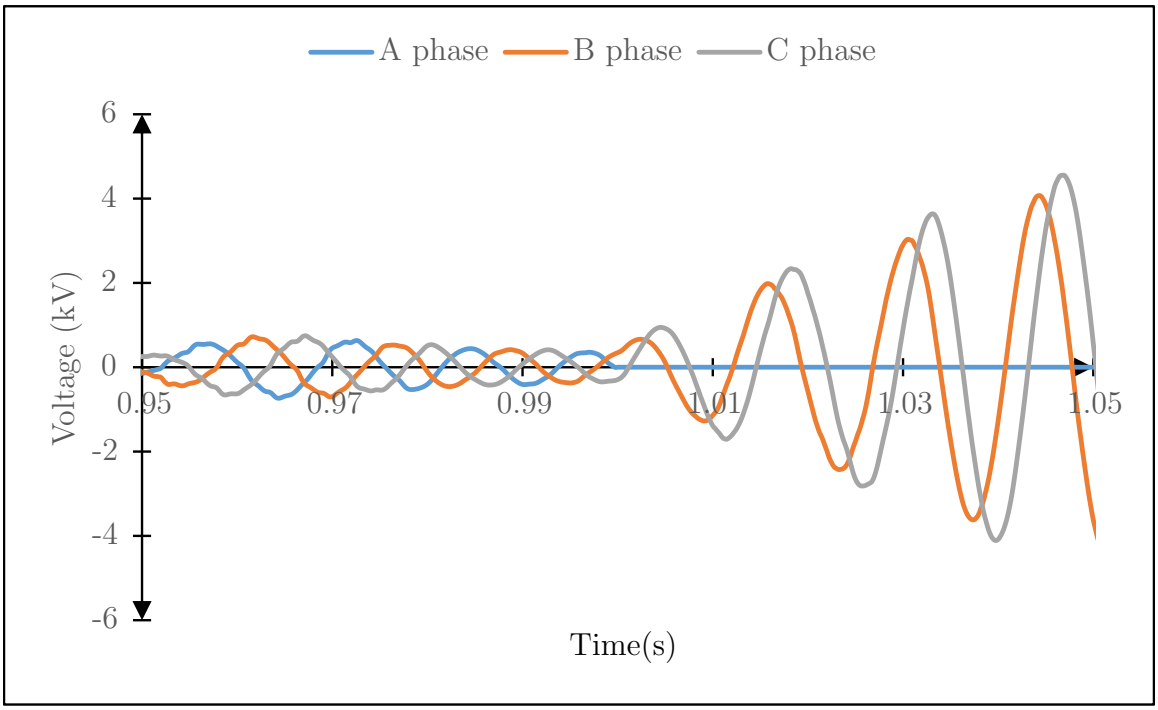

Figure 2.14: Voltage waveform of Bus-4 in grid-connected mode for fault at F-1

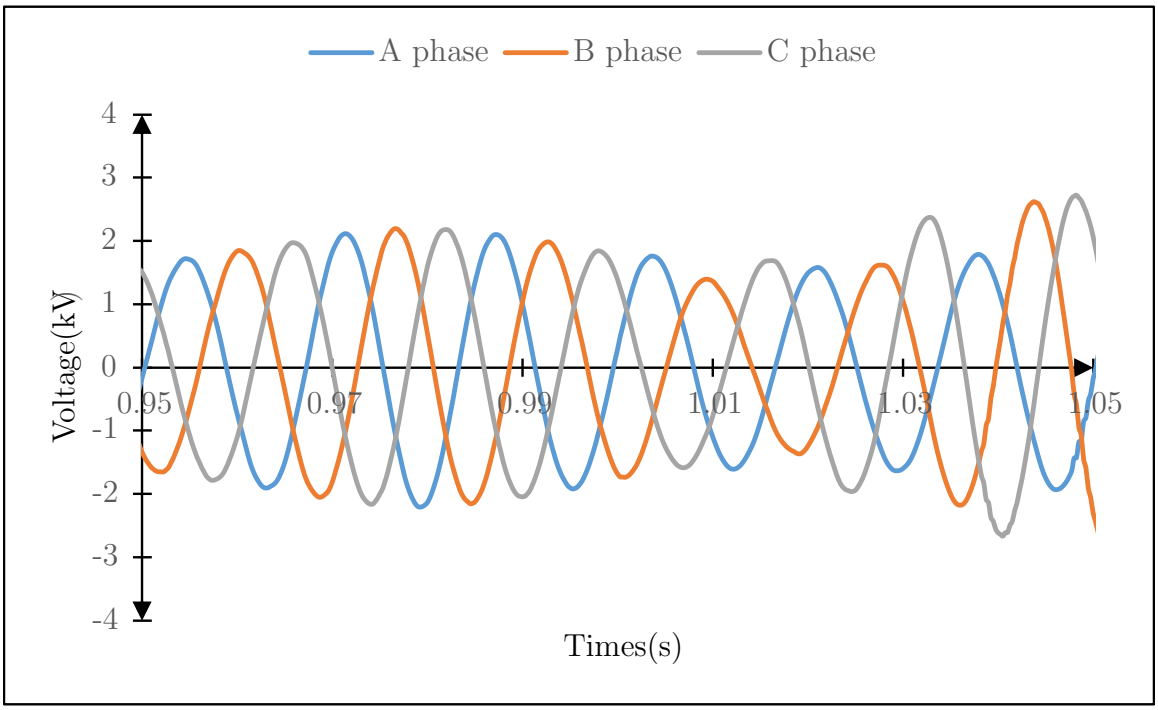

Figure 2.15: Voltage waveform of Bus-5 in grid-connected mode for fault at F-1

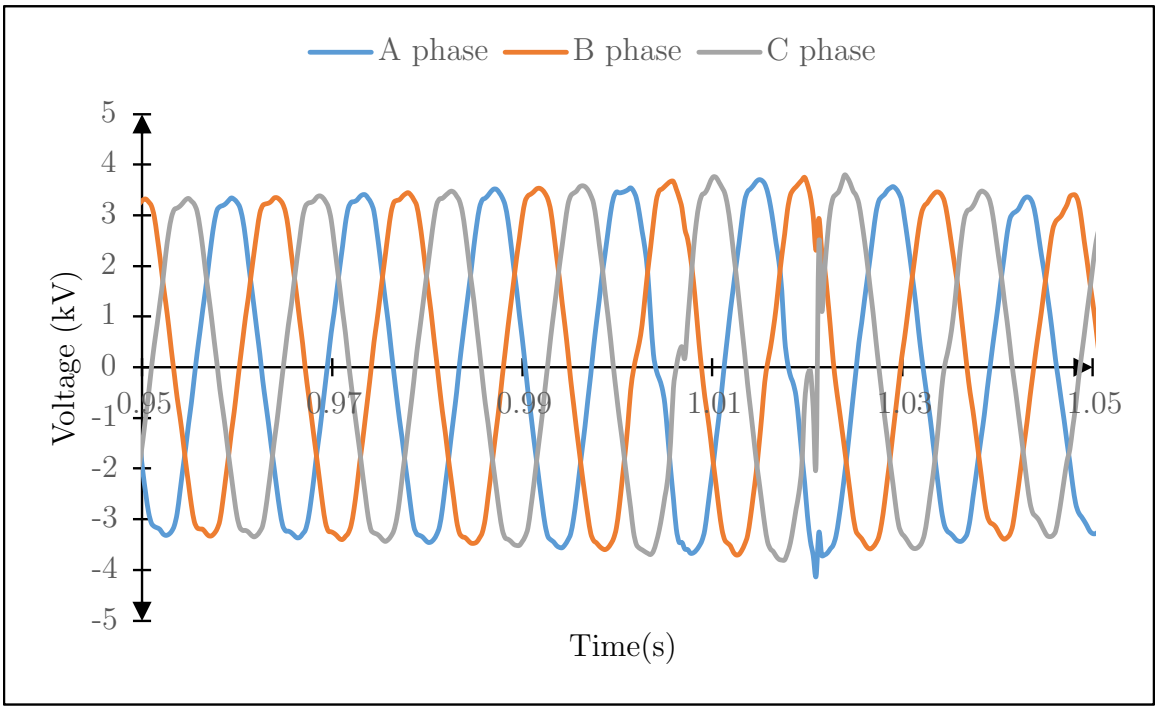

Figure 2.16: Voltage waveform of Bus-6 in grid-connected mode for fault at F-1

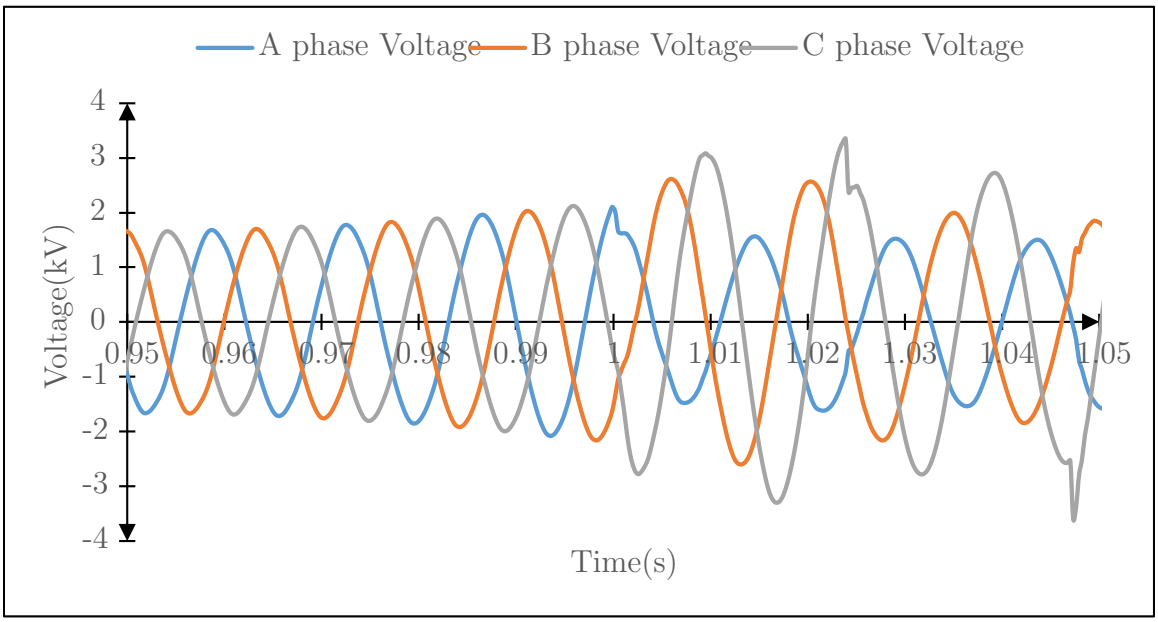

Figure 2.17: Voltage waveform of Bus-1 in off-grid mode for fault at F-1

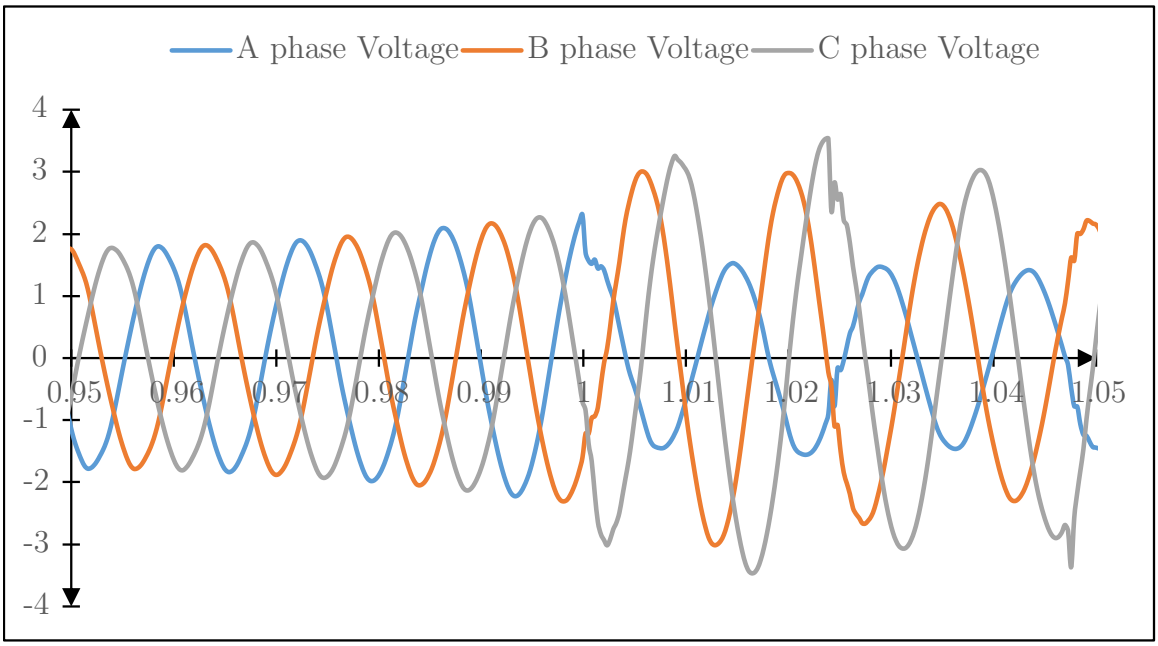

Figure 2.18: Voltage waveform of Bus-2 in off-grid mode for fault at F-1

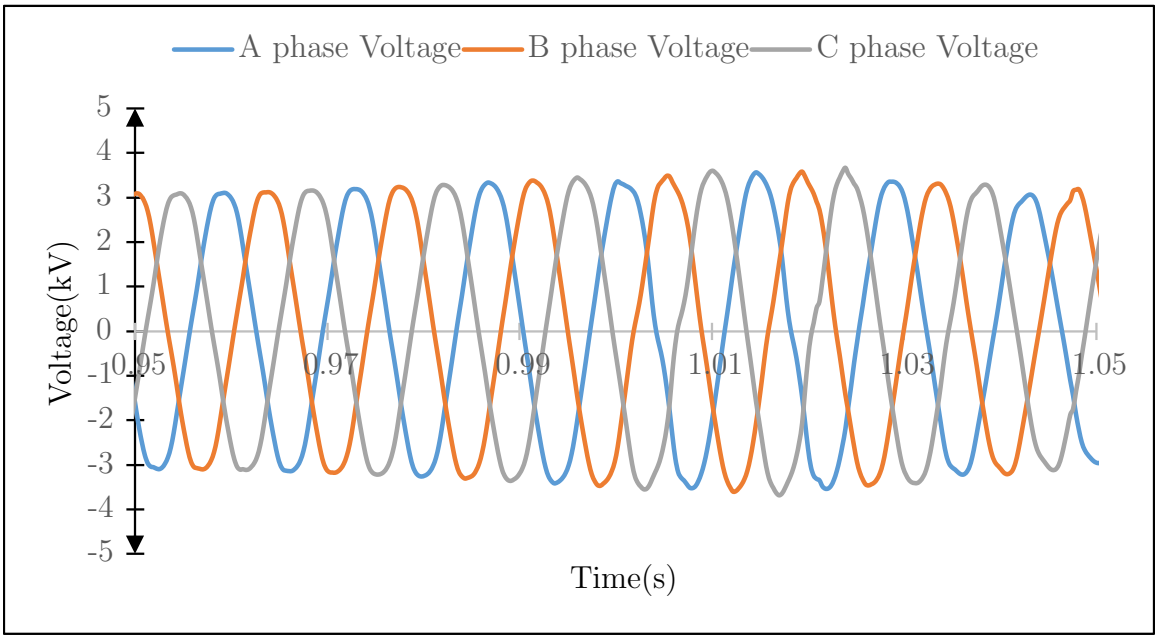

Figure 2.19: Voltage waveform of Bus-3 in off-grid mode for fault at F-1

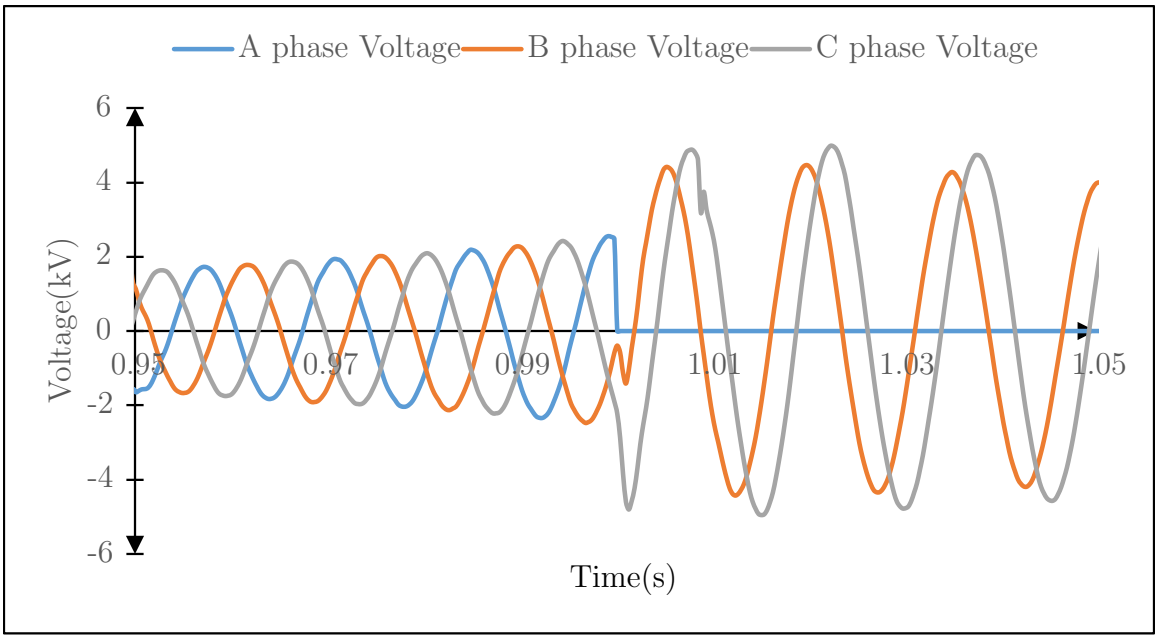

Figure 2.20: Voltage waveform of Bus-4 in off-grid mode for fault at F-1

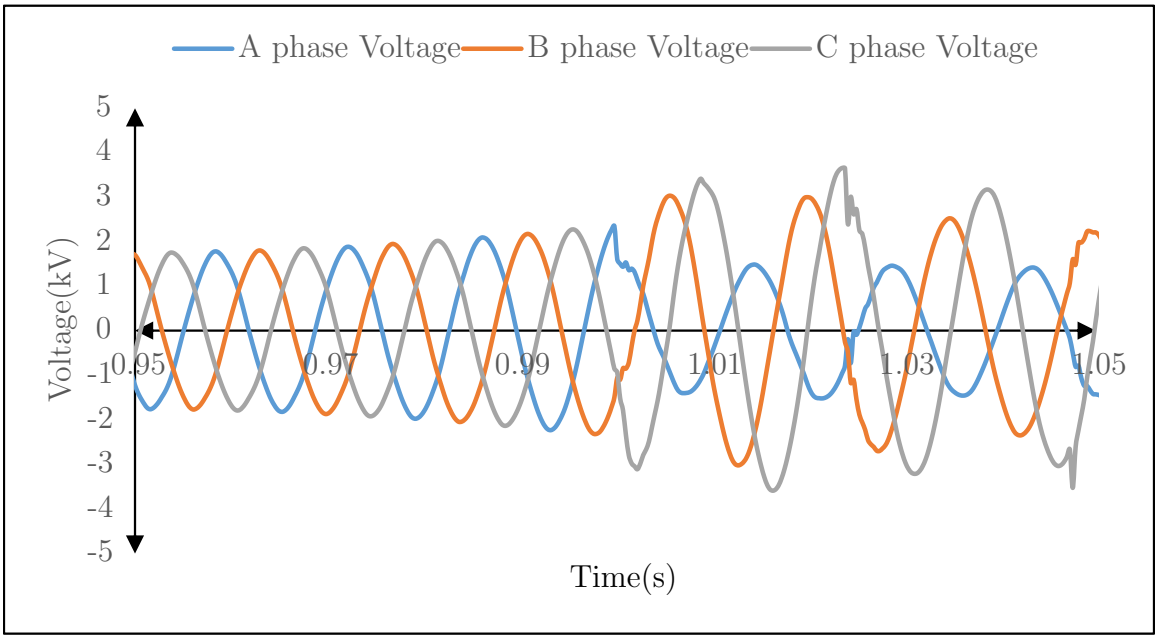

Figure 2.21: Voltage waveform of Bus-5 in off-grid mode for fault at F-1

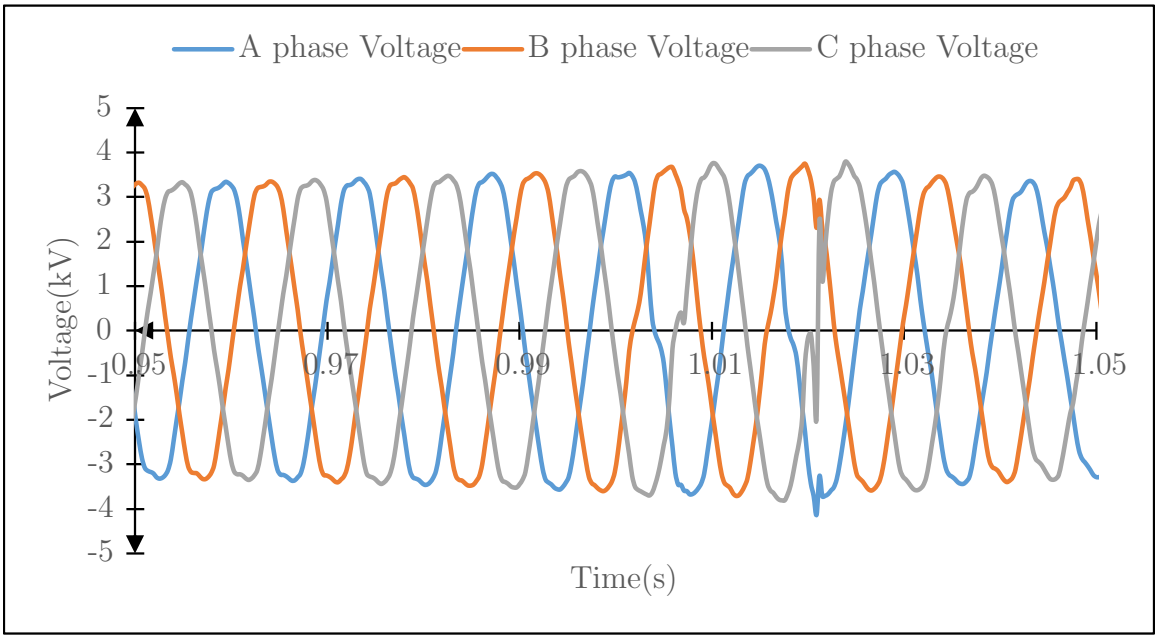

Figure 2.22: Voltage waveform of Bus-6 in off-grid mode for fault at F-1

observed from Fig. 2.23 that the current in all the phases has increased significantly. The grid supplies the zero sequence current through the transformer neutral point. At the same time, the current supplied by the PV inverter is almost balanced, which can be seen in Fig. 2.24.

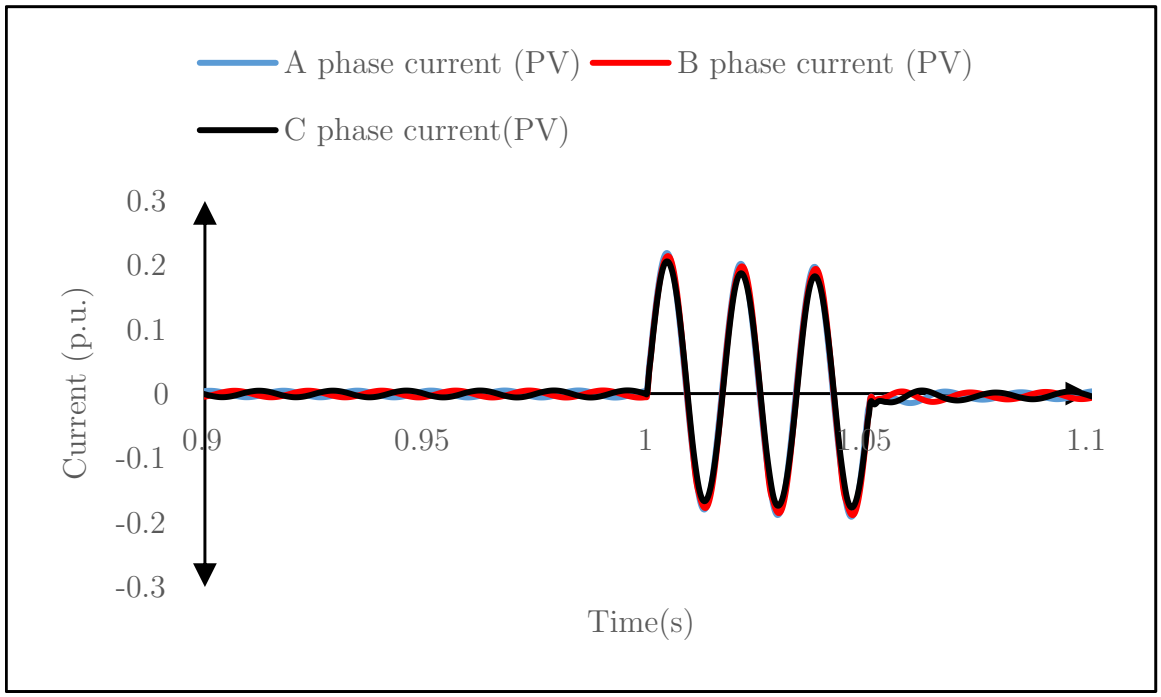

Figure 2.23: Current waveform on grid side of the PV inverter during fault F-1

Some of the protection schemes work on sequence components of current; therefore, analyzing the sequence currents supplied by the inverter during fault F-1 is worthwhile. Fig. 2.25 shows the sequence components of current from the inverter during fault F-1. The positive sequence current increases during a fault, while the negative sequence current is negligible. Since the inverter does not supply an unbalanced current during an unsymmetrical fault. From Fig. 2.25, it can be seen that the zero sequence current is absent since the PV- inverter is interfaced to the grid by the Delta-Star transformer; this blocks the zero sequence current reflected on the delta side. The results shown in this section 2.3 highlight the unusual fault behaviour of the inverter-based resources in microgrids.

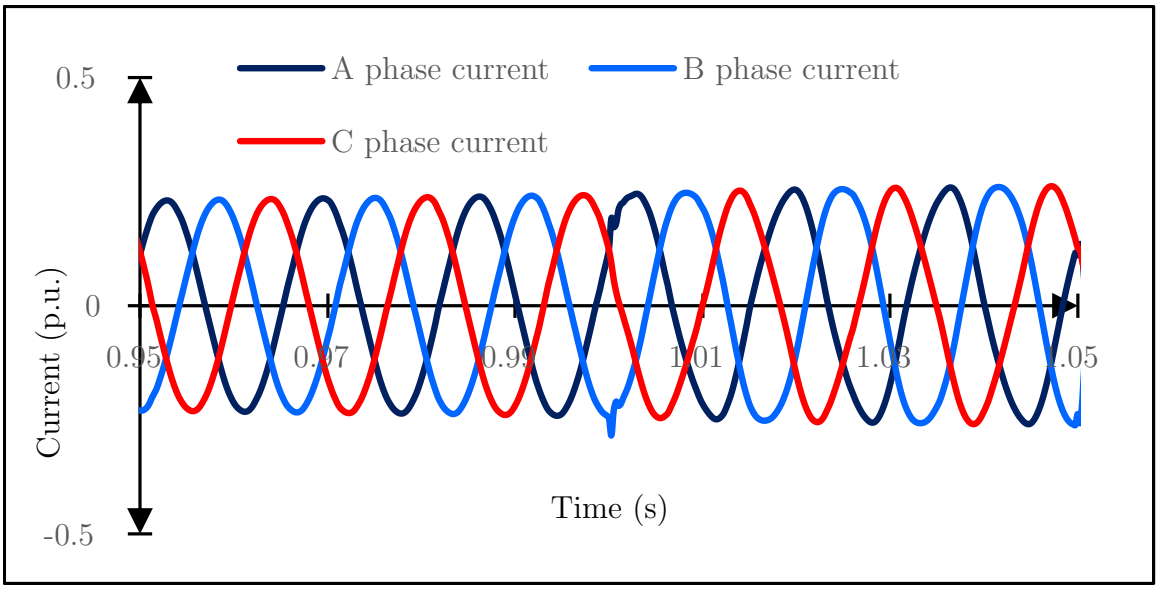

Figure 2.24: Current waveform from the PV inverter side during fault F-1

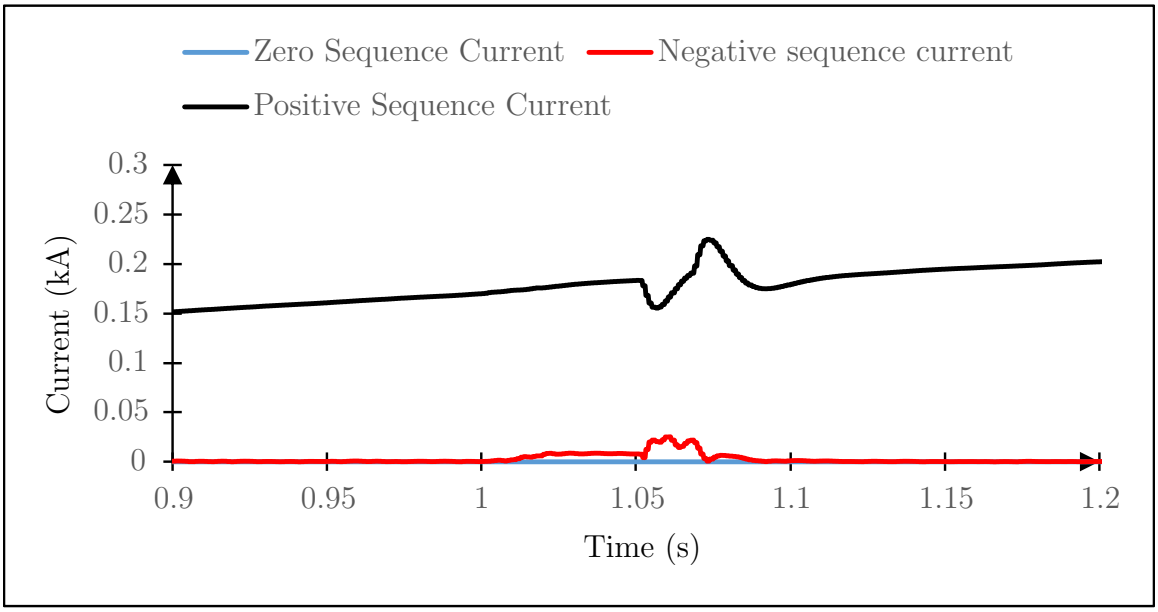

Figure 2.25: Sequence currents by PV inverter during fault F-1

2.4 Microgrid Protection: Current Practices and their Issues

Microgrids are part of the power system, which is constantly under fault for various reasons explained in the chapter-1. The role of the protection system is to identify, locate and isolate the faulty segment to keep the balance of the system operational. In the previous section, we found that the magnitude of the fault current remains nearly equal to the pref-fault value, so detecting a fault and differentiating it from no-fault is challenging for microgrids with inverter-based resources.

The interaction of power system protection in the presence of inverter-based resources in microgrids is one of the foundation pillars this thesis outlines. This section discusses the different types of protection methods and their issues when protecting a microgrid with inverter-based resources.

2.4.1 Types of Microgrid Protection Schemes

Currently, the microgrids are protected by traditional methods such as fuses, overcurrent and earth fault relays, directional relays, differential relays, and distance relays [27]. These protection methods have been designed for the power system network dominated by synchronous generators. Due to the lack of a microgrid protection relay, utilities or electricity operators have to rely on traditional protection relays. Some of the commonly used protection practices in power systems are :

1. *Overcurrent and earth fault protection relay (50,51,50N,51N)*: Overcurrent and earth fault protection relays work on the principle of rise in the current. When the current sensed by the relays increases above a threshold value, the relay declares the fault. [28–31]

2. *Directional protection relay (67,67N)*: This protection scheme utilizes two components, magnitude of current as well its direction of the current. The relay

realizes the fault when the magnitude of the current is above the threshold and the direction of the current is either forward or reverse [28–31].

3. *Differential protection relay[87)*: Differential protection utilizes the current input from the ends of a feeder and checks the current difference; if it is above the set point, the relay issues a trip signal. Two types of differential protection relays are commercially available, one which uses dual-slope characteristics and another is an alpha plane differential relay [28–31].

4. *Distance protection relay(21)*: These relays calculate the fault loop impedance using voltage and current. This impedance is compared with the impedance of the line under protection. Based on calculated magnitude and angle, the relay decides the fault and no-fault [28–31].

5. Under voltage protection: This method requires voltage input to the relay. It declares the abnormality in the system when the voltage drops below the set point.

2.4.2 Challenges in Microgrid Protection

The protection techniques described in section 2.4.1 pose many challenges with inverter-based resources in a microgrid.

Overcurrent and earth fault relays depend highly on the large magnitude of fault current. This technique is well-established and widely used in distribution networks and works perfectly where the grid supplies the current. However, this case is invalid with the microgrid operating in islanded mode [32, 33]. It can be seen from Fig. 2.24 the current supplied by the PV-inverter is almost the same as the pre-fault value. The energy resources in a microgrid are present in various locations; some are intermittent, such as solar and wind. Their participation with microgrids is highly volatile. As a result, the magnitude of the fault current is not fixed and is dynamic. Therefore, providing a fixed overcurrent protection setting for any microgrid topology becomes tedious [34]. The signature of fault current is ambiguous with inverter-based

resources since it is dictated by its control algorithm [35–39]. Several grid codes are defined as a guide for the interconnection of distributed energy resources with the grid and their functionalities under different situations; one is IEEE-1547:2018 [40]. Some grid codes and standards have introduced the functionality of requirement to remain interconnected with the power grid during an unbalanced event for inverter interfaced resources. This grid code defines the voltage support by inverter-interfaced resources by injecting positive sequence reactive power current [40, 41]. The consequence of these grid codes results in the change of power factor during a fault by injecting reactive power with fixed or reduced active power. Therefore, during a fault, the angle between voltage and current can change in a wide variety, keeping constant fault current. So, in general, the fault current of inverter-based resources for the different manufacturers and different voltage conditions (at the interface point) is different. At the same time, the response of a synchronous generator is independent of its make.

Since various sources are involved in a microgrid, the direction of current flow during a fault is not unidirectional. Unlike the traditional, radial power system results in a unidirectional flow of current during a fault. To mitigate this problem, directional relays are employed in the microgrid. Commercially available relays use positive sequence, negative sequence, or sequence voltage-polarized directional relays [42]. In [42], the decision for directional forward or reverse is based on apparent impedance calculation, and the sign of the cosine component determines the forward or reverse direction. The quantity for computing the torque equation is positive, negative, or zero, depending on phase or ground faults. The negative sequence directional element faces a challenge due to a very low negative sequence fault current delivered by inverter-based resource [43]. In the case of a positive sequence directional element, the voltage and current magnitude are enough to produce the desired torque. Still, the cosine angle term, which determines the direction, indicates a false value due to the presence of inverter-based resources [43]. Therefore, protection with the conventional directional poses security issues in the presence of inverter-based resources.

Another type of protection scheme that is used for the protection of microgrids is distance protection. When a type-III wind turbine generator feeds a microgrid during a three-phase fault, the short circuit current drops after two cycles because the wind turbine generator loses the excitation due to the fault. Consequently, the relay detects the fault in 2 cycles but cannot confirm it as a fault because of a sudden drop in current [44]. A similar incident of maloperation of distance relay is observed with a type-IV wind turbine generator, where the relay operates successfully for a three-phase fault but fails to operate for a three-phase with resistance [45]. In the case of distance relays with quadrilateral characteristics, the reactance element underreaches for internal resistive faults with negative sequence current polarization and overreaches with zero sequence current polarization. In the case of three-phase faults, a significant shift in angle between polarizing and operating quantity jeopardizes the security of the protection relay [46].

Another protection technique uses an undervoltage relay to identify a fault at the coupling point. If voltage is reduced by 0.88 pu at Point of Common Coupling (PCC), it declares fault in the microgrid. However, such schemes fail to differentiate between a voltage drop due to dynamic load change or due to a fault [47].

The voltage-restrained over-current protection technique is used for the protection of the microgrid [48]. This technique provides sensitivity to the overcurrent relay by monitoring the voltage of the relay and is used as a backup to overcurrent relays in generator protection [49]. This scheme suffers from the issue of undervoltage due to load generation imbalance. It is hard to differentiate a high-resistance fault since the change in voltage is minimal for a high-resistance fault, and the current magnitude is very low.

In adaptive relaying, the relay setting is adopted based on the change in network topologies and configurations in this protection method. This technique requires the status of disconnect or circuit breakers to identify the network's physical state [50]. Such techniques [51] are complex to implement and require fast transmission of the status of the network. This kind of scheme is affected by the sudden change in load or generation where the network re-configures quickly. Also, these protection

scheme does not respond well during load-shedding. In [52], adaptive coordination techniques using IEC 61850 communication protocols are explained, but they fail to respond during transient network conditions.

A different strategy for microgrid protection is based on multiple overcurrent settings with different scenarios. A feature in a numerical relay that allows the user to provide different settings based on the different operations. This method uses multiple setting groups for different microgrid combinations based on operation, resources, and loads [53, 54]. Such a protection method is suitable for small or limited-capacity microgrids where limited permutation and combination are possible. For large networks with dynamic loading, such schemes are not appropriate.

Another strategy for microgrid protection involves a data mining model where a neural network-based mining model is trained for different types of faults [55]. A model's training is limited to a specific architecture, types of resources, and a specific voltage. Also, the fault current signature of a particular inverter with different control strategies is different. Further, these models cannot differentiate between fault and transient events such as transformer energization, motor starting, and capacitor switching.

Strategy using superimposed current phasors from two ends of a feeder and using trigonometric function is proposed in the article [56]. This scheme has suffered from issues related to resistive faults and open circuit faults. Such schemes are not suitable for microgrid protection from all types of faults.

2.5 Summary

This chapter sets the base for the remainder of the thesis. First, different types of inverter and their basic functional module was introduced. The basic control architecture of grid following and grid forming inverter was discussed. Second, the fault response of various inverters in a medium-voltage microgrid was described. Also, the sequence current delivered by the inverter during a fault was shown. Thirdly, the

commonly used protection techniques in distribution systems are discussed. Finally, the challenges faced in protecting microgrids with conventional protection schemes were discussed. The research on microgrid protection has two approaches. One involves the modification of a traditional algorithm of relay; another is developing a microgrid protection relay. As such, in terms of the protection system, this thesis focuses on developing a new protection scheme for microgrids.

Chapter 3

Proposed Protection Scheme for Microgrids: Centralized Approach

This chapter is based on the following publication: **J.Sharma,** T.S. Sidhu "A New Protection Scheme for Feeders of Microgrids with Inverter-Based Resources" in *Journal of Electric Power Systems Research*, 2023

3.1 Introduction

As outlined in Chapter 2, traditional and non-traditional protection methods are adversely affected by the presence of inverter-based resources in a microgrid. This chapter aims to provide a solution for the protection of microgrids, which is the basis of this thesis. In this chapter, a novel centralized protection technique for microgrids is explained in detail. This work aims to design a simple technique that requires a modest amount of data. The algorithm was developed using sampled values as per IEC 61850-9-2 in the real-time digital simulator.

This chapter is organized as follows: First, section 3.2 explains the Modelling of the centralized protection method. Section 3.3 explains the protection technique. Section 3.4 explains the hardware setup used for implementing the protection technique. Section 3.4 describes the software for implementing the protection technique and the algorithm for protection, and section 3.5 concludes this chapter.

3.2 Centralized Protection Architecture: Overview

There is no formal definition of a centralized protection method by any standards. The IEEE-PSRC working group committee K15 defines it as a system of high-performing computing capable of providing protection, control, monitoring, communication and asset management [57]. The basic architecture of a centralized protection scheme is shown in Fig. 3.1

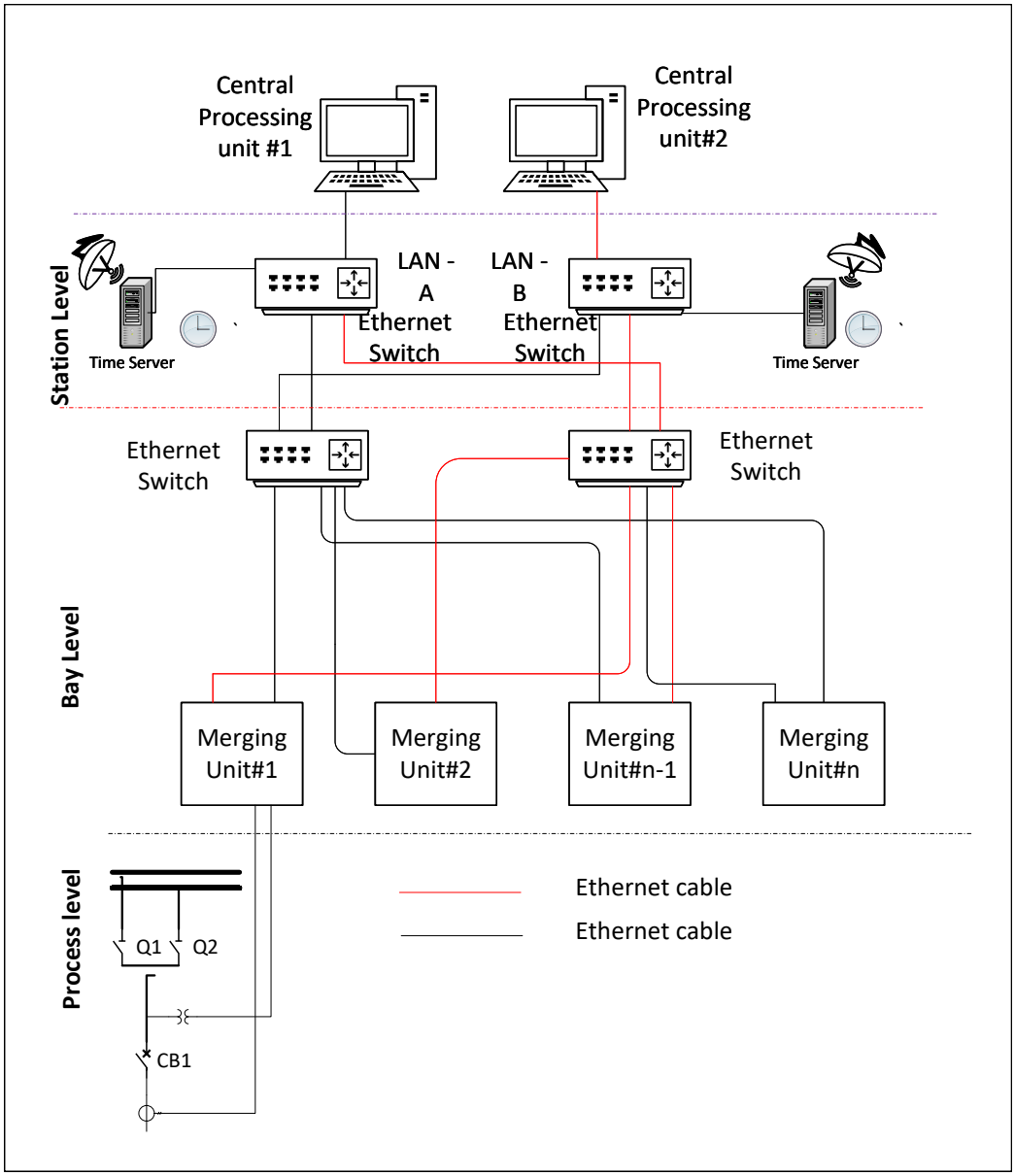

Figure 3.1: Centralized protection architecture

The key technical enabler for centralized protection and control is IEC 61850 standard [58]. The centralized protection architecture is divided into three levels, i.e. process, bay, and station. The perimeter of the process level covers the information from direct measuring instruments such as the current transformer, potential transformer and other equipment statuses. The data from the process level is transferred to the merging unit via copper cables or fibre optic cables. At the bay level, the merging unit is the interface between the central processing unit. The Merging unit also hosts a feeder's digital inputs and outputs; for example, it can communicate the digital status of isolators, breakers, or earth switches with the network and receive the trip or open commands from the central processing unit.

Depending on the required reliability and availability of the communication network [59], a suitable network architecture for centralized protection can be chosen. Two commonly used network redundancy protocols are High-availability Seamless Redundancy (HSR) Parallel-Redundancy Protocol (PRP). The redundancy shown in Fig. 3.1 is a PRP. The central processing unit receives the data at the station level. The data available to the central processing unit is synchronized substation time synchronizing servers; the most commonly used time synchronization protocol is simple Network Time Protocol (SNTP). SNTP servers are kept at the station level to avoid latency. The ideal solution for time synchronization is a GPS satellite clock, which provides an accuracy of 1μs [60].

The Central Processing Unit (CPU) is a computer where the protection and control algorithm is developed. The CPU has multiple protection functionalities depending on the requirement of the network or equipment under protection. The significant advantages of centralized protection architecture are reduced management and maintenance of the devices. Since a large substation or plant will have many IEDs, each IED will have its configuration, setting files and firmware version. On the other hand, Centralized protection architecture will have a limited number of devices, fewer settings, and limited device maintenance. The technologies that support centralized protection are non-invasive current sensors, a digital communication interface for low-power instrument transformers, merging units, advancement in communication

technology, and synchronization technology.

3.3 The Technique

The inputs for any protection unit are currents and voltages from the power system network. These quantities are the source of information for the microprocessor inside the protection unit to process the algorithm. The voltages and currents are sampled, and fundamental phasors of voltages and currents are estimated using the Discrete Fourier Transform (DFT) based on the principled described in [61]. The phasors are synchronized to a common time reference. The fundamental frequency phasors of voltages and currents of each phase are utilized to compute the positive sequence phasors of voltages and currents. To understand the protection technique, consider a two-node microgrid with inverter-based resources connected at both ends, as shown in Fig. 3.2. The direction of the current measurement is shown with the arrow. The fundamental frequency positive sequence voltage and current phasors estimated at the bus A and bus B are $V_{A1}\angle\theta_{A1}$, $I_{A1}\angle\alpha_{A1}$, $V_{B1}\angle\theta_{B1}$ and $I_{B1}\angle\alpha_{B1}$ respectively. The

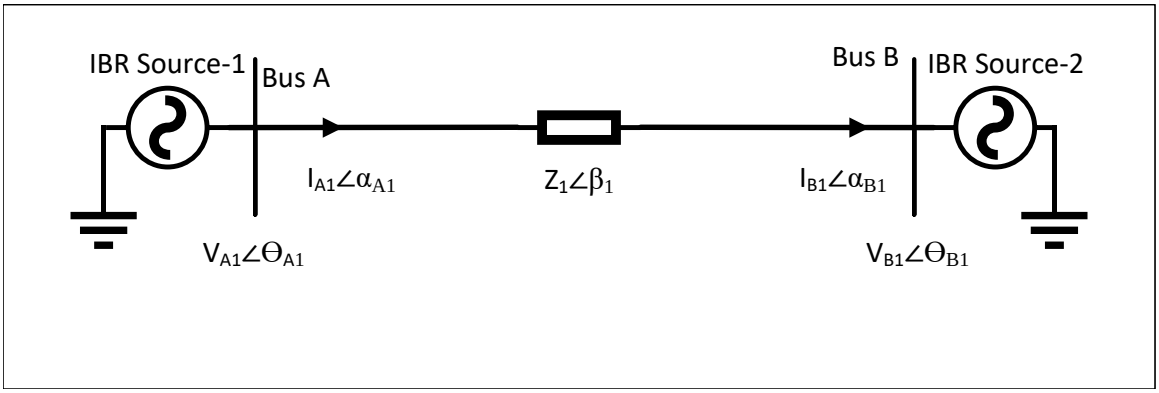

Figure 3.2: Two node microgrid with inverter-based resources on each end

voltage at bus A can be written as

$$V_{A1}\angle\theta_{A1} = I_{A1}\angle\alpha_{A1}.Z_1\angle\beta_1 + V_{B1}\angle\theta_{B1}. \tag{3.1}$$

$$Z_1\angle\beta_1 = \frac{V_{A1}\angle\theta_{A1} - V_{B1}\angle\theta_{B1}}{I_{A1}\angle\alpha_{A1}}. \tag{3.2}$$

$Z_1\angle\beta_1$ is the positive sequence impedance of the feeder as estimated from Bus A using positive sequence voltage and current phasors at Bus A and Bus B.

Similarly, the voltage at Bus B will be,

$$V_{B1}\angle\theta_{B1} = (-I_{B1}\angle\alpha_{B1}).Z_1\angle\beta_1 + V_{A1}\angle\theta_{A1}. \tag{3.3}$$

$$-Z_1\angle\beta_1 = \frac{V_{B1}\angle\theta_{B1} - V_{A1}\angle\theta_{A1}}{I_{B1}\angle\alpha_{B1}}. \tag{3.4}$$

From (3.2) and (3.4) it can be written as

$$Z_1\angle\beta_1 + (-Z_1\angle\beta_1) = 0 \tag{3.5}$$

-$Z_1\angle\beta_1$ is the positive sequence impedance of the feeder as estimated from Bus B using positive sequence voltage and current phasors at Bus B and Bus A. Under no-fault condition and when the phasors are synchronized then $I_{A1}\angle\alpha_{A1}$ is equal to $I_{B1}\angle\alpha_{B1}$. It can be observed from (3.2) and (3.4) that when there is no fault, the vector sum of the estimated feeder impedances $Z_1\angle\beta_1$ and -$Z_1\angle\beta_1$ is zero. This vector summation of impedances is called 'Discrepant Impedance'(ΔZ).

3.3.1 Assumptions in Protection Technique

While implementing the proposed protection technique, the following assumptions are made:

1. Voltage and current samples are available to the centralized protection unit from the ends of the feeders.
2. Voltage and current samples are time-stamped.
3. The network used for communication has sufficient bandwidth.

3.3.2 Protection Technique Characteristics and Operating Criteria

Theoretically, it is proven in section 3.3 that the discrepant impedances are zero during a no-fault condition. However, in practical situations, the errors encountered during measurements of currents and voltages need to be considered. The maximum error of Current Transformer (CT) used for the protection application as per IEEE std C57.13 is +/- 1%, and for potential transformer, it is +/- 1.2% [62] Therefore, it is suggested that the minimum setting for the protection technique shall be

$$\Delta Z \gg 0.05 \mid Z_1 \mid . \tag{3.6}$$

. The protection technique will declare a fault if the discrepant impedance shown in 3.6 is greater than 5% of the feeder impedance. Fig. 3.3 represents the protection technique's operating characteristics. The circle near the origin is a no-fault region. Ideally, it should be zero; instead of a circle, it would be a point at the origin. The region outside the circle is a fault region. The protection trip logic is shown in Fig. 3.4. The discrepant impedance is computed continuously in real-time. To ensure the security of the protection technique, a counter is added that increments by one whenever the computed discrepant impedance is greater than the threshold setting. The counter decrements by one whenever the discrepant impedance is less than the threshold setting. This adds security to the protection during transient conditions. Whenever the counter records the five consecutive values of discrepant impedance exceed the set value, the central processing unit issues a trip command to the breaker. So, the time taken by the processing unit to decide on fault and no-fault is 5 x(1/ Sampling time).

3.3.3 Modeling of the Centralized Protection Technique

In this section, the modelling of the centralized protection technique is discussed. The protection scheme was modelled on the RSCAD environment. Modelling of the protection technique involves the following steps:

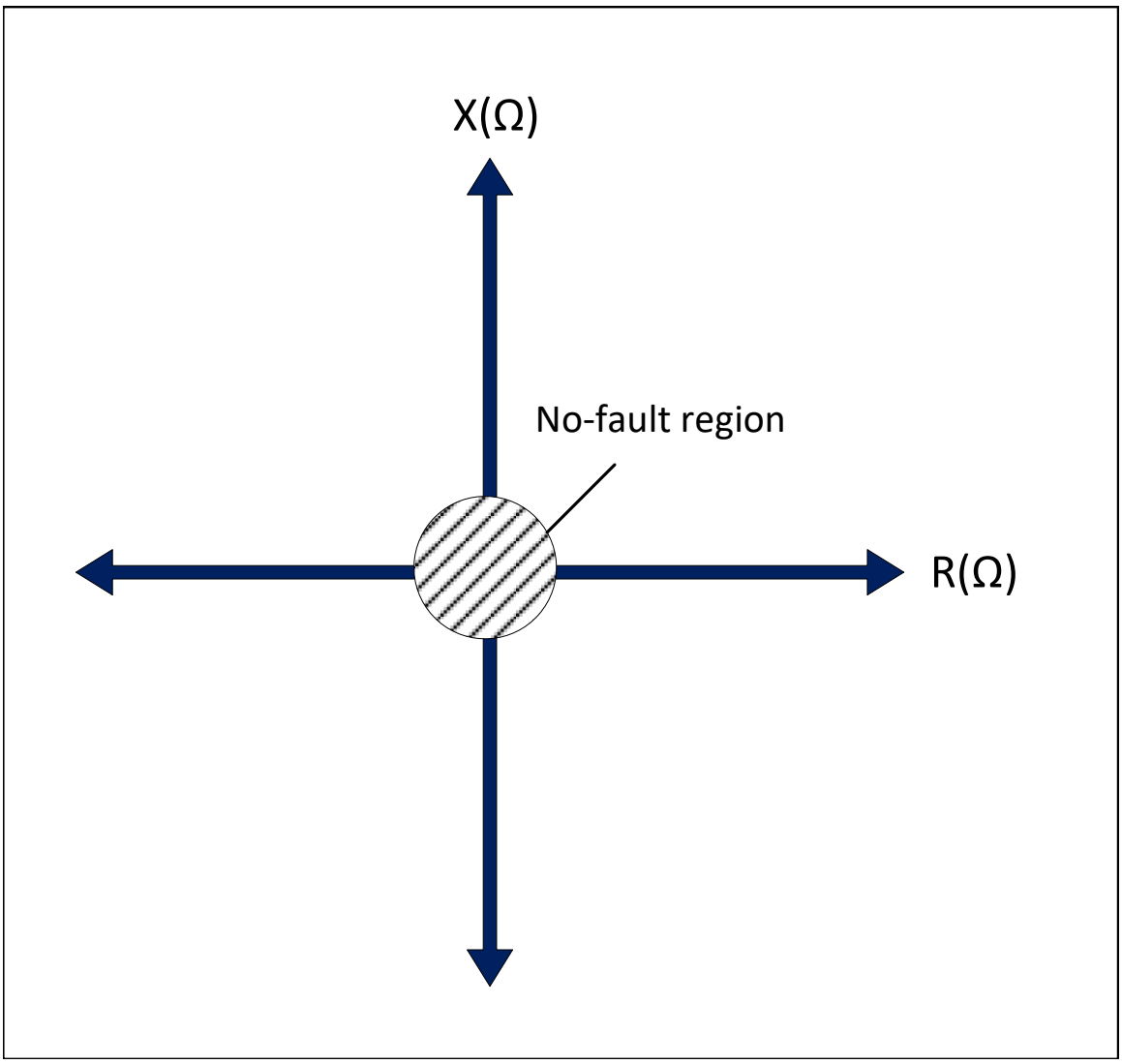

Figure 3.3: Operating characteristics of the protection technique

1. Modeling of Low Power Instrument Transformer (LPIT).

2. Downsampling of the received signal

3. Extraction of fundamental voltage and current phasor

4. Calculation of positive sequence voltage and currents

5. Computation of discrepant impedance

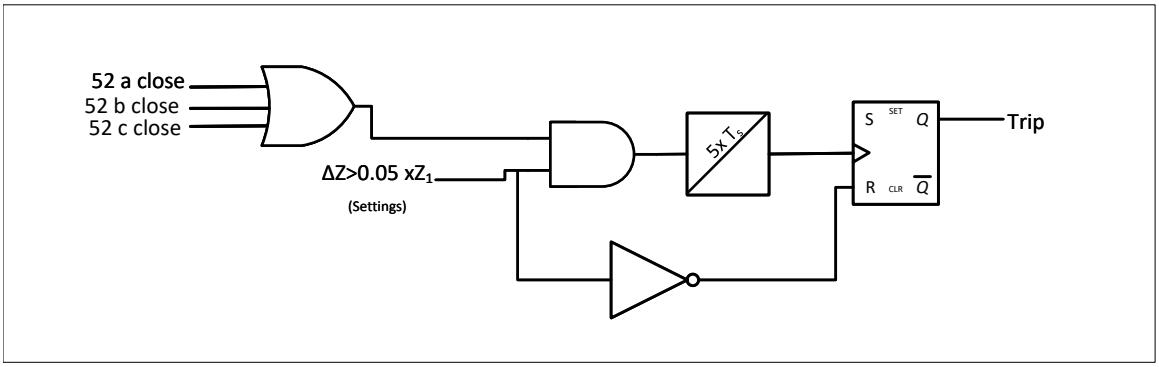

Figure 3.4: The protection logic

Modeling of Low Power Instrument Transformer (LPIT)

The input quantities, such as three-phase voltages and currents from one of the feeders, are interfaced with low-potential instrument transformers according to IEC 61869-9 [63].

An illustrative block diagram of a low-power instrument transformer is shown in Fig.3.5. It shows the three-phase currents and voltages from the secondary current are interfaced at the physical boundary of this device. The first interface is the instrument transformer's high voltage primary and its conversion, and the second is the merging unit. The converter, the interface between primary and secondary, is an integral part of the LPIT. Another interface to LPIT is a synchronizing signal. Fig. 3.6 represents the LPIT model.

According to IEC 61869-9, the sampled valued signal publishes the SV stream at 80 samples per power system frequency cycle. Therefore, for a 60 Hz system, the sampling rate shall be 4800 Hz. In Fig. 3.6, a) represents the output mode and b) represents the input mode. The output mode publishes the sampled stream of 8 signals, i.e. three phase currents and a neutral current, three-phase voltages and a neutral voltage. A quality bitmap also accompanies each channel. Simulation Flag (simulation bit) each Sampled Value (SV) stream is settable using the "Sim Flag" input in the component. The input channel configurations of the component (such as data type, data format, units, channel scaling etc.) should match those of the inbound SV stream for proper subscription. The input subscribes to the sampled signals

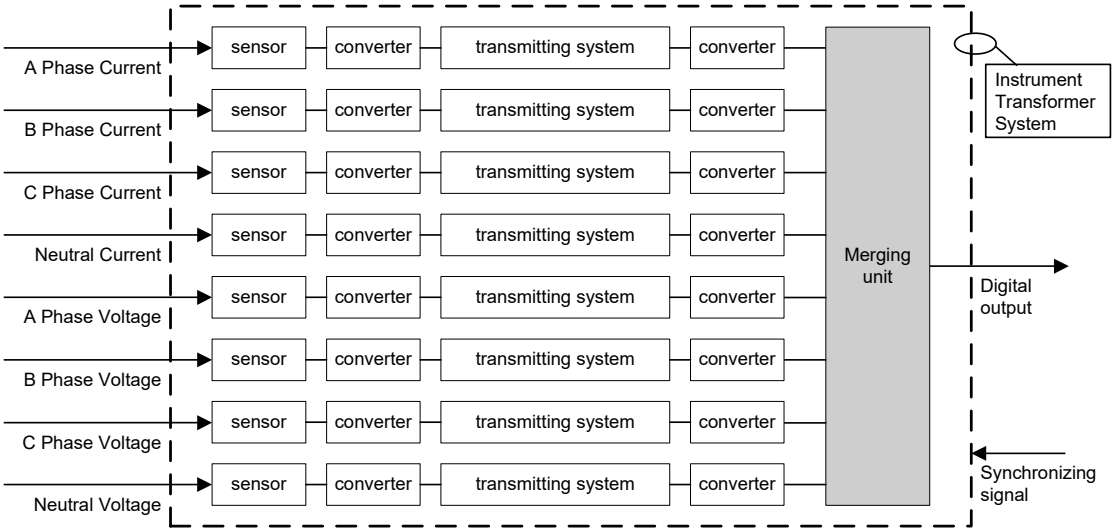

Figure 3.5: Block diagram of low potential instrument transformer [63]

published with the sampling rate set by the output mode. A sampled value(SV) communication link between subscriber and publisher is as per IEC 61850 process bus standards.

Downsampling of the Received Signal

The digital protection technique requires analog signals to be sampled at a specific rate. In our case, LPIT sends a sampled signal stream at 4.8 kHz. This sampled data could be stored in a cyclic buffer to be stored to a permanent record if a relay operation occurs. Because our protection cycle is generally set to 16 times per cycle, we will again down-sample at a rate of 960 kHz or twelve times per cycle. The sampled signals are passed through a moving average filter. The moving average filter acts as a digital low-pass filter to the sampled signals.

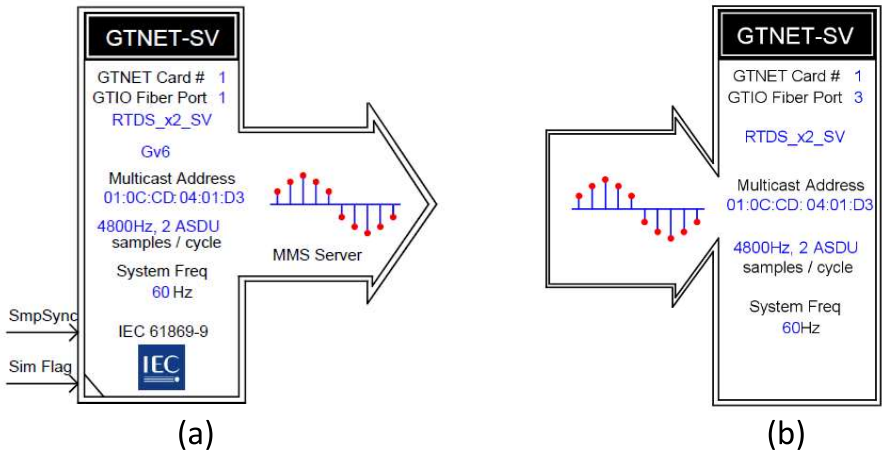

Figure 3.6: LPIT model in RSCAD

[64]

Extraction of Fundamental Voltage and Current Phasors

After downsampling the currents and voltage samples, the sampled signals are processed to extract fundamental phasors of currents and voltages. A full-cycle discrete Fourier transform is used for the extraction of the magnitude and phase of the input signal. A phase input signal is provided to DFT from a PLL, whose inputs are the bus voltages or line currents corresponding to the input signal. This phase input signal's period defines the fundamental frequency used to compute the DFT. This signal is a phase reference to the DFTfunction. For DFT to function, more than two samples per cycle of the frequency signal to be extracted are required. For example, the number of samples required to extract a fundamental frequency signal is three. To extract the 3rd harmonic signal, the number of samples shall be seven. The output of DFT is updated every time a new sample is taken. DFT's response is affected by the DC decaying component in the input signal [65]. Therefore, a DC removal block is

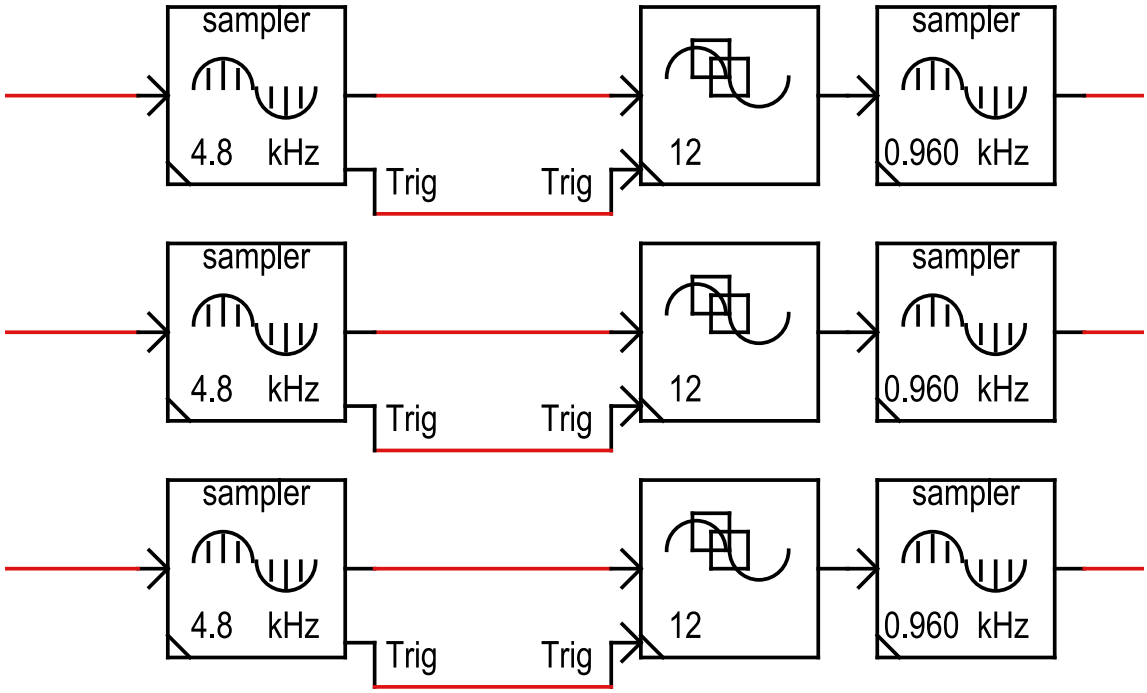

Figure 3.7: Down sampling and low pass filtering

applied before the samples are delivered to the DFT block to extract the fundamental frequency phasor of voltages and currents.

Calculation of Positive Sequence Voltage and Current

The synchronized phases A, B and C phasors are obtained from the DFT block. The positive, negative and zero sequence voltages and currents are computed from these synchronized phasors using symmetrical component methods [66]. The symmetrical component matrix can be written as

$$\begin{bmatrix} V_{a0} \\ V_{b0} \\ V_{c0} \end{bmatrix} = \begin{bmatrix} 1 & 1 & 1 \\ 1 & a & a^2 \\ 1 & a^2 & a \end{bmatrix} \begin{bmatrix} V_a \\ V_b \\ V_c \end{bmatrix} \tag{3.7}$$

Where V_{a0},V_{a1}, and V_{a2} are the zero, positive and negative sequence voltages of the A phase. The sequence voltages of other phases can be computed by providing a phase shift of 120°. The sequence currents are obtained as

$$\begin{bmatrix} I_{a0} \\ I_{b0} \\ I_{c0} \end{bmatrix} = \begin{bmatrix} 1 & 1 & 1 \\ 1 & a & a^2 \\ 1 & a^2 & a \end{bmatrix} \begin{bmatrix} I_a \\ I_b \\ I_c \end{bmatrix} \tag{3.8}$$

Calculation of Discrepant Impedance

After all the steps defined in subsection 3.3.2, the discrepant impedance for each sample is computed following the protection technique explained in section 3.3. Fig. 3.8 represents a complete flow diagram of the modelling process.

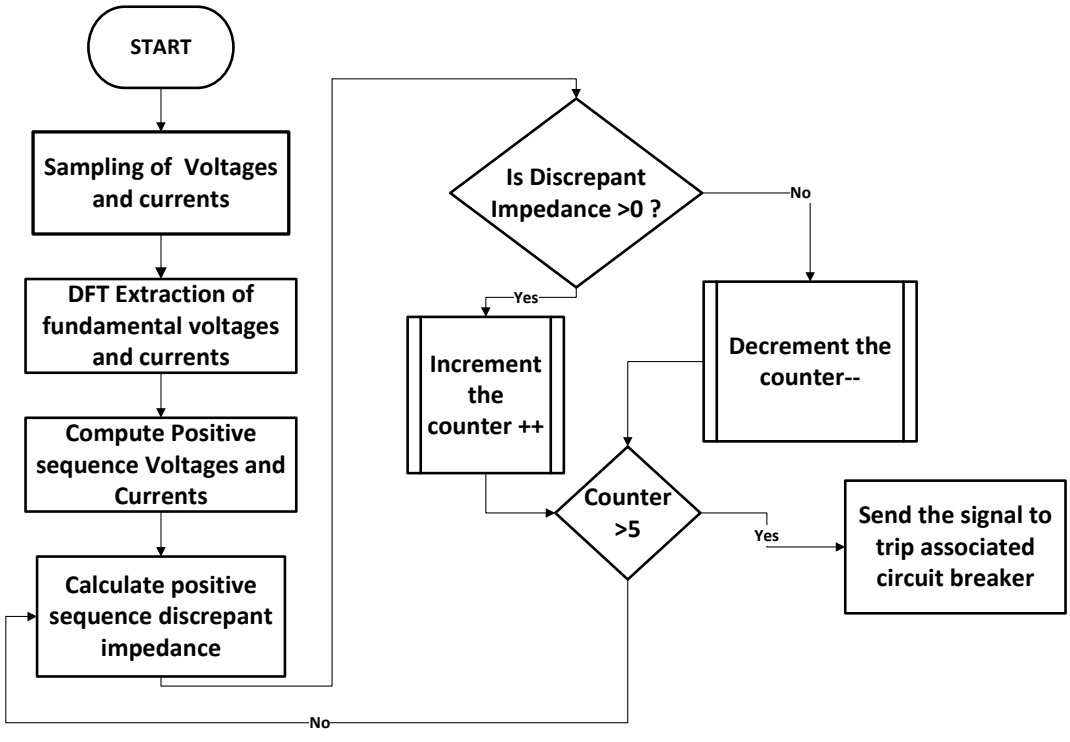

Figure 3.8: Flowchart for the modelling of the protection technique.

3.4 Hardware Setup for Implementing The Centralized Protection

The hardware used for the proposed protection system consists of two Gigabit-Transreceiver Network (GTNET) cards, one Gigabit-Transreceiver Network version 2 (GTNETx2) card,Gigabit-Processor Card (GPC) processor cards, a Gigabit Work Station Interface (GTWIF) card, an Ethernet switch, and Fiber optic and CAT-6 cables. All these cards are housed in a Real-time digital simulator rack.

3.4.1 GTNET and GTNETx2 Cards

The GTNET and GTNETx2 network cards enable real-time data exchange between the RTDS and external systems. GTNET and GTNETx2 cards are used to interface different network protocols. In this thesis, the IEC-61850-9-2 sampled values protocol is considered for transferring the voltages and current samples. A GTNETx2is a new version of GTNET cards. A GTNET card is a protocol converter that accepts data from the switch via CAT-6 cable and sends the information to GPC cards. GTNET and GPC cards are interfaced through fibre optic cables, and GTNETto an Ethernet switch is via CAT 6 cables. Also, a GTNET card is used for sending information from the GPC card to the Ethernet switch via Local Area Network (LAN) cable. GTNET and GTNETx2 cards are configured to publish and subscribe sampled values of voltages and currents. The GTNET card sends and receives the data at 80 samples/cycle rate. GTNET card uses the destination IP address of SV packets to identify the intended SV stream. GTNET card filters out other packets and is not processed.

3.4.2 GPC cards

GPC cards are processor cards used to simulate the power system, and control system components modelled within RTDS. The RTDS rack used for this project has five

GPC cards. Each GPCcard has two processors running at 1 GHz. GPC card includes fiber ports for connecting various I/O cards such as GTNET, GTDI(digital input), GTAO(Analog input), GTAI(analog input) and GTDO(digital output). Each GPC card is assigned a power system or control system component up to 66 nodes. 1 processor on a GPCcard within an RTDS rack is commonly assigned to the power system network (i.e. computation of node voltages, passive branches, etc.).GPCprocessors are allocated to handle the different power system components (e.g., machines, transmission lines, transformers, etc.) that comprise the simulated power system model.

Control system components Generally, one processor on a GPC card inside a rack handles the control system components modelled in the RTDS. Simulation situations with many controllers may dedicate more resources to the control components than a single GPC processor. Data is also sent between control system components and GT I/O cards linked to the GPC's fiber ports.

3.4.3 GTWIF cards

Each RTDS rack consists of one GTWIF card. The GTWIF card provides communication between RTDS rack and the workstation computer that is running RSCAD software. This communication is over a CAT-6 cable. The RSCAD/RunTime software connects with the GTWIF card's real-time operating system to transmit and receive messages related to plot updates and user-initiated events (for example, changing a set point via a Slider, Switch, or other similar RunTime component). The GTWIF card is also utilized for data connection with the computer workstation to load new simulation cases and start and terminate simulations. The GTWIFcoordinates data communication between processors over the rack's backplane. GTWIF can be connected directly to the HMI workstation or through the Ethernet switch.

3.4.4 The Hardware Setup

Fig. 3.9 shows the hardware used for implementing the protection technique. GTWIF, GPC and GTNET(subscriber) cards are housed in a RTDS panel. The ethernet switch

Figure 3.9: Hardware setup for modelling of centralized protection-Subscriber

for interfacing between the subscriber, publisher and GPC card is also placed inside the RTDS panel.

The publisher's GTNET card is placed inside the NOVACOR. NOVACOR is a generation-2 real-time digital simulator. The NOVACOR sends the sampled value data through an ethernet switch. The publisher hardware setup is represented in Fig. 3.10. The protection algorithm is developed on the GPCprocessor card of RTDS, and the power system mode is developed inside the NOVACOR.

Fig. 3.11 represents the real-time test platform for developing and testing the proposed protection scheme. All RTDS cards are shown outside the rack to explain and depict communication relationships. However, all the cards are in the RTDSrack. RTDS rack contains five giga-processor cards(GPC), workstation interface cards (GTWIF) and gigabit transceiver network interface cards (GTNET-SV).

Figure 3.10: Hardware setup for modelling of centralized protection-Publisher

A workstation interface card(GTWIF) is used for communication between RTDS and work station running the RSCAD software. GTWIF and the workstation communicate over an ethernet-based CAT-6 local area network (LAN) cable. RSCAD software communicates with GTWIF in real-time to send or receive messages associated with plots and updates. GTWIFalso coordinates the communication between processors within the rack, which is connected through fiber optic cables

Two gigabit transceiver network interface cards are GTNET-SV-1 and GTNET-SV-2. GTNET-SV-1 publishes the sampled values of currents and voltages according to IEC 61869-9 from one end of the feeder and GTNET-SV- 2 publishes sampled values of voltages and currents from another end. GTNET-SV-1 and GTNET-SV-2 are connected to the GPC processor via fiber optic cables and to an ethernet switch over CAT-6 LAN cable. The sampled values of voltages and currents from the ends of the feeder are transmitted to the central processing unit through an ethernet switch over CAT-6 LAN cable. The protection algorithm, developed in the central processing

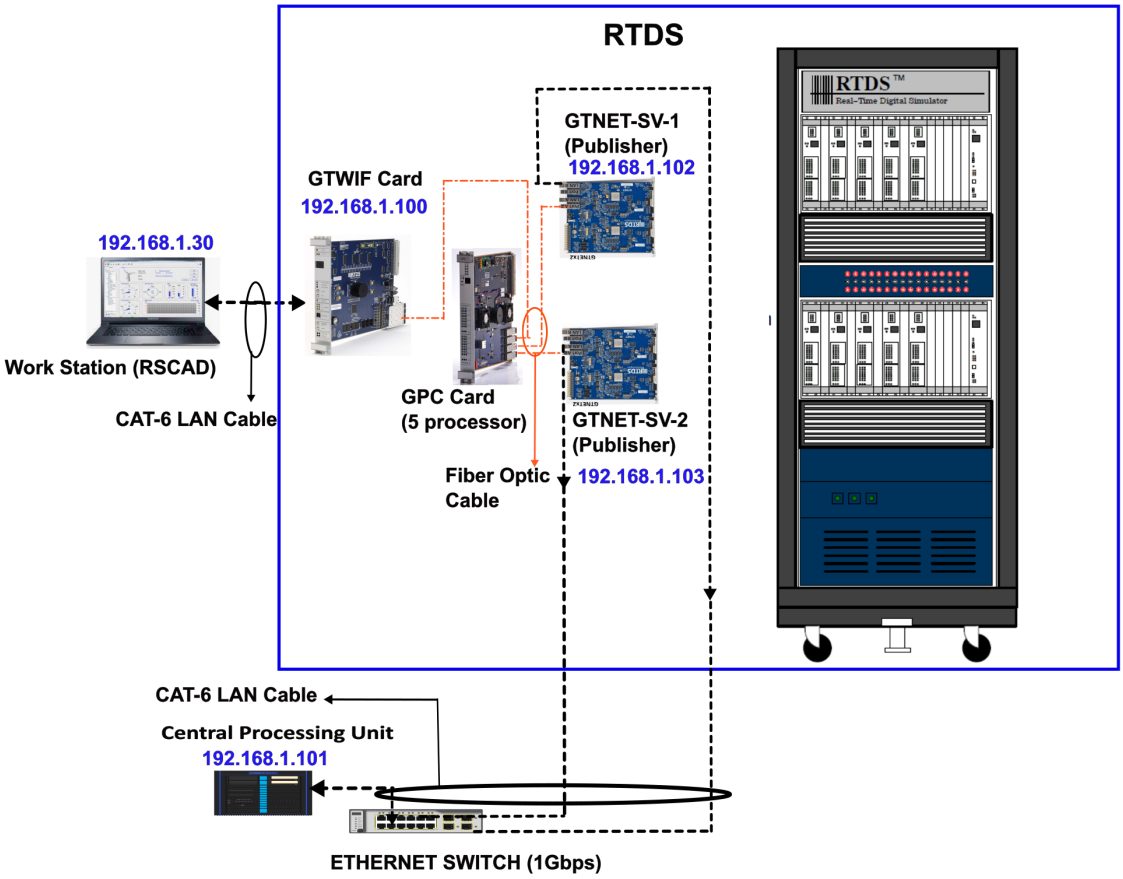

Figure 3.11: A simplified overall network architecture of the hardware setup

unit, continuously computes the discrepant impedances.

3.5 Summary

This chapter explains the design and implementation of the centralized discrepant impedance-based protection technique using IEC-61869-9-2 sampled values. The Mathematical analysis of 'discrepant voltages' is explained with two node microgrid for internal faults. The protection scheme does not require copper wires to interface current and voltage transformers with µCPU, instead, it uses digital instrument transformers. The protection technique uses positive sequence currents and voltages in a network dominant with inverter-based resources. The hardware setup includes publisher and subscriber of sampled values of voltages and currents, processor GPC and NOVACOR. The protection technique is simpler and easy to implement and also identifies the fault segment of the network. This technique can be used for any power system network independent of the capacity, voltage level, and type of resources.

Chapter 4

Performance Evaluation of the Protection Technique on High Voltage -IEEE-9 Bus System

This chapter is based on the following publication: **J. Sharma**, T. Sidhu, "A new protection scheme for feeders of microgrids with inverter-based resources," *Journal of Electric Power Systems Research, Elsevier, Vol. 224, 2023*

4.1 Introduction

The challenges to the protection of microgrids are reported in Chapter 2. A digital protection scheme using sampled values is proposed in Chapter 3. This chapter describes implementing and testing a sampled value-based protection system for protecting high- and medium-voltage microgrids [67]. The protection system includes the identification of a faulted segment of the microgrid. The performance of the protection system was tested in the laboratory. Some test results are included in this chapter.

4.2 IEEE-9 Bus System with Inverter-Interfaced Resources

A benchmark IEEE-9 bus system with inverter interfaced resources, as shown in Fig. 4.1, was used to evaluate the proposed protection scheme on high voltage system

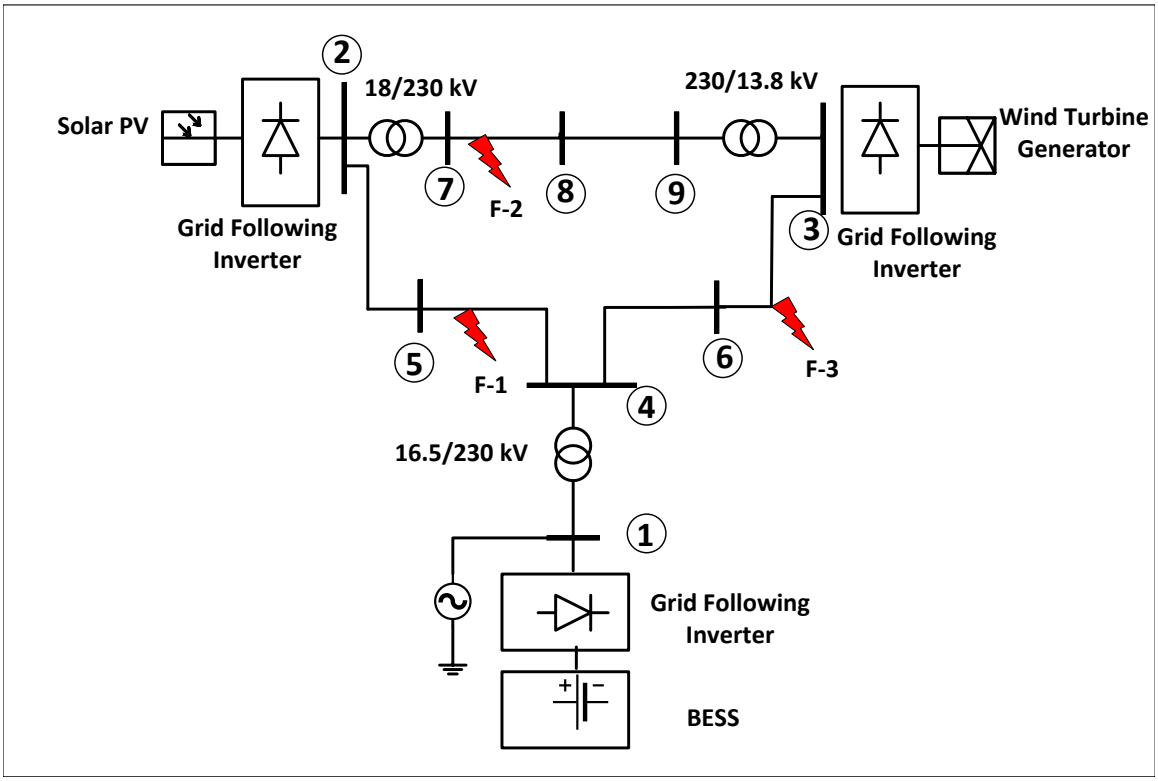

Figure 4.1: IEEE-9 bus system with grid forming and grid following inverters

Table 4.1: IEEE-9 bus system load and generation details.

Bus No.	Source/Load	Capacity(MVA)	Voltage(kV)	Real Power(MW)	Reactive Power(MVAr)
1	IBR	200	16.5	66.9	161.1
2	IBR	200	18.0	163.6	5
3	IBR	200	13.8	89.9	-5
5	Load	-	230	125	5
6	Load	-	230	90	3
8	Load	-	230	100	3

In this study, the modified model from reference [68] is our experiment's foundation. Detailed load data, generation data, and line parameters can be found in

Table 4.1. Fig.4.1 illustrates the microgrid's network structure, which consists of three inverters, feeders, and loads. Among these inverters, two are functioning as grid-forming inverters, while one operates as a grid-following inverter. Each of these inverters boasts a 200 MVA rating. Solar and wind energy resources are harnessed through the grid-following inverters, while a battery source is linked through the grid-forming inverter. The loads connected to the buses are characterized as constant impedance loads, and the transmission lines are represented using a pi model. The proposed protection philosophy has undergone rigorous validation across various scenarios, encompassing fault types, fault locations, and the diversity of inverters within the network, whether in grid-connected or islanded operation modes. This comprehensive validation process ensures the robustness and versatility of the protection strategy under diverse conditions and configurations, thus bolstering its applicability and reliability in real-world power systems.

4.2.1 Test Results for Line-to-Ground Fault at F-1

Various faults were simulated on the IEEE-9 bus test system to demonstrate the effectiveness of the protection technique. Consider a single-phase fault, denoted as F-1, at a specific location along feeder 4-5, precisely 30% from its starting point, from bus 4, when the network is in islanded mode. The voltage levels at various buses throughout this fault and these voltage variations are presented in Fig. 4.2.

It's important to note that before the fault, the voltage values at these buses were consistently near the 1 per unit (p.u.) mark, which is the reference voltage under normal operating conditions.

To better understand the system's behaviour during this fault event, we examined the discrepancies in impedance both before and during the fault, as illustrated in Fig. 4.3 and Fig. 4.4. Intriguingly, the analysis revealed that the calculated discrepant impedances, measured from the two ends of the transmission line, remained within the range expected for a no-fault region before the fault occurred.

In theory, the differences in impedance should be absolutely zero. However, it's

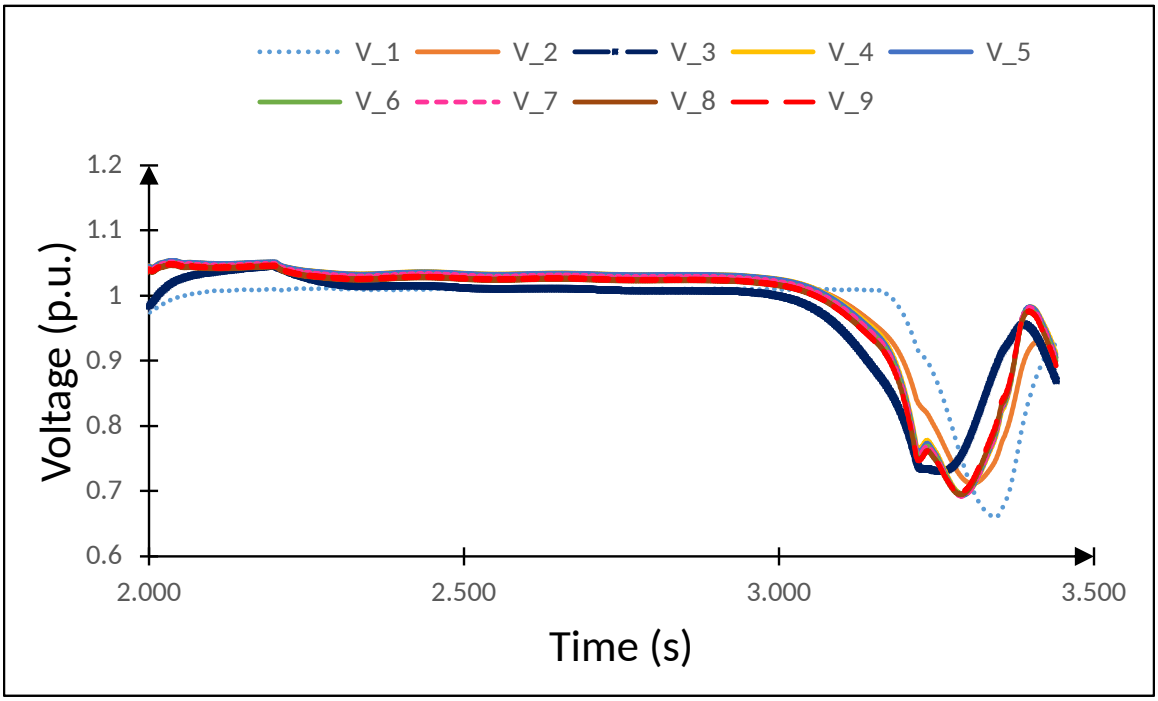

Figure 4.2: Magnitude of voltages during fault at F-1

essential to recognize that our modelling approach plays a role in this discrepancy. In this model, the feeders are modelled using a simplified pi model. Yet, our protection technique treats feeder impedances as lumped values, neglecting the capacitances. This distinction in modelling methodologies means that, in practice, we don't observe an ideally zero impedance difference during non-fault conditions due to shunt capacitances.

While the fault occurs, the discrepancies in impedance are situated within the fault region, which is evident in Fig 4.3. It's worth noting that the circle depicted in Fig 4.3 isn't particularly large. This is primarily a consequence of the limitations imposed by fault currents in a grid dominated by inverters, which typically range from 1.2 to 2 times the pre-fault current.

In the specific context of fault F-1, we have plotted the discrepant impedances estimated for the healthy feeders in Fig. 4.5. This figure shows that these impedance discrepancies are clustered around the origin point and exhibit a maximum value of 0.3 Ω. This 0.3 Ω value accounts for just about 1% of the line impedances. This

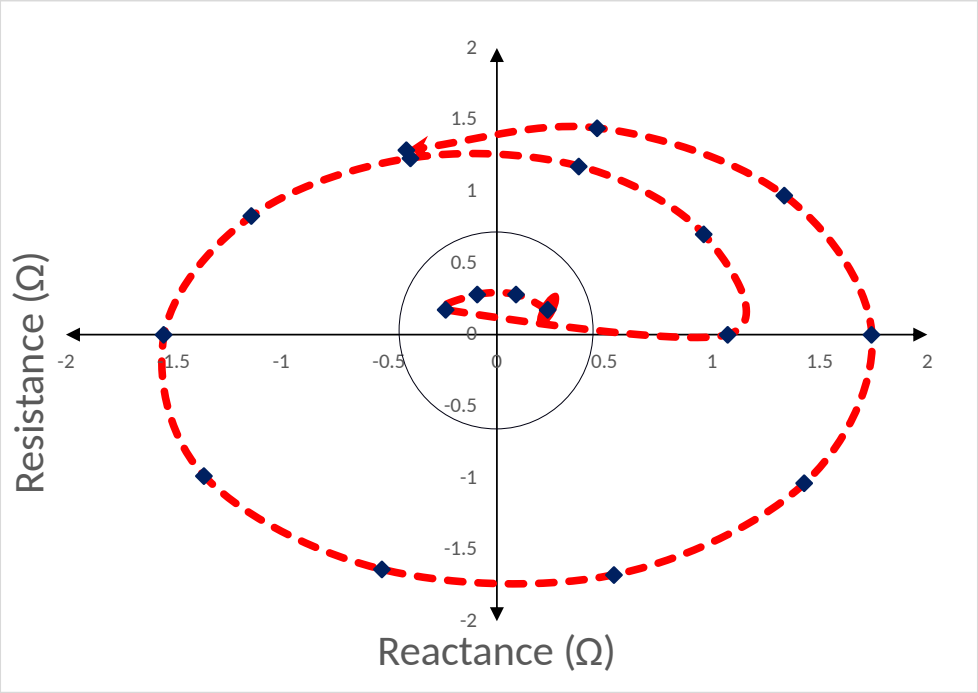

Figure 4.3: Discrepant impedances during the fault at F-1

observation underscores that discrepant impedances of healthy feeder has a minor impact on fault F-1. The values of these discrepant impedances do not precisely align with the origin point. This deviation occurs due to the influence of fault F-1 on the broader network. It's crucial to recognize that our microgrid functions in an islanded mode, relying solely on inverter-based resources. In such an isolated mode, any fault occurring in one part of the network can have ripple effects, impacting voltages and currents in other sections. This phenomenon arises due to the microgrid's characteristics, including its low short-circuit capacity and zero inertia.

However, what's particularly noteworthy is that our proposed relay scheme continues to function effectively without any malfunction. Despite the inherent challenges of islanded operation and the interconnected nature of faults in such a setup, our protection scheme reliably operates as intended.

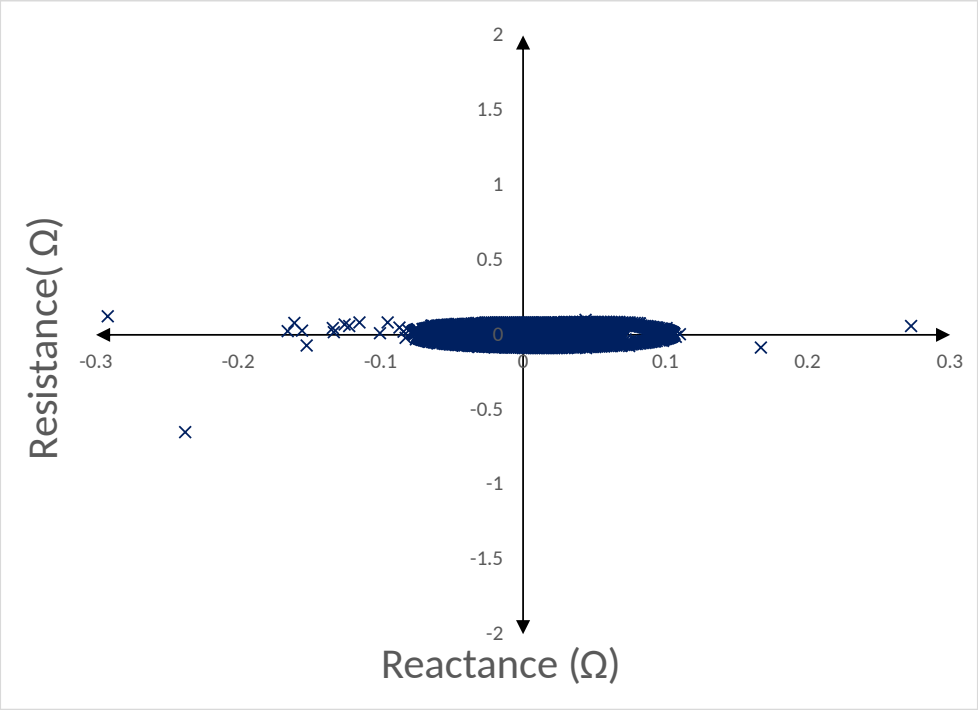

Figure 4.4: Discrepant impedances before the fault at F-1

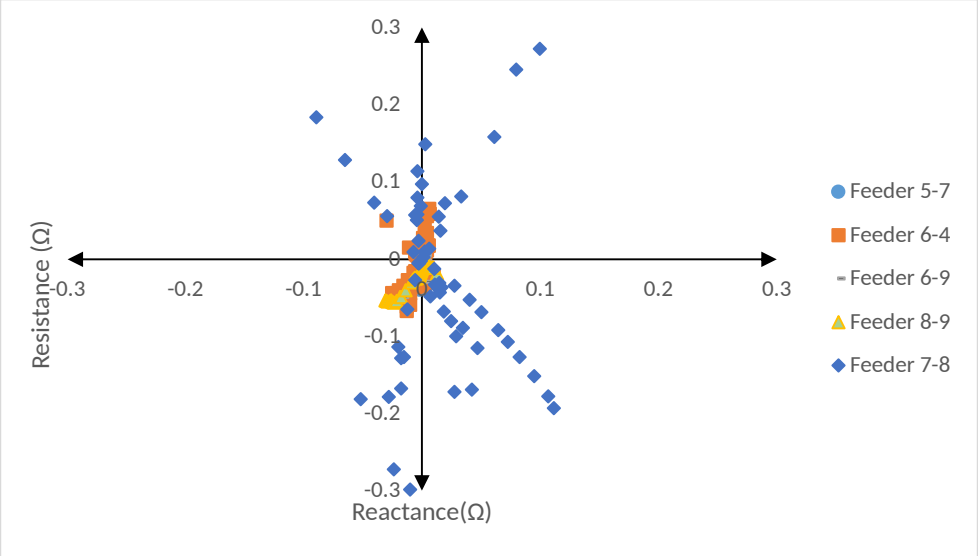

Figure 4.5: Discrepant impedances of healthy feeder during the fault at F-1

4.2.2 Test Results for Line-to-Line Fault at F-2

To understand the behaviour of the proposed protection technique, a line-to-line fault, F-2, is simulated on the feeder between bus-7 and 8 at 60% of line length from bus-7. In Fig. 4.6, you can observe the calculated discrepant impedances for the feeder section between buses 7 and 8. This deviation of discrepant impedances from the no-fault region to the fault region is a reliable indicator of a fault in the system.

However, it's essential to consider the broader network context. In Fig. 4.7, an overview of the discrepant impedances for the rest of the system outside the feeder 4-5. The values plotted in Figure 9 consistently remain within the range expected for a no-fault condition. This implies that the rest of the system, unaffected by fault F-2, continues to exhibit impedance characteristics in line with normal operation.

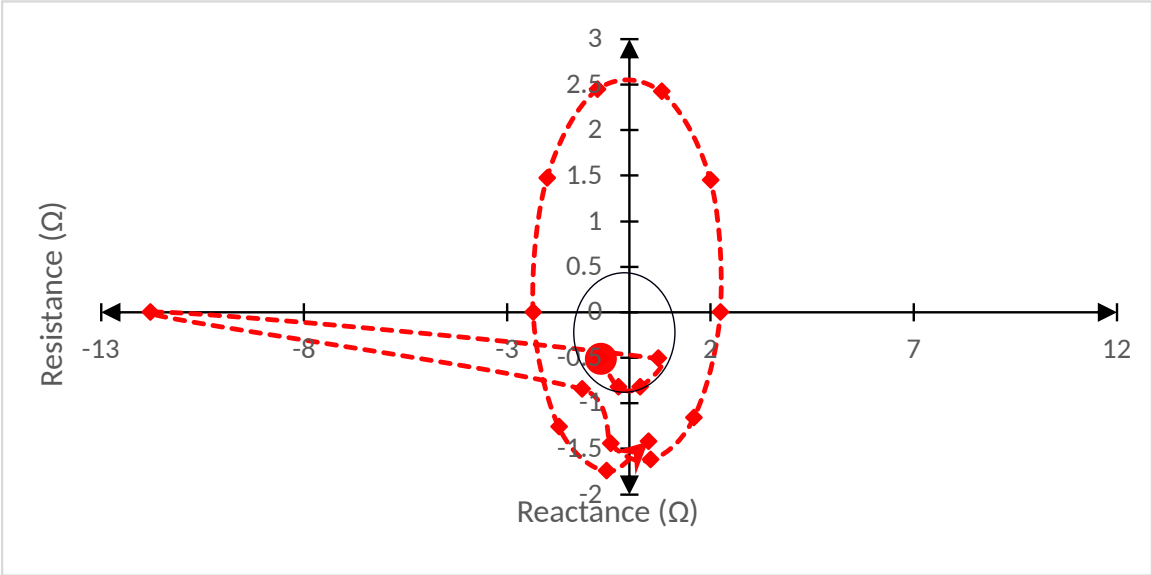

Figure 4.6: Discrepant impedances of feeder between bus 7and 8 during the fault at F-2

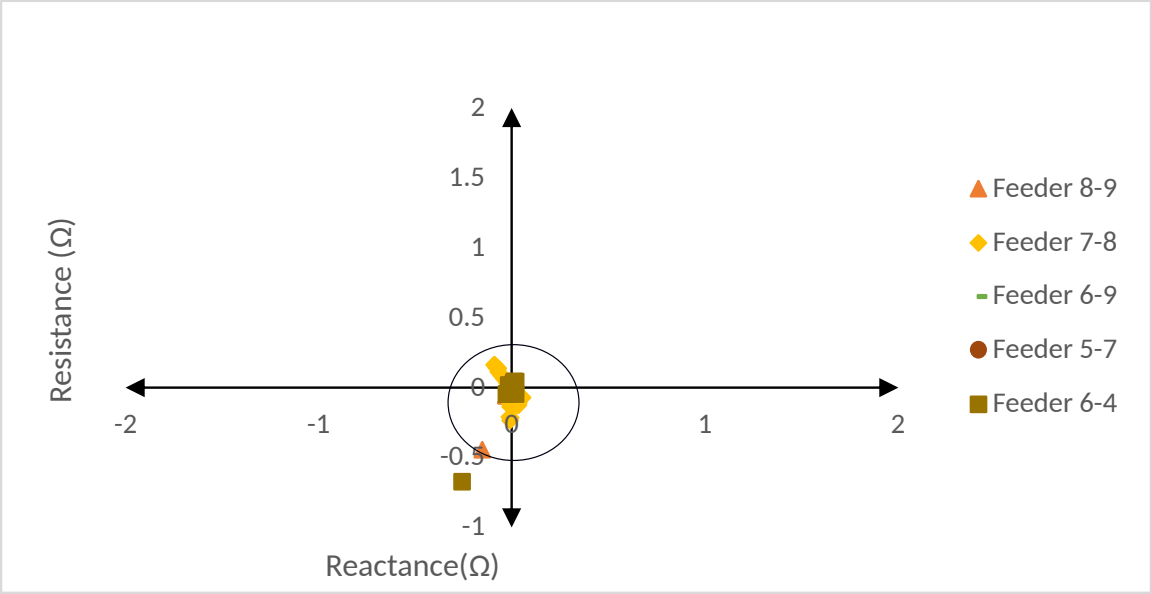

Figure 4.7: Discrepant impedances of healthy feeder during a fault at F-2

4.2.3 Test Results for Line-to-Line-to-Line Fault at F-3

A three-phase fault within a power system represents a severe electrical fault in which all three phases of an alternating current (AC) power network become electrically linked, usually due to a short circuit. To examine the performance of the suggested protection method, a simulated three-phase fault has been introduced at location F-3 along the feeder connecting bus-3 and bus-6. The discrepant impedances associated with this fault are illustrated in Fig. 4.8.

Conversely, Fig. 4.9 illustrates the corresponding impedances for unaffected, healthy feeders. In the case of the faulty feeder, these discrepant impedances are situated within the fault region, directly indicating the presence of a fault. However, for the healthy feeders, these discrepant impedances are located in regions unaffected by the fault.

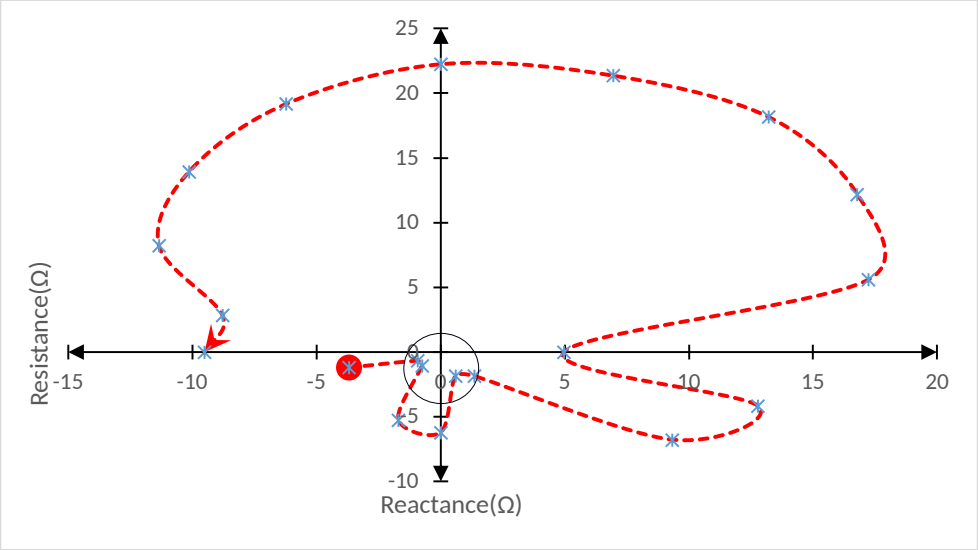

Figure 4.8: Discrepant impedances of a feeder during a fault at F-3

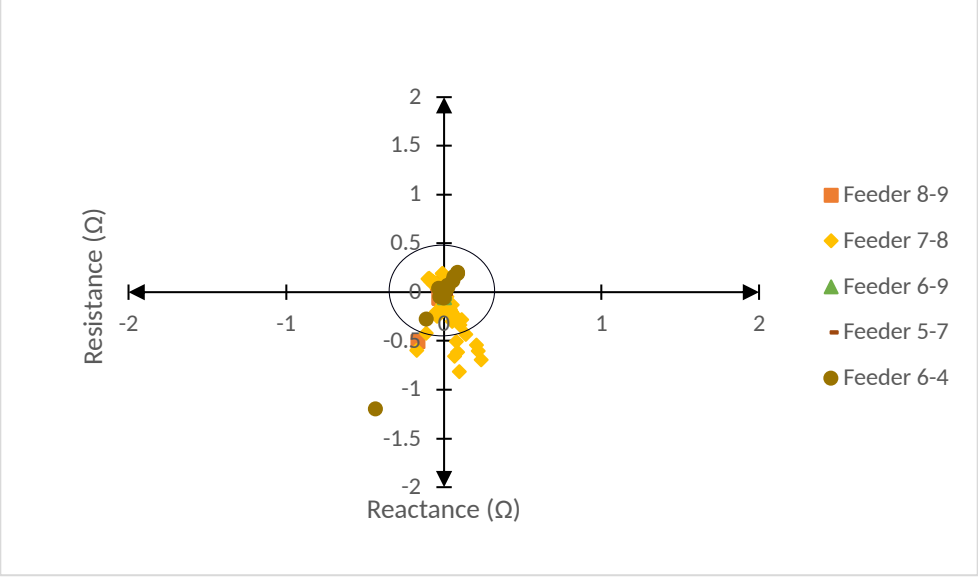

Figure 4.9: Discrepant impedances of healthy feeders during a fault at F-3

4.2.4 Test Results for High Resistance Faults

High-resistance faults are characterized by their higher impedance, which limits the current flow but can still result in various fault detection issues. Since the fault current is limited, the high resistance fault will pose more difficulty when the system operates in an islanded mode.

To assess the effectiveness of the proposed protective system in handling high resistance faults, we conducted a simulation involving a Line-to-Ground (L-G) fault at location F-1. This simulation introduced a fault resistance of 6Ω, which equates to approximately 200% of the feeder's impedance.

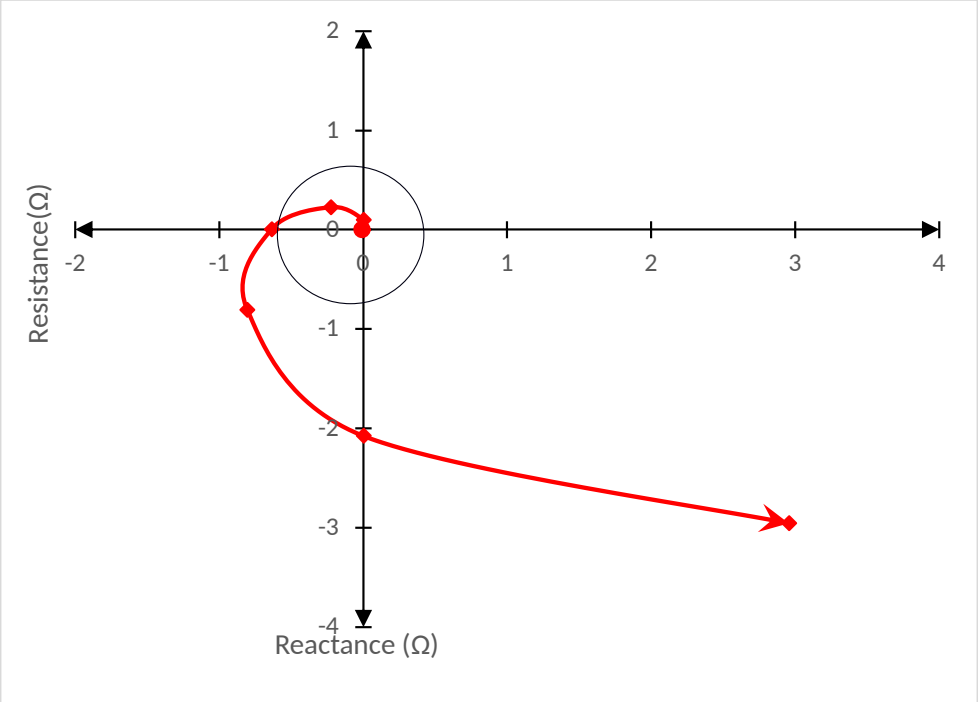

Figure 4.10: Discrepant impedances of a feeder between bus 4-5 during a high resistance fault at F-1

The results, as depicted in Fig. 4.10, clearly indicate the presence of discrepancies in impedance within the faulted region, confirming the occurrence of a fault. In contrast, the impedance discrepancies observed in healthy feeders during this fault scenario all fall within the no-fault region, with their values consistently low.

4.2.5 Test Results for Line-to-Ground Fault at F-1 in Grid-Connected Mode

Faults in grid-connected mode refer to electrical faults or anomalies that occur within a system while it is actively connected to the larger electrical grid. The fault current magnitude will be higher in grid-connected mode than in islanded mode.

During grid-connected operation, when a single-phase fault materializes at location F-2 along feeders 4-5, the relay system estimates impedance variations, as illustrated in Fig. 4.11.

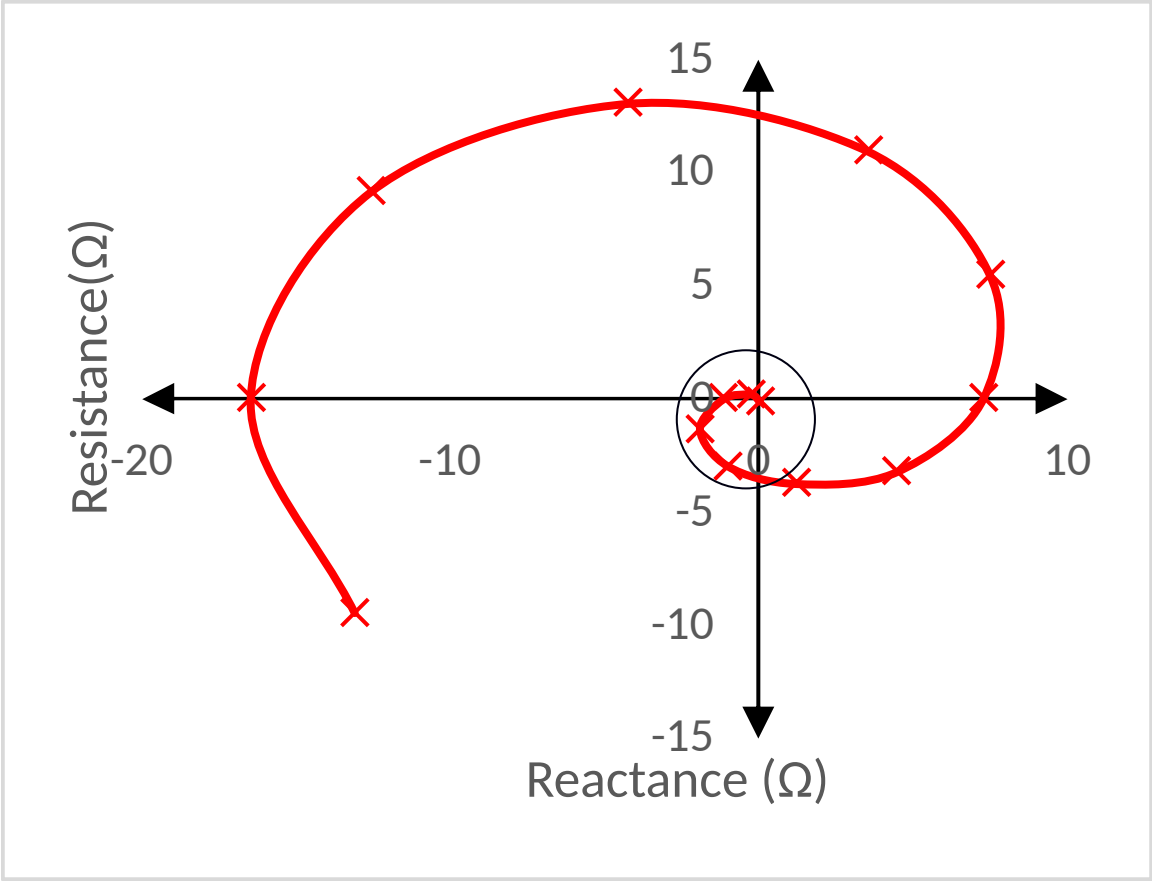

Figure 4.11: Discrepant impedances of a feeder between bus 4-5 for at F-1 during grid-connected mode

Before the fault, the impedance values are situated within the no-fault region. However, when the fault transpires, the impedance estimations significantly shift into

the fault region. Conversely, the discrepant impedance estimations persist within the no-fault region for the remaining feeders throughout the fault event. This consistent pattern signifies that these other feeders remain unaffected by the fault, maintaining their normal operating conditions.

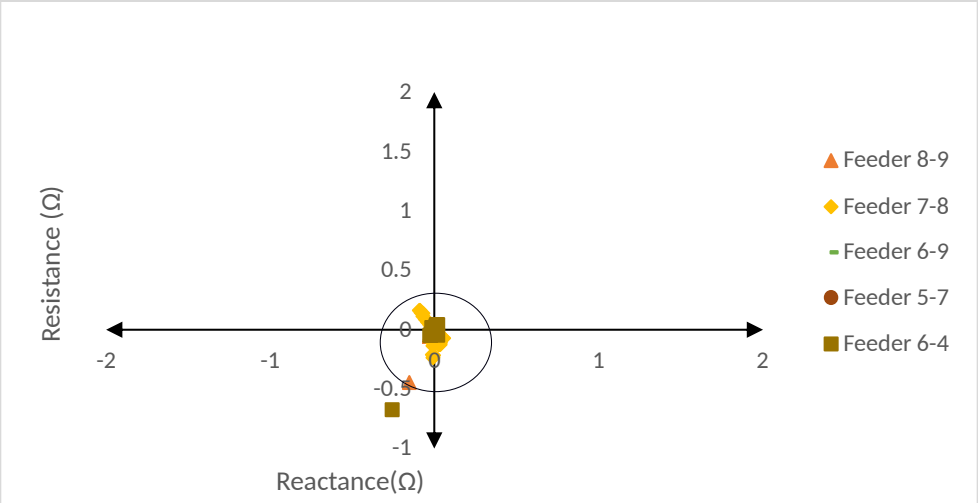

Figure 4.12: Discrepant impedances of healthy feeder during a fault at F-1 in grid-connected mode

4.3 Summary

The evaluation protection technique for detecting the faults on the IEEE-9 bus benchmark system with inverter-based resources is discussed in this chapter. The protection technique was tested on grid-following, grid-forming inverters in grid-connected and islanded modes of operation and test results are presented for various faults in this chapter. The results indicate that the protection technique is stable for external faults and operates for the fault in its protection zone. In other words, the protection technique is reliable.

Chapter 5

Performance Evaluation of the Protection Technique on a Low Voltage Micogrid

5.1 Introduction

Chapter 4 introduced a protection technique that demonstrated strong performance in high-voltage systems supplied by IBRs. The initial studies used PSCAD/EMTDC, an offline software. This chapter, however, shifts its focus towards the real-time application of this protection technique using RTDS. The experimentation phase is now on a low-voltage microgrid associated with the Consortium for Electric Reliability Technology Solutions (CERTS) initiative.

Within the scope of this research, the CERTS microgrid was meticulously developed in RSCAD. The development of the protection scheme was executed on a CPU NOVACOR. This chapter provides a comprehensive overview of the CERTS microgrid's modelling, delves into the intricacies of designing and implementing the protection scheme, and presents the results of rigorous testing under diverse scenarios. Furthermore, the chapter elaborates on the communication aspects essential for the successful implementation of this protection scheme in real-time applications [69].

5.2 Performance Evaluation

The centralized protection technique was tested on 480 V low voltage CERTS microgrid. The following section describes the microgrid and test setup.

5.2.1 CERTS Microgrid

A low-voltage CERTS (Consortium for Electric Reliability Technology Solutions) microgrid is designed to operate at 480 V. Within this microgrid topology, there are two inverter-coupled photovoltaic resources, namely PV-1 and PV-2, each with a capacity of 100 kW, and they are connected to nodes N-6 and N-8, respectively. Furthermore, an inverter-coupled BESS, capable of generating 90 kW, is linked to node N-3. A diesel generator (DG) with an output capacity of 100 kW is integrated into the network at node N-4. The graphical representation of this configuration is illustrated in Fig 5.1.

The DG is an essential backup power source, ensuring an uninterrupted energy supply during contingencies. Complementing these generation assets are four load banks, each with a capacity of 50 KVA, strategically interconnected at nodes N-1, N-4, N-7, and N-8. These load banks represent the critical end-users within the microgrid, and their distribution is planned for load balancing.

The microgrid's connectivity to the utility grid is facilitated through a 13.2/0.480 kV transformer, representing the interconnection point. The photovoltaic resources PV-1 and PV-2 are equipped with grid-following inverters, while the BESSutilizes a grid-forming inverter; all are designed per the guidelines outlined in the IEEE-1547 standard [40]. These inverters play a pivotal role in harmonizing the microgrid's operations with the utility grid while enabling seamless transitions between various operational modes.

Furthermore, to facilitate the protection of the feeders of the microgrid, each feeder node is outfitted with digital instrument transformers. These transformers enable the real-time acquisition of voltage and current data, which is subsequently transmitted

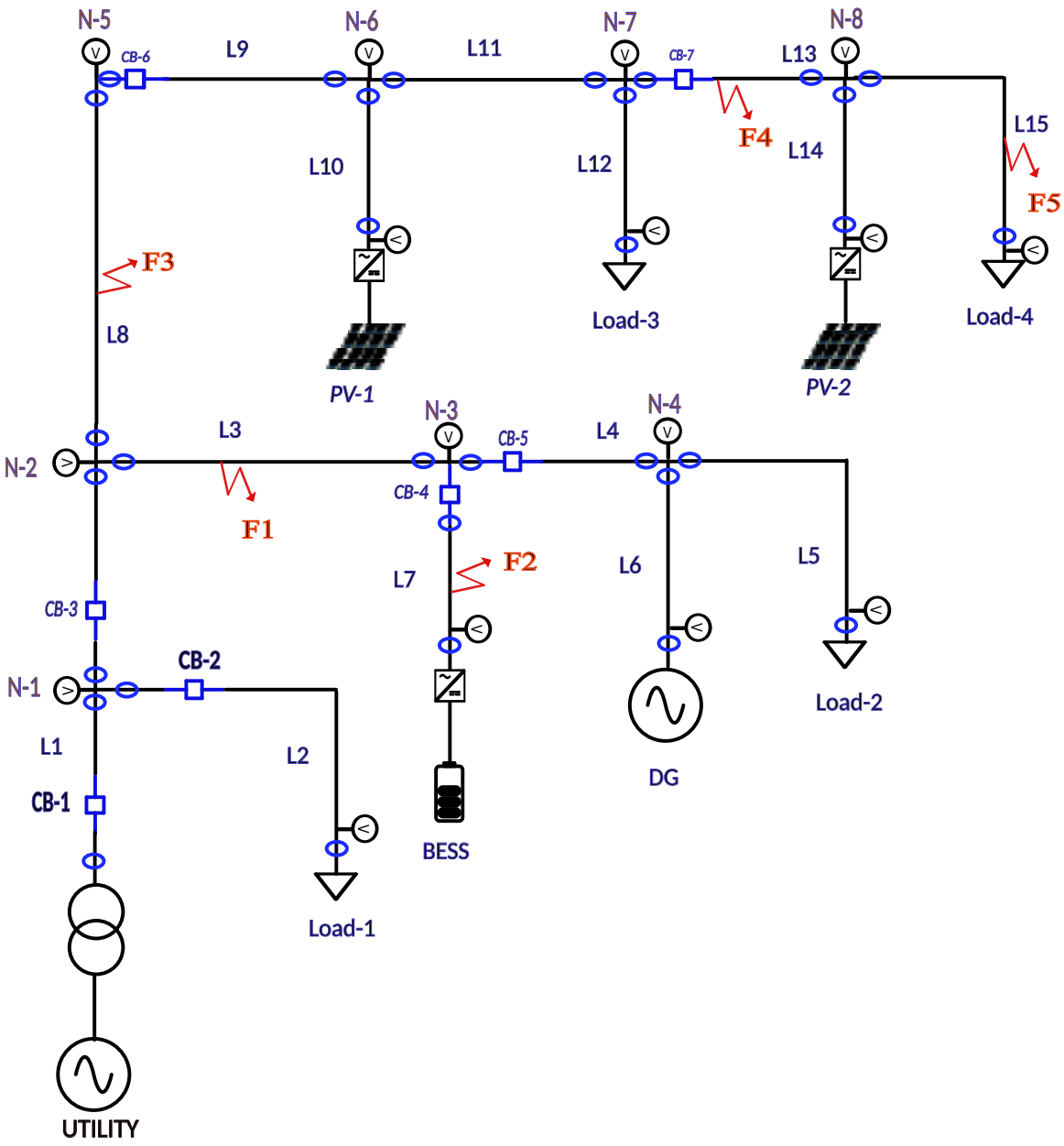

Figure 5.1: CERTS Microgrid

to a centralized processing unit.

The operation mode of the microgrid, be it in a grid-connected or islanded state, is governed by the circuit breakers. CB-1, for instance, functions as the interface breaker with the utility grid, effectively controlling the microgrid's mode of operation. Meanwhile, CB-2 takes charge of managing feeders L2, CB-3 assumes responsibility for feeders L3 and L8, CB-4 exercises control over feeders L7, CB-5 regulates feeders

L4, L6, and L5, CB-6 , manages the feeders L9, L10, and L11, and CB-7 wields authority over the feeders L13, L14, and L1.

5.2.2 Experimental Setup

Fig. 5.2 illustrates the real-time test platform employed for simulating the proposed protection scheme within the context of the CERTS microgrid. This platform consists of two distinct racks, Rack-1 and Rack-2, each serving specific roles in the simulation setup. The integration between these racks is achieved through a point-to-point global bus hub cable, which facilitates the synchronization of simulation time steps.

Rack-1 is equipped with an RTDS (Real-Time Digital Simulator) from NOVACOR and is primarily responsible for modeling the CERTS microgrid. On the other hand, Rack-2 houses an RTDS with GPC (Generic Processor Card) capabilities, which is dedicated to implementing the protection scheme. Both racks have gigabit transceiver network interface cards (GTNET-SV) to enable seamless communication.

The GTNET-SV card plays a pivotal role as it acts as a carrier for the publication and subscription of sampled values related to three-phase voltages and currents over the LAN (Local Area Network) following the IEC 61869-9 standard. In this configuration, the publisher GTNET-SV card in Rack-1 transmits sampled values of voltages and currents according to IEC-61869-9 at 80 samples per cycle sampling rate. Rack-2, in turn, receives these sampled values through a GTNET-SV subscriber card. The communication between the two racks is facilitated via GT fiber ports and fiber optic cables, ensuring high-speed and reliable data transfer. These sampled values are synchronized with a 1 PPS (Pulse Per Second) internal clock of the RTDS, ensuring precise timing.

The communication protocol adopted for data exchange between the processors and the Human Machine interface (HMI) PC is IEC 61850, a widely recognized standard for substation automation.

The sampled values of voltages and currents received from both ends of the feeders arrive at a rate of 80 samples per cycle. These sampled values are down-sampled

through a moving average process to effectively compute discrepant impedances, resulting in 10 samples per cycle. Fundamental frequency phasors of voltages and currents are computed using full-cycle Discrete Fourier Transform (DFT) analysis. This information, combined with the principles described in section 2 of the study, is used to calculate the discrepant impedances for all feeders within the network at each sampling interval, corresponding to 1/480 seconds.

The protection scheme operates based on pre-defined criteria discussed in chapter-3, where the threshold values for discrepant impedance and trip counters are set. When the trip counter reaches a predetermined value, typically set at five, a trip command is issued to the breaker associated with the faulty feeder via the LAN, effectively isolating the faulted section of the microgrid.

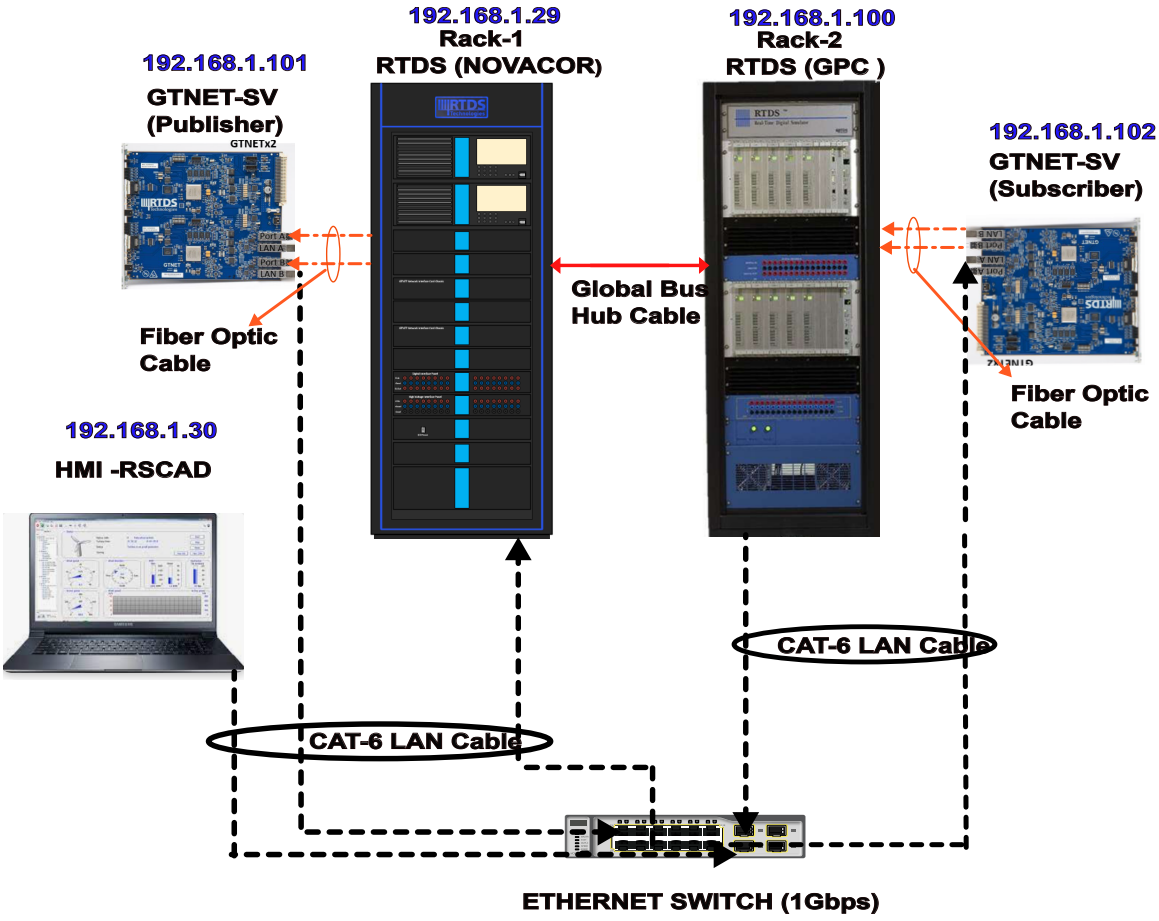

Figure 5.2: Real-Time test setup of the microgrid protection

It is important to know the discrepant impedances of all the feeders in the mi-

crogrid to identify the faulted feeder from the rest of the network. The computed discrepant impedances of feeders-A, B, and C are ZA, ZB and ZC, respectively. Assuming a fault F1 on the feeder-A, the discrepant impedances of the feeder-A will fall in the fault region, whereas those for the feeders B and C are in the no-fault region. The faulted segment of the network can then be identified based on Table 5.1

Table 5.1: Faulted feeder identification matrix

Discrepant impedance (ΔZA)	Discrepant impedance (ΔZB)	Discrepant impedance (ΔZC)	Faulted feeder
1	0	0	Feeder-A
0	0	1	Feeder-C
0	1	0	Feeder-B
1	1	0	Feeder-A and B
1	0	1	Feeder-A and C
0	1	1	Feeder-B and C

Note: 1 represents that the discrepant impedances are in the fault region, and 0 represents that the discrepant impedances are in the no-fault region.

5.3 Performance Results

Several faults under various operating conditions were performed on a real-time test bench to evaluate the protection technique's performance. It was found that the protection technique is dependable and secure.

5.3.1 Performance with Different Operating Modes

To assess the performance of the proposed protection scheme, an array of simulated fault scenarios, encompassing both symmetrical and asymmetrical faults, have been systematically executed within the CERTS microgrid. Specifically, four distinct fault types were intentionally introduced at the midpoint of feeder L7, denoted as F1, as visually represented in Fig 5.1. These fault categories encompass line-to-line (AB) faults, three-phase (ABC) faults, line-to-line-to-ground (BCG) faults, and line-to-ground (AG) faults. The primary objective was to comprehensively scrutinize the protection scheme's response and ability to detect and mitigate these varied fault conditions effectively.

Figs. 5.3 and 5.4 depict R-X plots, illustrating the discrepant impedances associated with these four diverse fault types. These plots provide a clear visual representation of the impedance behaviour during fault occurrences. Remarkably, the trajectory of discrepant impedances exhibited in Figs. 5.3 and 5.4 consistently falls within the fault region for all fault types, regardless of whether the microgrid operates in grid-connected or islanded mode. This observation reaffirms the scheme's robustness and reliability in promptly identifying and addressing faults, irrespective of the operational context.

Furthermore, an analysis of the discrepant impedances of healthy feeders reveals that they consistently remain close to zero, as evidenced in Fig. 5.5 both before and after the fault is cleared.

Remarkably, the discrepant impedances of all unaffected or "healthy" feeders remain within the non-fault region throughout the fault event—before, during, and after the fault is cleared by the circuit breaker CB-4. This exceptional performance aligns seamlessly with the predefined protection criteria, affirming the scheme's efficacy in safeguarding the microgrid against various fault scenarios. Importantly, this protective scheme's performance remains consistent and independent of the microgrid's operational mode, further underscoring its versatility and reliability.

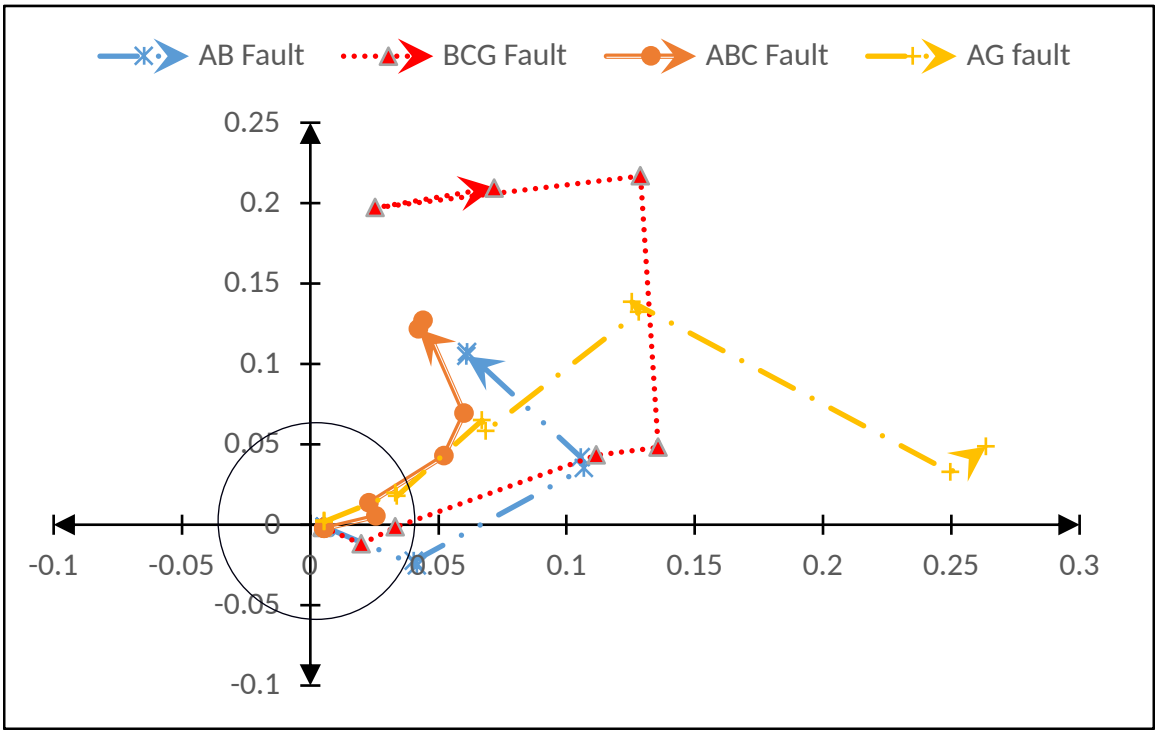

Figure 5.3: Discrepant impedances of feeder L7 for fault at F1 during grid-connected mode

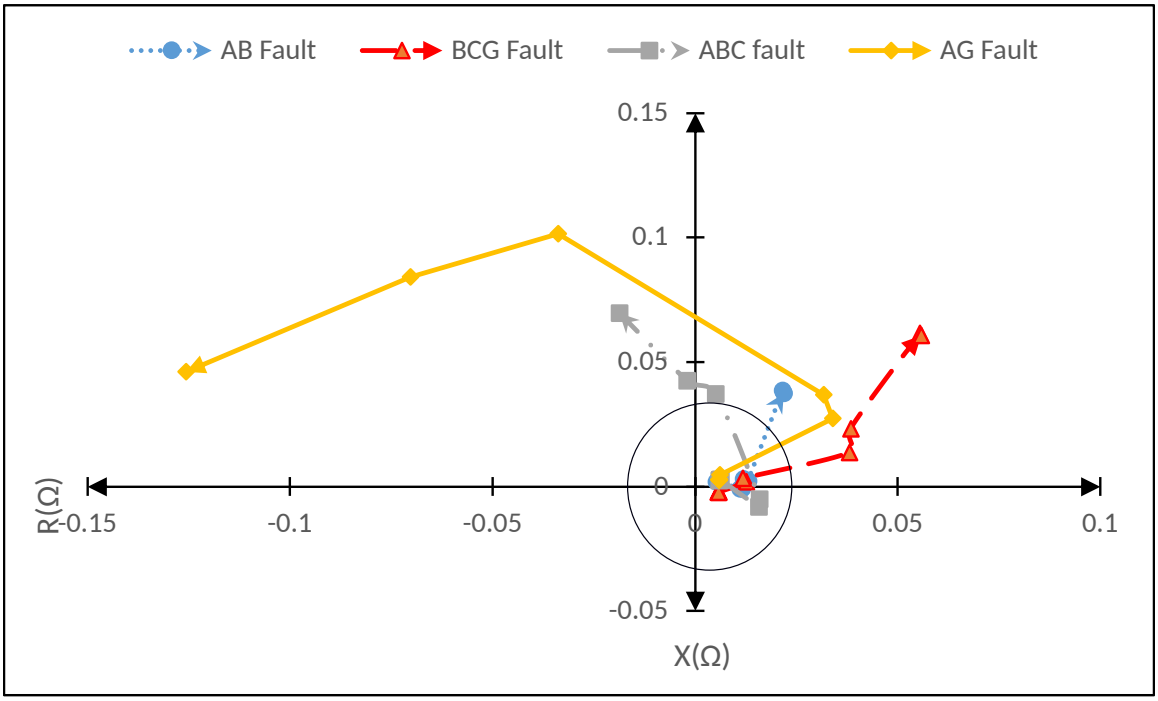

Figure 5.4: Discrepant impedances of feeder L7 for fault at F1 during islanded mode

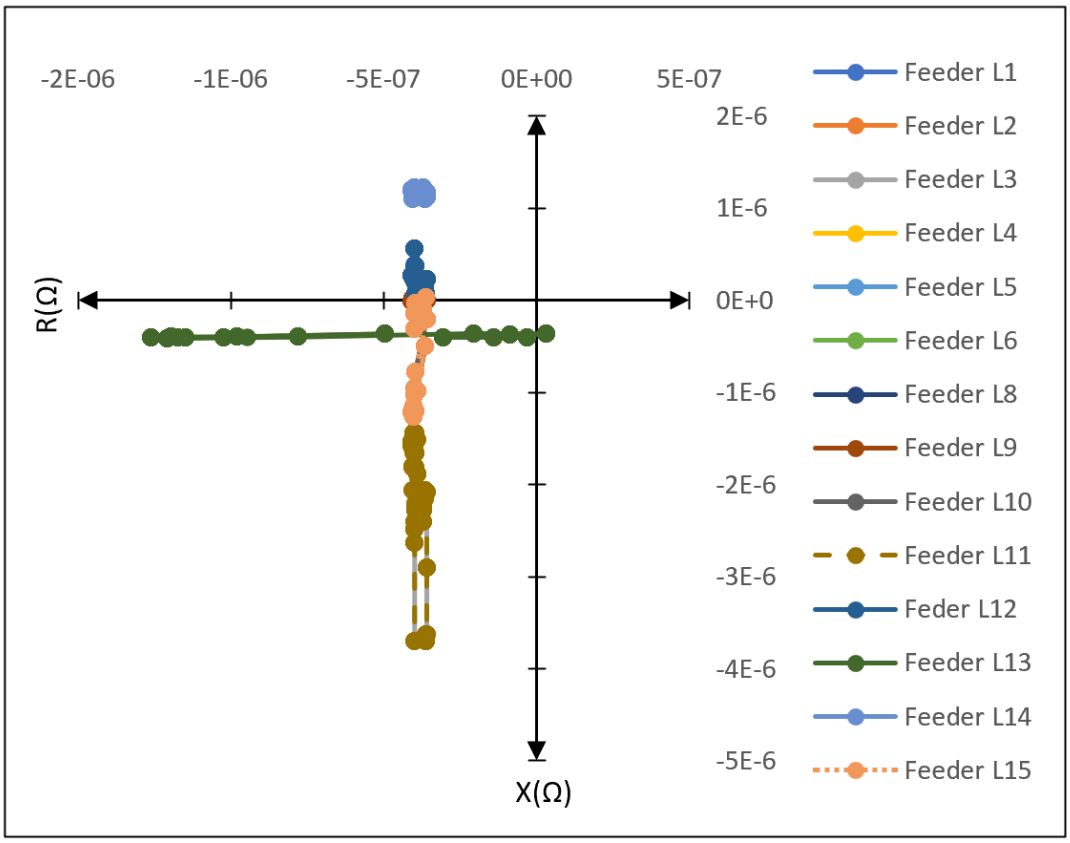

(c)

Figure 5.5: Discrepant impedances of healthy feeders for fault at F1 on L7 before, during and after the fault is cleared

5.3.2 Performance with High Resistance Faults

The protection scheme's performance assessment extends to high-resistance faults, which present a distinctive challenge due to their low current magnitudes. These challenges are further exacerbated in islanded operational modes, where the current levels are typically diminished. Therefore, the proposed protection scheme is evaluated for its effectiveness in handling high-resistance fault scenarios.

A single-line-to-ground fault denoted as F3, is deliberately introduced at the midpoint of feeder L13, featuring a range of fault resistances that span from Rf= 0.0172Ω (equivalent to 100% of the feeder impedance) to Rf= 0.086Ω (representing 500% of the

feeder impedance), and further extending to Rf= 0.172 Ω (equivalent to 1000% of the feeder impedance). This comprehensive examination encompasses a broad spectrum of fault resistances to assess the protection scheme's performance thoroughly.

Fig.5.6 and 5.7 serve as graphical representations, offering insights into the outcomes of the analysis conducted on AG (line-to-ground) faults with varying fault resistances, both in grid-connected and islanded operational modes.

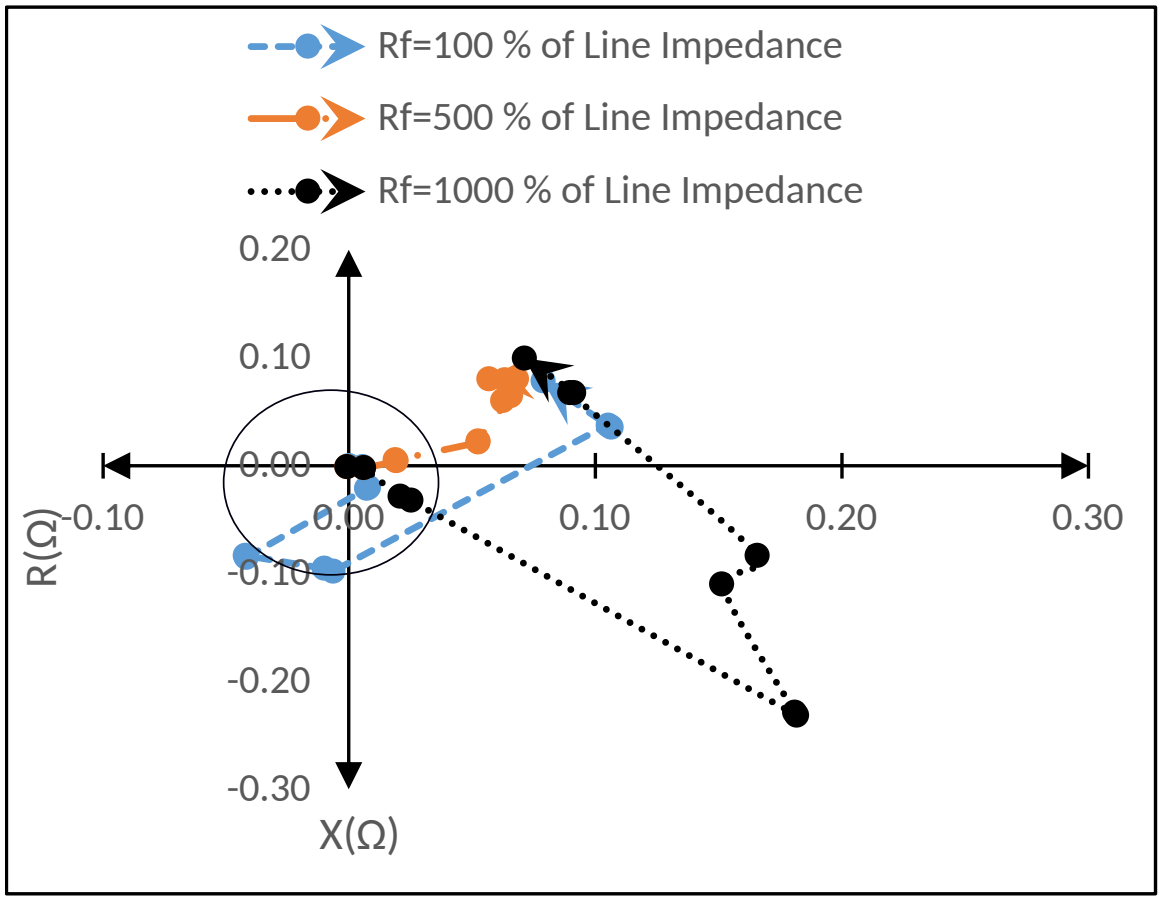

Figure 5.6: Discrepant impedances of feeder L13 for fault at F3 during grid connected mode

An observation from Figs. 5.6 and 5.7reveals that irrespective of the range of fault resistances applied, the trajectories of discrepant impedances consistently deviate from the no-fault region in both grid-connected and islanded operational modes. This phenomenon underscores the robustness and adaptability of the protection scheme when confronted with high-resistance faults. It effectively detects and responds to

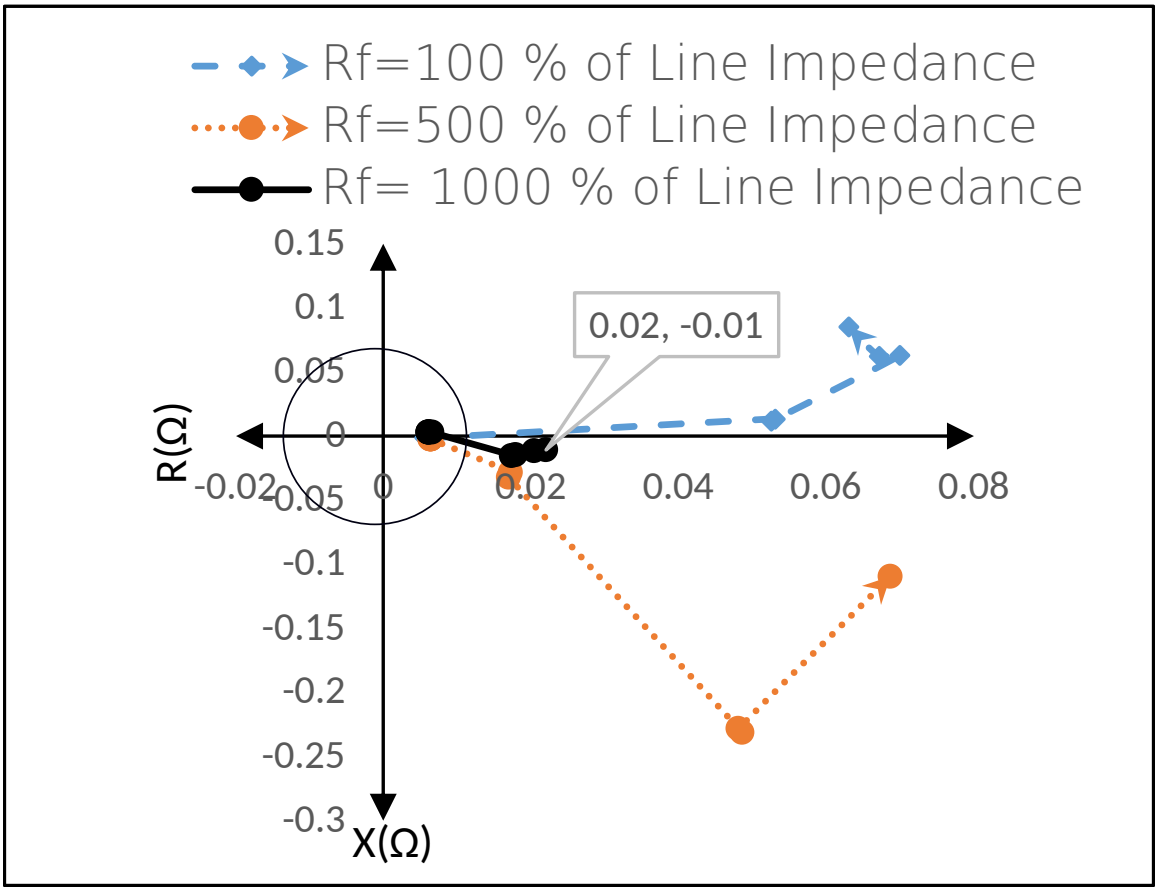

Figure 5.7: Discrepant impedances of feeder L13 for fault at F3 during islanded mode

these faults across a broad spectrum of fault resistances, demonstrating its reliability in safeguarding the microgrid.

5.3.3 Effect of Broken Conductor Faults

Detecting faults involving broken conductors poses a substantial challenge, particularly when these conductors remain suspended and do not make contact with the ground. In such cases, the fault condition can be pretty severe, and timely detection is critical for maintaining grid stability and safety. Considering both islanded and grid-connected operational modes, the proposed protection scheme's effectiveness is rigorously evaluated in scenarios involving an open circuit fault within feeder L9.

To provide a specific example, let's consider a scenario where phase A of feeder L9 experiences a break but remains suspended without making contact with the

ground. Consequently, the current in phase A becomes zero, while the positive sequence current remains present, thanks to the current flow in the other two phases. This situation highlights the intricate nature of detecting open circuit faults, where traditional methods may not readily identify the issue.

The trajectory of discrepant impedances during the occurrence of the broken conductor fault is meticulously captured in Fig. 5.8. A noteworthy observation from this depiction is that the discrepant impedance trajectory deviates from its initial position and eventually converges to a specific point, as indicated in Fig. 5.8. Notably, the magnitude of the settled value of discrepant impedances during an open circuit fault registers at 0.019 Ω. Remarkably, this value accounts for 98%of the positive sequence impedance of the feeder (0.0172Ω), a value significantly exceeding the defined protection scheme setting, which is typically set at 3%of the positive sequence feeder impedance (0.000516 Ω).

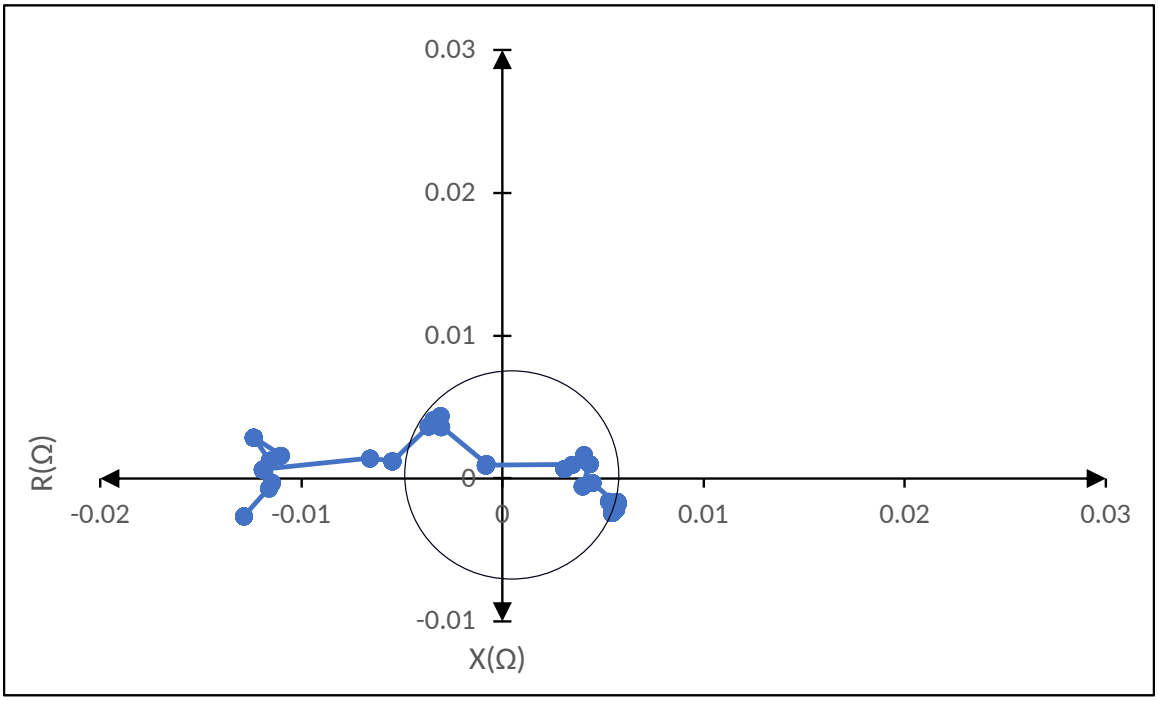

Figure 5.8: Discrepant impedances of feeder L9 during an open circuit fault on phase A

This empirical evidence substantiates the effectiveness of the proposed protection scheme in detecting and responding to open circuit faults, even in complex scenar-

ios where conductors remain suspended. By successfully identifying the fault and triggering protective actions, the scheme reinforces the integrity and resilience of the microgrid, ensuring that faults of this nature do not go unnoticed or unaddressed. Hence, the proposed protection scheme serves as a reliable and robust solution for mitigating open circuit faults and enhancing the overall reliability of the microgrid system.

5.3.4 Effect of Change in Microgrid Topology

Renewable energy sources inherently exhibit intermittent energy generation patterns, which can lead to variations in the availability of these resources within microgrids. Consequently, these fluctuations in resource availability can trigger changes in the microgrid's overall topology. As a direct consequence of these topological changes, the fault current characteristics within the microgrid also undergo alterations, mainly when the microgrid operates in islanded mode, disconnected from the primary utility grid.

A comprehensive testing regime is executed to validate the resilience and adaptability of the proposed protection scheme in the face of such dynamic topological variations. This testing encompasses various combinations of energy resources while the microgrid remains in islanded mode. To illustrate this, let's consider a scenario where a line-to-ground fault, denoted as F3, is near node N7. In this test setup, different combinations of resources are introduced, including PV, BESS, and DG.

The resulting R-X plot of discrepant impedances, as depicted in Fig. 5.9, provides valuable insight into the behaviour of the protection scheme under these varying conditions. Notably, Figure 16 portrays a significant shift in the trajectory of discrepant impedances, transitioning from a no-fault region to a fault region when a fault occurs at F3 under different resource combinations. These combinations include scenarios where the microgrid operates with PV and BESS, PV and DG, and BESS and DG, respectively.

The implications drawn from the outcomes of Fig. 5.9 reinforce the robustness

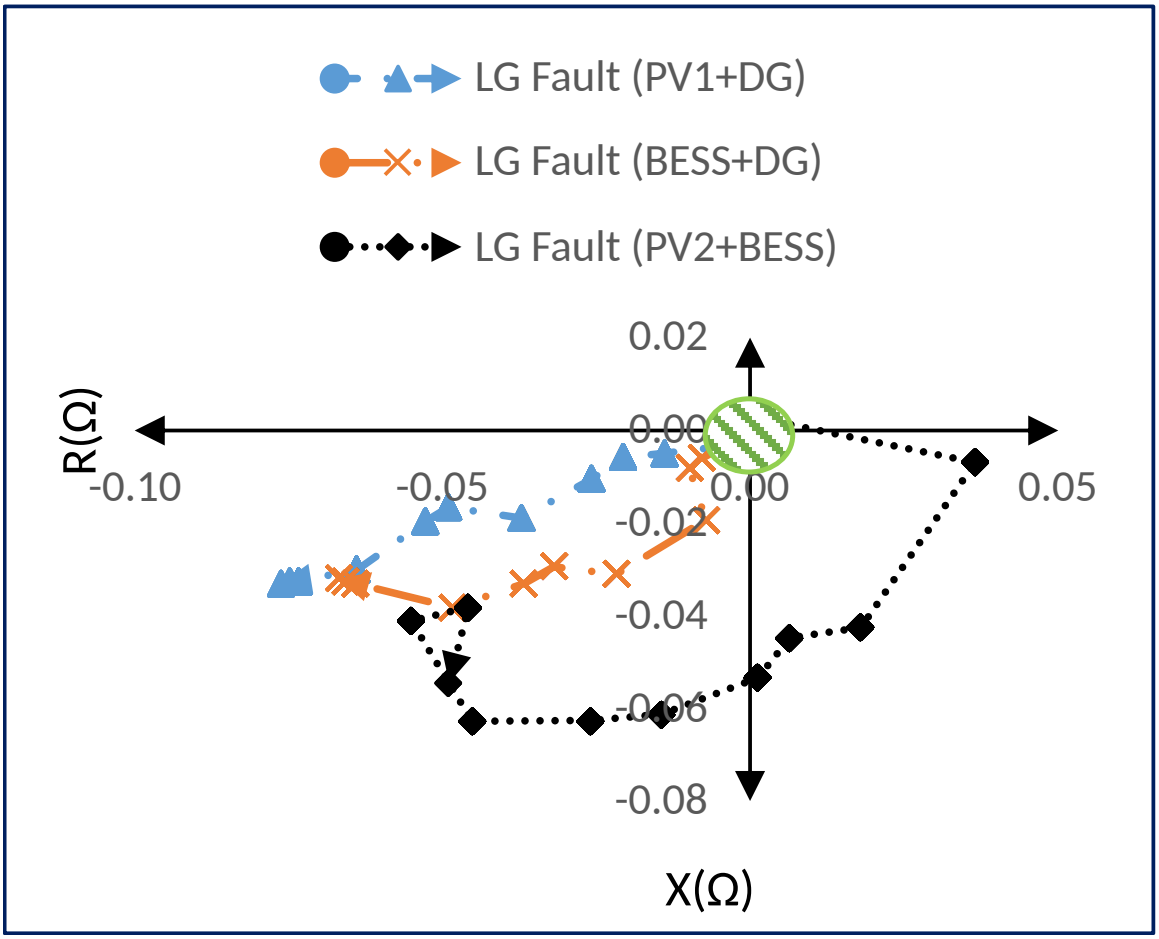

Figure 5.9: Discrepant impedances of feeder L13 during a close-in fault on phase A

and versatility of the proposed protection scheme. It effectively adapts to the dynamic changes in microgrid topology resulting from variations in the availability of renewable energy resources. Furthermore, the scheme showcases its reliability in the presence of different resource combinations contributing to the microgrid, ensuring that fault detection and mitigation remain consistent and appropriate regardless of these dynamic factors.

In conclusion, the comprehensive test results in Fig. 5.9 affirm that the proposed protection scheme functions adeptly and is inherently independent of shifts in microgrid topology and the specific mix of resources integrated into the microgrid system. This resilience bolsters the scheme's suitability for safeguarding the integrity and reliability of microgrid operations under real-world conditions where resource availability

may vary.

5.3.5 Effect of Voltage Imbalance in the Microgrid

In low-voltage distribution systems, maintaining perfect balance is challenging, primarily due to single-phase loads that tend to introduce imbalances in the network. These single-phase loads, in turn, contribute to voltage imbalances within the system. According to IEEE standard 1250-2018, low-voltage networks' recommended degree of imbalance is limited to 3% of the nominal voltage. This imbalance in voltage is responsible for the persistent existence of negative sequence voltage and current flows within the system, even under non-fault conditions.

As a result of these inherent imbalances, protection schemes that rely on negative sequence quantities can suffer from misoperation due to the network's unbalanced nature; it becomes imperative to enhance the sensitivity of these protection schemes to prevent unwarranted trips. Furthermore, earth fault protection based on residual overcurrent, which essentially sums up the three-phase currents, may yield erroneous results, even in scenarios with no faults.

To thoroughly analyze the proposed protection scheme's performance in such unbalanced conditions, an unbalanced load, referred to as Load-2, is introduced into the microgrid. Specifically, we consider feeder L5, which features an unbalanced load configuration where Phase A has a load of 10 KVA, Phase B has 20 KVA, and Phase C has 30 KVA. Under no-fault conditions, the computed discrepant impedance is displayed in Fig. 5.10, revealing that it falls below the predetermined set value. This outcome stems from the fact that the protection scheme leverages positive sequence components of voltage and current, which remain unaffected by the presence of unbalanced loads. However, when a line-to-ground and line-to-line fault, denoted as F4, occurs on feeder L5, the discrepant impedance shifts into the fault region, as demonstrated in Fig. 5.11. A key observation derived from Fig. **??** and Fig. **??** is that, despite the presence of unbalanced loads, the discrepant impedance during non-fault conditions remains below the 3%threshold relative to the feeder impedance. Conversely, during

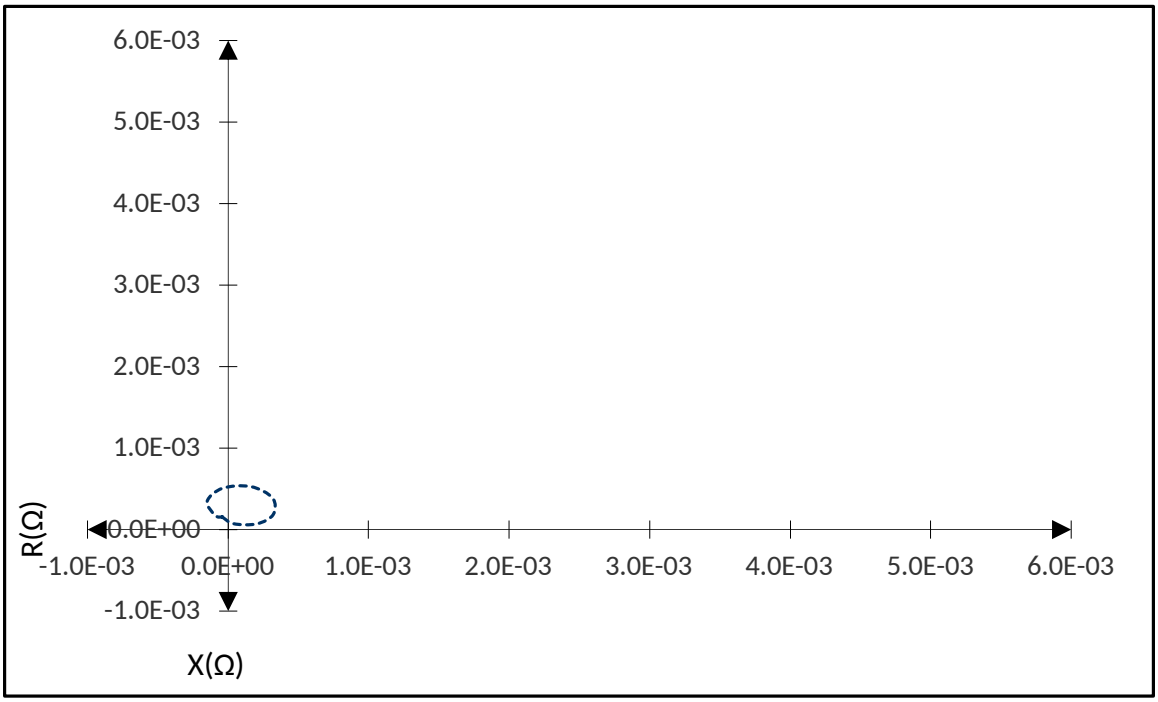

Figure 5.10: Discrepant impedances of feeder L4 during no-fault with unbalance load

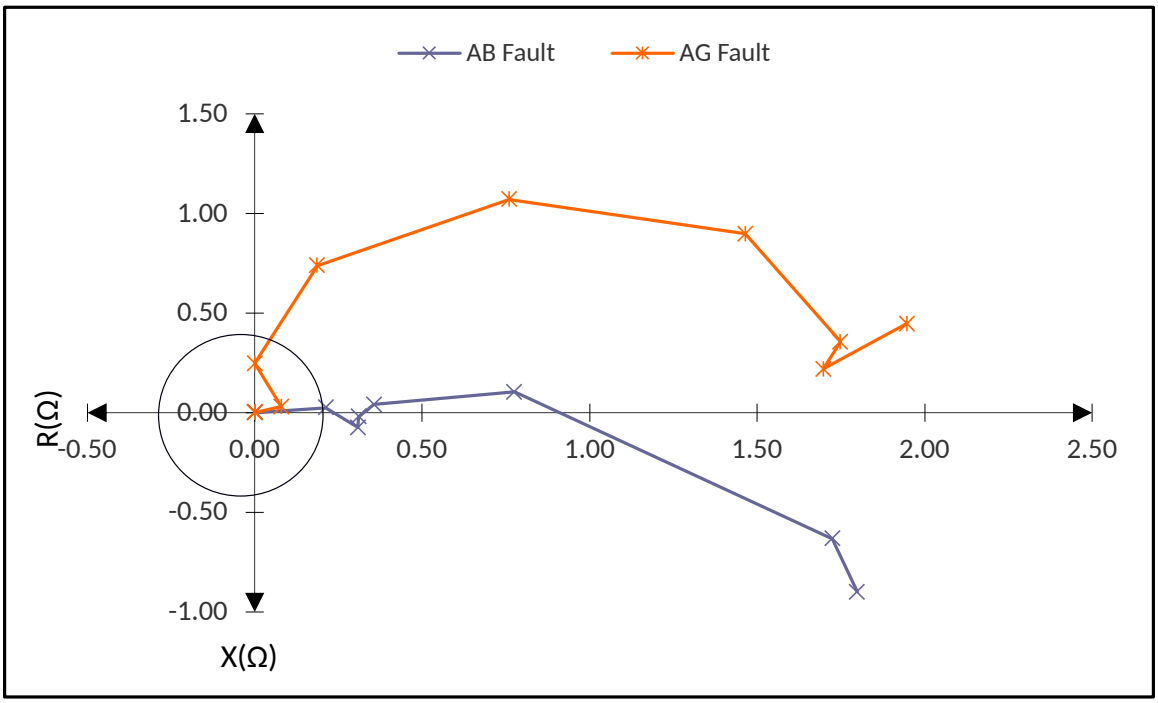

Figure 5.11: Discrepant impedances of feeder L4 during a faut

fault conditions, the discrepant impedance consistently exceeds the values observed under no-fault circumstances.

This empirical evidence underscores the robustness of the proposed protection scheme when confronted with unbalanced load conditions. The scheme effectively discriminates between fault and non-fault conditions by focusing on positive sequence components, mitigating the risk of erroneous trips. Consequently, the scheme proves its suitability for deployment in unbalanced low-voltage distribution systems, where single-phase loads can introduce significant voltage imbalances while ensuring accurate fault detection and protection.

5.4 Comparison With Differential Protection

In the domain of feeder protection, a commercially established differential relay, predicated upon an α-plane characteristic, has been deployed for practical applications. This relay operates by ascertaining the ratio between the current measured remotely and the locally observed current. In scenarios without faults, this ratio remains camouflaged within the confines of the stable region, as depicted in Fig. 5.12. Conversely, in the event of a fault occurrence, this ratio traverses into the trip region, as expounded in reference [70].

To gauge the efficacy of this relay in a microgrid that integrates inverter-based resources specifically, a line-to-ground fault is created within phase A of feeder L13 at the designated point F3. This fault resistance value (Rf) of 0.0172 ohms, mirroring precisely 100% of the feeder's impedance. This fault was created during the microgrid's islanded mode of operation. The α-plane differential relay, crucially, draws its requisite inputs from the current measurements conducted at both extremities of feeder L13.

Noteworthy, Fig. 5.12 schematically shows that the trajectory of the A-phase current initiates from the coordinates (-0.025, -0.03) strategically positioned within the stable region of the relay's characteristic curve. Remarkably, it consistently abstains

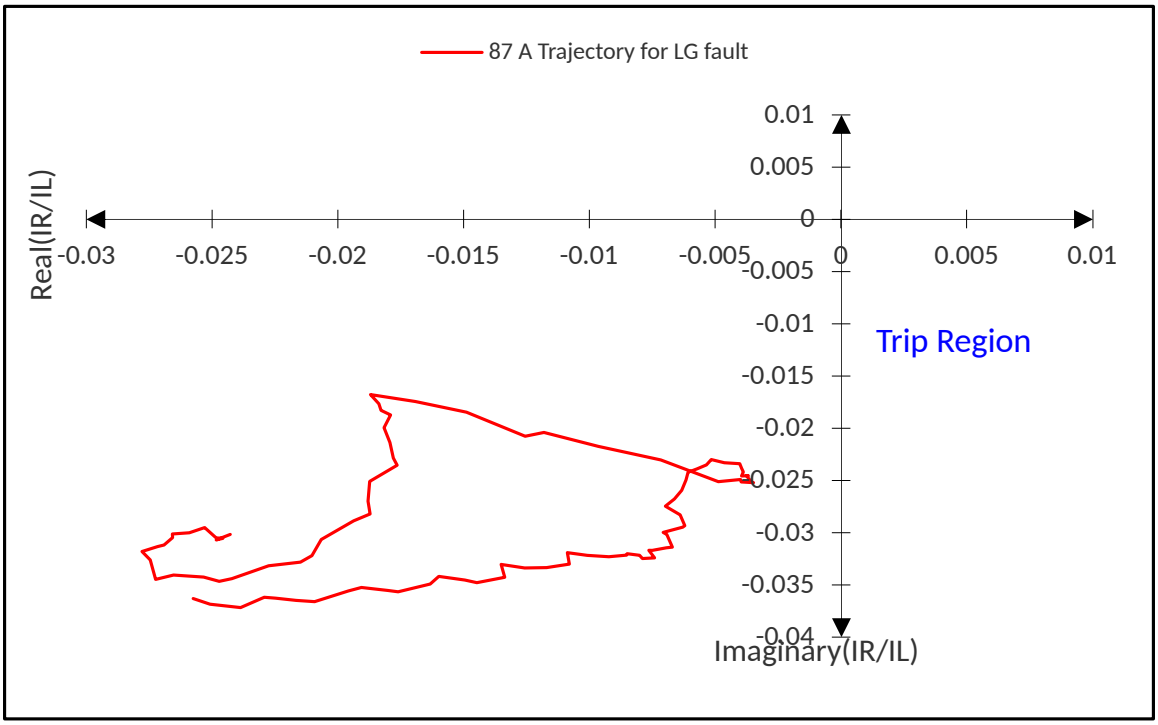

Figure 5.12: α-Plane operating characteristic of a differential relay

from entering into the trip region despite the occurrence of the fault. This behaviour can be attributed to the dynamic nature of the current's phase angle during a fault event, mainly when the inverter-based resource injects reactive current to stabilize the bus voltage.

In contrast, the performance evaluation of the protective scheme is meticulously executed for the identical fault scenario. This assessment is visually encapsulated in Fig. 5.13. Notably, this alternative approach hinges upon discerning discrepancies in the positive sequence impedance. The findings corroborate the method's capability to accurately detect the fault, as elegantly demonstrated in Fig. 5.13

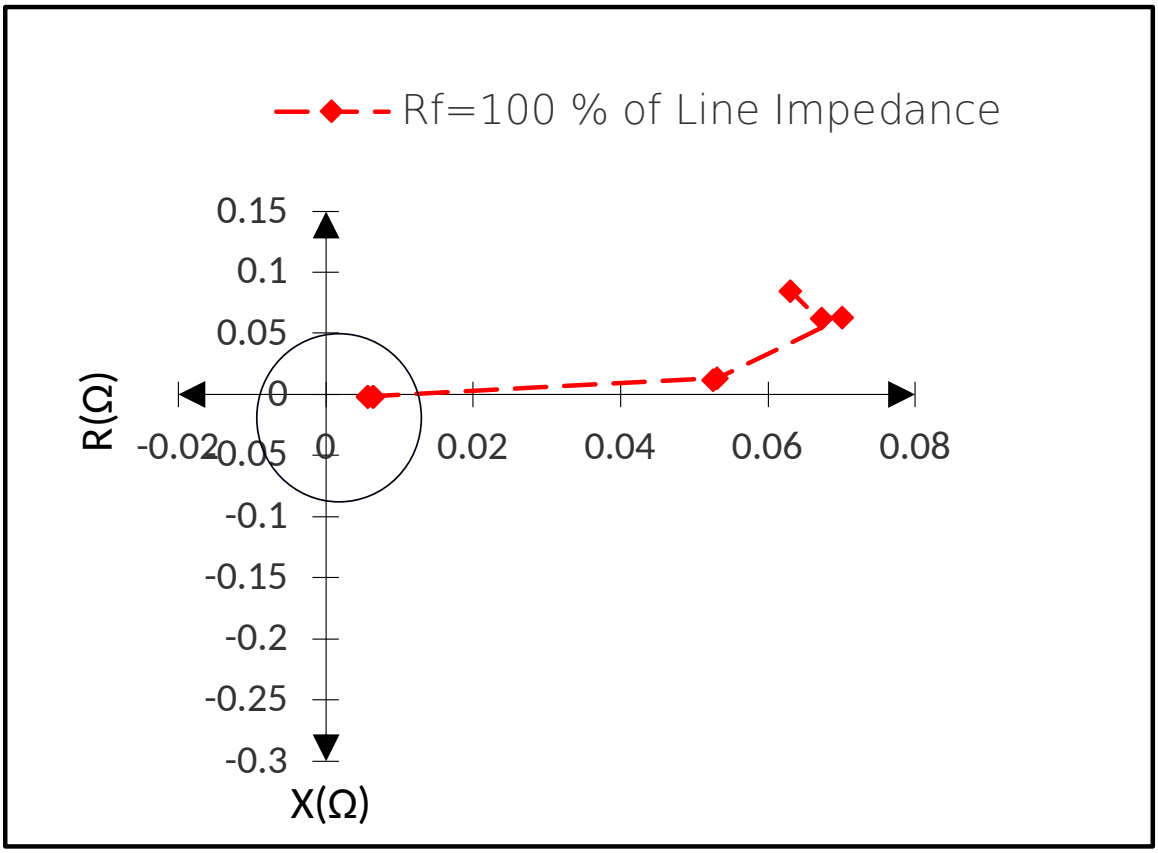

Figure 5.13: Discrepant impedances of feeder L13 for fault at F3 during islanded mode for resistive fault

5.5 Communication Aspects

Communication is pivotal in numerous protection schemes within the power industry, including the one proposed in this paper. When designing a protection scheme, it is essential to consider three major communication aspects, which are outlined below:

5.5.1 Bandwidth Requirements

Bandwidth is a critical metric that indicates the capacity of data transmitted within a network over a specific time frame. In power systems, various types of data traffic are prevalent on a process bus, including sampled values and GOOSE (Generic Object-Oriented Substation Event) messages. A sampled value frame comprises sampled value data, sampled value identifier, and Ethernet frame overhead. During the testing

phase of the proposed scheme, the length of a sampled value frame was measured at 120 bytes (960 bits) using third-party software, namely 'Wireshark'.

Engineers dimensioning the network's bandwidth must consider the frame length, the number of digital instrument transformers, and the sampling rate. The bandwidth (BW) consumed by the sampled value messages in the network is determined by the following formula:

$$BW = \frac{L_f.S.N_t}{10^6} \tag{5.1}$$

Here, L_f is the length of sampled value frame in bits, S is the number of samples per second, N_t is the number of digital instrument transformers, and BW is the bandwidth in Mbps.

Referring to Fig. 5.1, it is determined that 38 digital current and potential transformers are needed. These instruments generate 4800 samples per second. Substituting these values into (5.1) yields a bandwidth requirement of 175.10 Mbps for the CERTS microgrid with the proposed protection scheme. A similar procedure can be applied to calculate the bandwidth requirement for any microgrid.

5.5.2 Loss of Samples

The proposed protection scheme relies on communication to transmit sampled value messages from digital instrument transformers to a central processing unit. In cases of unforeseen contingencies, there is a possibility that sampled packets may be lost while traversing the network. It is essential to assess the impact of sample loss on the effectiveness of the proposed protection scheme.

To investigate this, the discrepant impedances of feeder L6 were monitored under no-fault conditions with and without sample loss. The GTNET-SV publisher suppresses the output sampled value data stream. Without sample loss, the discrepant impedance values should ideally be zero. Five voltages and currents are simultaneously suppressed, and the discrepant impedance is computed.

Table 3 provides insight into the computed discrepant impedance, which is less than 3%of the feeder impedance when there is no sample loss. This resilience to sample loss can be attributed to the down-sampling of received samples within the proposed protection scheme.

The same resilience to sample loss is observed when six consecutive samples are lost. However, when seven consecutive samples are lost, the discrepant impedance falls within the fault region. This implies that the proposed protection scheme can tolerate the loss of up to six consecutive samples when down-sampling is applied, reducing the original sampling rate from 4800 Hz to 480 Hz. For scenarios involving more than six consecutive sample losses, the lost samples can be reconstructed using the interpolation method described in [71]

Table 5.2: Change in Discrepant Impedance Due to Loss of Samples in No-fault Condition

Feeder Impedance Z_1 (ohm)	No. of Samples lost	$\lvert\Delta Z\rvert/Z_1$ (%)
0.01724	0	0
0.01724	5	0.149
0.01724	6	0.179
0.01724	7	4.18

5.5.3 Loss of Synchronization

The proposed protection scheme requires synchronized samples from both ends of the feeder. The synchronization signal may be lost. In this case, the digital instrument transformer shall go into the holdover mode. For the holdover, the digital instrument

transformer shall continue to send the sampled values at the specified sampling rate. The minimum holdover time shall be five seconds, which means the digital instrument transformers shall continue to send the signals for at least five seconds as if the synchronization signal is still present. Once the synchronization is resumed, the sampled values shall continue synchronizing the new pulse.

5.6 Summary

This chapter explored the response of the proposed protection technique on a CERTS low-voltage microgrid. The protection technique is evaluated under different operating scenarios and for resistive and open circuit faults. The response of the proposed protection scheme was appropriate for islanded and grid-connected modes and for a microgrid operating without a synchronous generator such as DG. Further, the protection system was verified for its performance with a commercially available alpha-plane differential relay. It can be concluded that the alpha-plane differential relay doesn't operate for high resistive faults in a microgrid with IBR, while the proposed protection scheme performs well. Also, the proposed protection scheme requires a low bandwidth network and fewer copper wires for practical implementation. The protection scheme is inherently resilient to losing a limited number of samples consecutively.

Chapter 6

Summary and Conclusions

6.1 Summary and Conclusions

The modern power system is changing every day and experiences a fault that is beyond the control of engineers and operators. These currents' signature differs from legacy power generators such as synchronous generators. The first chapter of the thesis describes the power system protection concepts, causes of faults and the need for a protection scheme for inverter-dominated microgrids. The primary objective of the work reported in this thesis was to design, implement and evaluate the protection technique. Using simulation software and real-time digital simulator.

Chapter 2 of the thesis takes a deeper dive into the faults that can impact microgrids featuring inverter-based generators. It examines the distinct signature of fault currents occurring within microgrids, whether they operate in grid-connected or islanded modes. The chapter also scrutinizes the limitations of existing protection methods commonly used by utilities when a dedicated microgrid protection relay is absent. These conventional practices often involve over-current, undervoltage, differential, direction, and distance relay techniques. However, the chapter elaborates on the issues and challenges associated with these traditional methods, highlighting their shortcomings in addressing the unique characteristics of fault currents in inverter-dominated microgrids.

Researchers and engineers have made progress in designing adaptive overcurrent protection using machine learning for the microgrids. These methods and their limi-

tations are discussed in Chapter 2.

Chapter 3 of this thesis introduces an innovative protection technique and outlines its modelling on a centralized microcomputer. This novel approach offers simplicity and efficiency, requiring only a modest amount of sampled voltage and current values for its operation. The modelling process for this protection technique encompasses several crucial steps, including signal sampling, signal acquisition, downsampling, signal conditioning, and phasor estimation. Additionally, Chapter 3 defines the trip characteristics of the protection technique and elaborates on the underlying trip logic. The central microcomputer initiates a trip action when the impedance discrepancy for any feeder exceeds a predetermined threshold for five consecutive instances.

Moving on to Chapter 4, it provides a comprehensive description of the benchmark system featuring inverter-based resources. This chapter seeks to evaluate the effectiveness of the previously introduced protection technique. Various types of faults occurring at different network segments under various operating modes are simulated and analyzed. To visualize the performance of the protection technique, characteristic curves are plotted on the R-X (reactance-resistance) plane. The results and findings presented in this chapter demonstrate that the proposed protection technique excels at blocking external faults while appropriately responding to internal faults.

Furthermore, the performance assessment of the protection technique extends to real-world scenarios. Chapter 5 details the evaluation of the protection technique using a real-time operating system and a real-time digital simulator. The CERTS microgrid, developed within the RSCAD software on the RTDS platform, serves as the testing ground for this assessment. The protection algorithm itself is implemented on the NOVACOR microcomputer. Rigorous testing is conducted under a range of fault scenarios, various operating conditions, and situations involving high resistances. The results conclusively confirm the dependability and security of the protection technique, demonstrating its robustness and effectiveness in real-time applications. The protection technique is independent of microgrid architecture, type of resources and control strategy of resources. Further, the protection technique is independent of the mode of operation, i.e. grid-connected mode and islanded mode. The protection

scheme works for high resistance faults up to 500% of feeder resistance for CERTS microgrid feeder. The protection scheme works for resistive faults, while the alpha-plane differential relay does not operate. Further, the protection can sustain the loss of five consecutive samples without affecting the trip setting.

6.2 Suggestions for Future Research

It has been demonstrated in this thesis that the proposed protection technique is capable of protecting microgrids. The laboratory testing of the system has provided satisfactory results. Future work involves:

1. Testing of protection techniques in real-world microgrids.
2. Testing of protection technique on transmission connected with inverter-based generators of different types and controls.
3. Effect of CT saturation and very high impedance faults(100 ohm) on the protection technique.
4. Combined control and protection unit for microgrids.
5. Development of the backup protection scheme.

References

[1] International Renewable Energy Agency, "IRENA (2018), global energy transformation: A roadmap to 2050, International Renewable Energy Agency, Abu Dhabi, [Online]. Available: www.irena.org/publications," tech. rep., International Renewable Energy Agency.

[2] Canadian Renewable Energy Association, "Powering Canada's Journey to Net-Zero, [Online]. Available: https://renewablesassociation.ca/ ."

[3] "IEEE Std-2030.9 Recommended Practice for the Planning and Design of the Microgrid," 2019.

[4] M. S. Sachdev and R. Das, "Understanding Microprocessor Based- Technology Applied to Relaying, PSRC, Working Group Report I-01, 2009,"

[5] "IEEE Std C37.91-2021 (Revision of IEEE Std C37.91-2008) IEEE Guide for Protecting Power Transformers," 2021.

[6] "IEEE Recommended Practice for Motor Protection in Industrial and Commercial Power Systems," tech. rep., IEEE. ISBN: 9781504436083.

[7] "IEEE Guide for AC Generator Protection," tech. rep., IEEE. ISBN: 9780738152509.

[8] M. W. Altaf, M. T. Arif, S. N. Islam, and M. E. Haque, "Microgrid Protection Challenges and Mitigation Approaches–A Comprehensive Review," *IEEE Access*, vol. 10, pp. 38895–38922, 2022.

[9] A. Simeon and S. Chowdhury, "Protection Challenges in a Stand-alone Microgrid: Case Study of Tsumkwe Microgrid," in *2020 IEEE PES/IAS PowerAfrica*, (Nairobi, Kenya), pp. 1–5, IEEE, Aug. 2020.

[10] A. E. P. Fernandez, J. M. Gers, and J. Quintero, "Challenges in Microgrid Protection," in *2019 FISE-IEEE/CIGRE Conference - Living the energy Transition (FISE/CIGRE)*, (Medellin, Colombia), pp. 1–6, IEEE, Dec. 2019.

[11] V. R. Mahindara, A. Priyadi, M. Pujiantara, M. H. Purnomo, A. Y. Saber, and E. Muljadi, "Protection Coordination Challenges for Microgrid Distribution Network with High Penetration Inverter-Based Resources," in *2020 IEEE Energy Conversion Congress and Exposition (ECCE)*, (Detroit, MI, USA), pp. 1618–1622, IEEE, Oct. 2020.

[12] M. A. Zamani, T. S. Sidhu, and A. Yazdani, "A Protection Strategy and Microprocessor-Based Relay for Low-Voltage Microgrids," *IEEE Transactions on Power Delivery*, vol. 26, pp. 1873–1883, July 2011.

[13] M. S. Rahman, T. F. Orchi, S. Saha, and M. E. Haque, "Multi-Agent Approach for Overcurrent Protection Coordination in Low Voltage Microgrids," in *2019 IEEE Power & Energy Society General Meeting (PESGM)*, (Atlanta, GA, USA), pp. 1–5, IEEE, Aug. 2019.

[14] M. A. Zamani, A. Yazdani, and T. S. Sidhu, "A Communication-Assisted Protection Strategy for Inverter-Based Medium-Voltage Microgrids," *IEEE Transactions on Smart Grid*, vol. 3, pp. 2088–2099, Dec. 2012.

[15] A. K. Soni, A. Kumar, R. K. Panda, A. Mohapatra, and S. N. Singh, "Adaptive Coordination of Relays in AC Microgrid Considering Operational and Topological Changes," *IEEE Systems Journal*, vol. 17, pp. 3071–3082, June 2023.

[16] S. Sahu, S. Ansari, and O. H. Gupta, "Protection of low voltage AC microgrid using discrete wavelet transform," in *2022 IEEE 9th Uttar Pradesh Section International Conference on Electrical, Electronics and Computer Engineering (UPCON)*, (Prayagraj, India), pp. 1–6, IEEE, Dec. 2022.

[17] A. S. Rana, K. Jnaneswar, and M. S. Thomas, "Fault Location Identification Using Hybrid Scheme in AC Microgrid," in *2023 International Conference on*

Recent Advances in Electrical, Electronics & Digital Healthcare Technologies (REEDCON), (New Delhi, India), pp. 391–396, IEEE, May 2023.

[18] D. Liu, A. Dysko, Q. Hong, D. Tzelepis, and C. D. Booth, "Transient Wavelet Energy-Based Protection Scheme for Inverter-Dominated Microgrid," *IEEE Transactions on Smart Grid*, vol. 13, pp. 2533–2546, July 2022.

[19] Z. Shuai, C. Shen, X. Yin, X. Liu, and Z. J. Shen, "Fault Analysis of Inverter-Interfaced Distributed Generators With Different Control Schemes," *IEEE Transactions on Power Delivery*, vol. 33, pp. 1223–1235, June 2018.

[20] North American Electric reliability Corporation (NERC), "Inverter Relay Manufacturer Coordination Meeting - April 2019 , [Online]. Available :https://www.nerc.com/comm/pc/pages/inverter-based-resource-performance-task-force.aspx," Apr. 2019.

[21] A. Yazdani and R. Iravani, *Two-Level, Three-Phase Voltage-Sourced Converter*, pp. 115–126. 2010.

[22] W. Du, F. K. Tuffner, K. P. Schneider, R. H. Lasseter, J. Xie, Z. Chen, and B. Bhattarai, "Modeling of grid-forming and grid-following inverters for dynamic simulation of large-scale distribution systems," *IEEE Transactions on Power Delivery*, vol. 36, no. 4, pp. 2035–2045, 2021.

[23] Y. Li, Y. Gu, and T. C. Green, "Revisiting grid-forming and grid-following inverters: A duality theory," *IEEE Transactions on Power Systems*, vol. 37, no. 6, pp. 4541–4554, 2022.

[24] Y. Gu and T. C. Green, "Power system stability with a high penetration of inverter-based resources," *Proceedings of the IEEE*, vol. 111, no. 7, pp. 832–853, 2023.

[25] P. Piagi and R. Lasseter, "Autonomous control of microgrids," in *2006 IEEE Power Engineering Society General Meeting*, pp. 8 pp.–, 2006.

[26] J. Sharma, K. T. Lulbadda, A. Golder, T. Sidhu, and S. S. Williamson, "Fault analysis of microgrids with inverter interfaced resources in grid-connected and islanded modes," in *2022 IEEE 1st Industrial Electronics Society Annual On-Line Conference (ONCON)*, pp. 1–6, 2022.

[27] J. Shiles, E. Wong, S. Rao, C. Sanden, M. A. Zamani, M. Davari, and F. Katiraei, "Microgrid protection: An overview of protection strategies in north american microgrid projects," in *2017 IEEE Power Energy Society General Meeting*, pp. 1–5, 2017.

[28] W. A. . Christopoulos, C., *Overcurrent and earth fault protection. In: Electrical Power System Protection*. Boston, MA: Springer, 1999.

[29] W. Elmore, *Protective Relays Their Theory and Applications*. New york: Marcel Dekker Inc., 2003.

[30] A. van C Warrington, *Protective Relays Their Theory and Practices Vol-I*. 11 New Fitter Lance EC4: Chapman and Hall Limited, 1968.

[31] A. W. Helmut Ungrad, Willibald Winkler, *Protection Techniques in Electrical Energy Systems*. Boca Raton: CRC Press, 1995.

[32] M. J. Reno, S. Brahma, A. Bidram, and M. E. Ropp, "Influence of inverter-based resources on microgrid protection: Part 1: Microgrids in radial distribution systems," *IEEE Power and Energy Magazine*, vol. 19, no. 3, pp. 36–46, 2021.

[33] N. Hatziargyriou, H. Asano, R. Iravani, and C. Marnay, "Microgrids," *IEEE Power and Energy Magazine*, vol. 5, no. 4, pp. 78–94, 2007.

[34] P. Naveen and P. Jena, "A review on issues and coordination strategies for over current protection in microgrid," in *2017 14th IEEE India Council International Conference (INDICON)*, pp. 1–6, 2017.

[35] D. Lagos, V. Papaspiliotopoulos, G. Korres, and N. Hatziargyriou, "Microgrid protection against internal faults: Challenges in islanded and interconnected operation," *IEEE Power and Energy Magazine*, vol. 19, no. 3, pp. 20–35, 2021.

[36] E. Sortomme, G. J. Mapes, B. A. Foster, and S. S. Venkata, "Fault analysis and protection of a microgrid," in *2008 40th North American Power Symposium*, pp. 1–6, 2008.

[37] Y. Xu, L. Mu, F. Zhang, Z. Mou, and J. Zhu, "Analysis of the fault characteristics of microgrid with inverter-interfaced distributed generators," in *2019 IEEE 8th International Conference on Advanced Power System Automation and Protection (APAP)*, pp. 386–390, 2019.

[38] G. Kou, L. Chen, P. VanSant, F. Velez-Cedeno, and Y. Liu, "Fault characteristics of distributed solar generation," *IEEE Transactions on Power Delivery*, vol. 35, no. 2, pp. 1062–1064, 2020.

[39] Z. Shuai, C. Shen, X. Yin, X. Liu, and Z. J. Shen, "Fault analysis of inverter-interfaced distributed generators with different control schemes," *IEEE Transactions on Power Delivery*, vol. 33, no. 3, pp. 1223–1235, 2018.

[40] "IEEE standard for interconnection and interoperability of distributed energy resources with associated electric power systems interfaces," *IEEE Std 1547-2018 (Revision of IEEE Std 1547-2003)*, pp. 1–138, 2018.

[41] "The grid code-national grid electricity transmission." [online at] https://bit.ly/35ktXE4.

[42] Schweitzer Engineering Laboratories, Inc. , "SEL-751 feeder protection relay." [online at] https://selinc.com/products/751/docs/.

[43] A. Hooshyar and R. Iravani, "A new directional element for microgrid protection," *IEEE Transactions on Smart Grid*, vol. 9, no. 6, pp. 6862–6876, 2018.

[44] S. De Rijcke, P. S. Pérez, and J. Driesen, "Impact of wind turbines equipped with doubly-fed induction generators on distance relaying," in *IEEE PES General Meeting*, pp. 1–6, 2010.

[45] A. Hooshyar, M. A. Azzouz, and E. F. El-Saadany, "Distance protection of lines emanating from full-scale converter-interfaced renewable energy power

plants—part i: Problem statement," *IEEE Transactions on Power Delivery*, vol. 30, no. 4, pp. 1770–1780, 2015.

[46] A. Banaiemoqadam, A. Azizi, A. Hooshyar, M. Kanabar, and E. F. El-Saadany, "Impact of inverter-based resources on different implementation methods for distance relays—part i: Phase comparators," *IEEE Transactions on Power Delivery*, pp. 1–11, 2023.

[47] V. Telukunta, J. Pradhan, A. Agrawal, M. Singh, and S. G. Srivani, "Protection challenges under bulk penetration of renewable energy resources in power systems: A review," *CSEE Journal of Power and Energy Systems*, vol. 3, no. 4, pp. 365–379, 2017.

[48] R. Mohanty, P. Chen, and L. A. Tuan, "Current restrained undervoltage protection scheme of converter dominated microgrids," in *15th International Conference on Developments in Power System Protection (DPSP 2020)*, pp. 1–6, 2020.

[49] "Voltage restrained overcurrent relay." [online at] https://library.e.abb.com/public/c1256d32004634bac1256e0f006bd0fc/1MRK509033-BEN_en_Voltage_restraint_overcurrent_relay_and_protection_assemblies_RXISK_2H_and_RAISK.pdf.

[50] B. Chattopadhyay, M. Sachdev, and T. Sidhu, "Adaptive relaying for protecting a distribution system-a feasibility study," in *[Proceedings] WESCANEX '91*, pp. 20–25, 1991.

[51] P. Mahat, Z. Chen, B. Bak-Jensen, and C. L. Bak, "A simple adaptive overcurrent protection of distribution systems with distributed generation," *IEEE Transactions on Smart Grid*, vol. 2, no. 3, pp. 428–437, 2011.

[52] F. Coffele, C. Booth, and A. Dyśko, "An adaptive overcurrent protection scheme for distribution networks," *IEEE Transactions on Power Delivery*, vol. 30, no. 2, pp. 561–568, 2015.

[53] M. N. Alam, S. Chakrabarti, and A. K. Pradhan, "Protection of networked microgrids using relays with multiple setting groups," *IEEE Transactions on Industrial Informatics*, vol. 18, no. 6, pp. 3713–3723, 2022.

[54] A. Barranco-Carlos, C. Orozco-Henao, J. Marín-Quintero, J. Mora-Flórez, and A. Herrera-Orozco, "Adaptive protection for active distribution networks: An approach based on fuses and relays with multiple setting groups," *IEEE Access*, vol. 11, pp. 31075–31091, 2023.

[55] S. Samal, S. R. Samantaray, and N. K. Sharma, "Data-mining model-based enhanced differential relaying scheme for microgrids," *IEEE Systems Journal*, pp. 1–12, 2022.

[56] B. Wang and L. Jing, "A protection method for inverter-based microgrid using current-only polarity comparison," *Journal of Modern Power Systems and Clean Energy*, vol. 8, no. 3, pp. 446–453, 2020.

[57] IEEE-PSRC, "Centralized substation and protection control." [online at] https://www.pes-psrc.org/kb/report/020.pdf.

[58] "IEC 61850-9-2:2011 :Communication networks and systems for power utility automation - Part 9-2," Sept. 2011. ICS 33.200 ISBN 978-2-8322-7886-4.

[59] "IEC 62439-3:2021 :Industrial communication networks – high availability automation networks – part 3: Parallel redundancy protocol (prp) and high-availability seamless redundancy (hsr)," Dec. 2021. ICS 25.040.40; 35.100.05,ISBN 978-2-8322-1059-5.

[60] "IEC/IEEE international standard - communication networks and systems for power utility automation – part 9-3: Precision time protocol profile for power utility automation," *IEC/IEEE 61850-9-3 Edition 1.0 2016-05*, pp. 1–18, 2016.

[61] *Mathematical Basis for Protective Relaying Algorithms*, ch. 3, pp. 55–108. John Wiley Sons, Ltd, 2009.

[62] "IEEE standard requirements for instrument transformers - redline," *IEEE Std C57.13-2008 (Revision of IEEE Std C57.13-1993) - Redline*, pp. 1–106, 2008.

[63] "IEC standard for digital interface of instrument transformers," *Instrument transformers - Part 9: Digital interface for instrument transformers*, pp. 1–127, 2016.

[64] "RSCAD instruction manual," *RSCAD Instruction Manual*, pp. 1–1520, 2016.

[65] T. Sidhu, X. Zhang, F. Albasri, and M. Sachdev, "Discrete-fourier-transform-based technique for removal of decaying dc offset from phasor estimates," *IEE Proceedings Generation Transmission and Distribution*, vol. 150, no. 6, pp. 745–752, 2003.

[66] C. L. Fortescue, "Method of symmetrical co-ordinates applied to the solution of polyphase networks," *Transactions of the American Institute of Electrical Engineers*, vol. XXXVII, no. 2, pp. 1027–1140, 1918.

[67] J. Sharma and T. S. Sidhu, "A new protection scheme for feeders of microgrids with inverter-based resources," *Electric Power Systems Research*, vol. 224, p. 109632, 2023.

[68] R. W. Kenyon, A. Sajadi, A. Hoke, and B.-M. Hodge, "Open-source pscad grid-following and grid-forming inverters and a benchmark for zero-inertia power system simulations," in *2021 IEEE Kansas Power and Energy Conference (KPEC)*, pp. 1–6, 2021.

[69] J. Sharma and T. Sidhu, "A low voltage microgrid protection scheme using digital instrument transformers," *IET Renewable Power Generation*, vol. Submitted.

[70] G. Benmouyal, "Line current differential protection," in *Line Current Differential Protection: A Collection of Technical Papers Representing Modern Solutions*, vol. 2, 2021.

[71] M. G. Kanabar and T. S. Sidhu, "Performance of iec 61850-9-2 process bus and corrective measure for digital relaying," *IEEE Transactions on Power Delivery*, vol. 26, no. 2, pp. 725–735, 2011.

APPENDICES

Appendix A

Line Parameters of the Micogrids

This appendix details line parameters used in the IEEE-9 bus system and CERTS microgrid.

A.1 Line Parameters of the IEEE-9 Bus System

This appendix provides the details of line parameters used in the IEEE-9 bus system.

Sequence	R(ohm/m)	XL (ohm/m)	XC(ohm/m)	Line Length (km)
Positive	1.07 x 10^-4	4.27 x 10^-4	2.5448 x 10^6	10
Zero	5.35 x10^-4	1.153 x10^-3	4.162 x10^6	10

A.2 Line Parameters of the CERTS Microgrid

The Line lengths and impedances of feeders of the CERTS microgrid are shown in the table below:

Sequence	R(ohm)	XL (ohm)	XC(M ohm)
Positive	0.019331	0.048191	0.007466
Zero	0.031944	0.085208	0.007466

Feeder	Line Length (m)
L1	0.915
L2	69
L3	23
L4	23
L5	69
L6	23
L7	23
L8	23
L9	25
L10	25
L11	69
L12	69
L13	46
L14	23
L15	69